PROPAGATION OF LEAKING MODES IN A PLANE SEISMIC WAVEGUIDE

Thesis by

Robert Alden Phinney

Submitted in partial fulfillment of the requirements

for the degree of Doctor of Philosophy

Division of Geological Sciences

California Institute of Technology

April 1961

Abstract

The work of Rosenbaum describing propagation of imperfectly trapped (leaking) modes in an acoustic waveguide is extended to two problems of geophysical importance. The problem of a liquid layer coupled to an elastic halfspace is considered first, in a paper entitled: Propagation of Leaking Modes in the Crustal Waveguide: The Oceanic PL wave. Theoretical results obtained in this first paper may be applied, after slight generalization, to the most general type of plane seismic waveguide. In a second paper, entitled: Propagation of Leaking Interface Waves, we discuss these generalizations and apply them to the fundamental problem of pulse propagation along a plane interface. The most important result of both papers is the description of the earliest-arriving signal traveling in the waveguide as a result of a transient point excitation.

Numerical results for both problems were obtained by solving the complex period equation on the Burroughs 220 computer. The programming framework and the numerical methods used are discussed in a third section of this thesis.

Table of Contents

CALIFORNIA INSTITUTE OF TECHNOLOGY
SEISMOLOGICAL LABORATORY

LEAKING MODES IN THE CRUSTAL WAVEGUIDE
PART I: THE OCEANIC PL WAVE

By

Robert A. Phinney

This research was partially supported by Contract No. AF-49 (638) 910 of the Air Force Technical Applications Center as part of the Advanced Research Projects Agency project VELA.

LEAKING MODES IN THE CRUSTAL WAVEGUIDE
PART I: THE OCEANIC PL WAVE[1]

Robert A. Phinney

Seismological Laboratory
California Institute of Technology
Pasadena, California

****

Abstract

The problem of the seismic signal associated with the earliest P-wave is treated from the modal point of view, where the signal is regarded as a quasi-surface wave, coupled both to the motion of the earth's layered surface and to body waves propagating in the underlying media. Predictions made for the particular model assumed are relevant to explosion and earthquake sources. The oscillations following the initial P motion are explained.

The transient solution obtained by Rosenbaum for leaking mode propagation in an acoustic waveguide has been generalized to describe propagation in an elastic halfspace overlain by a liquid layer. The early-arriving PL modes known from earthquake studies have been computed for several theoretical models to test the effect of the elastic

---

[1]Contribution No. 1013, Division of Geological Sciences, California Institute of Technology

constants on their dispersion and attenuation. Physical reasoning based on harmonic plane wave models, appears insufficient to predict many features of the exact dispersion and attenuation. The analogy between PL waves and normal modes in the case treated by Pekeris is exploited and it is also believed that PL waves are related to an attenuated pseudo-surface wave of a free solid halfspace. Late-arriving quasi-standing waves are treated briefly and their relevance to certain seismic phenomena is mentioned.

Introduction

The nature of the ground response to a transient seismic source, such as an explosion or an earthquake, has been approached from two complementary points of view which are mathematically tractable. Geometric ray theory predicts the amplitudes and travel times of energy travelling as compressional and shear waves in the earth. It has been especially valuable in interpreting the early part of a seismic signal containing the body waves P and S, as well as mixed phases such as PP, PS, PSP, etc., known from earthquake studies. Waveguide theory has heretofore concerned itself with the later portion of a seismogram consisting largely of oscillations perfectly coupled to the earth's layered surface, such as Rayleigh waves and Love waves. This theory has not accounted, however, for the principal energy in the early-arriving body waves, namely the oscillatory "tail" often associated with the P wave or the refraction arrival. Furthermore, early-arriving oscillations are often observed, which have no apparent relation to either known body waves or theoretically predicted surface waves. It is to such problems that this paper is addressed. The waveguide theory is generalized to a transient in such a way as to explain early-arriving waves which share certain properties of both body waves and surface waves (normal modes). It is hoped that this approach will eventually predict or confirm many details of seismograms

from transient sources which have been largely ignored up to now. Although a liquid surface layer is treated here the method can be extended to a solid surface layer. The results for the latter case will appear in a forthcoming paper.

In the past decade much has been learned about the properties of surface waves on a layered elastic halfspace. One is able to deduce the dispersion and particle motion for ordinary Love or Rayleigh waves by finding the zeroes, in the real domain, of a secular determinant, as a function of the frequency parameter ω. The definitive form of this theory is due to Pekeris [1948], who applied his results to a liquid layer lying over a liquid halfspace. Since then various authors have obtained the dispersive properties of surface waves in a sufficient variety of cases to learn a great deal about the properties of the earth's crust and upper mantle.

A common definition of "surface wave" states that, in the steady state (sinusoidal time dependence) the energy is restricted to the surface waveguide, causing the wave amplitudes to vanish exponentially with increasing distance from the waveguide. Consequently a set of source free potentials can be formed, equal in number to the boundary conditions. The latter generate a set of homogeneous linear equations whose vanishing determinant specifies the dispersion relations (phase and group velocity curves). An equivalent

viewpoint, utilizing the mutual constructive interference of plane waves totally reflected in the waveguide, arrives at the same result.

The plane wave interference idea strongly suggests that one may observe other types of surface waves, in which the total reflection criterion is not entirely satisfied. Modes of motion exist in which energy is systematically leaked into the halfspace. The constructive interference criterion will still select certain frequencies at which the leakage loss is small compared with that at neighboring frequencies; these frequencies will propagate as quasi-surface waves, damped exponentially in time and space, due to continual loss of energy from the waveguide.

Oliver and Major [1960] recently discussed a class of leaking waves known in earthquake seismology as PL waves. They are observed as early-arriving dispersed signals, coupled to the P wave velocity in the basement, and are dual to Rayleigh waves in the sense that the surface orbital motion is generally prograde elliptical. The PL wave is the oscillatory portion of the familiar refraction arrival and corresponds to the normal modes obtained by Pekeris for the liquid bottom problem.

Oliver and Major suggested that these leaking modes should correspond to minimum values (quasi-resonance) of the secular determinant. Proceeding on this basis, they computed dispersion curves for single layer crustal models

corresponding roughly to an oceanic and a continental crust. The Pekeris solution, however, is not sufficiently refined to yield damped modal solutions, so that the Oliver and Major curves, while intuitively reasonable, have no rigorous role in the Pekeris theory. Also, the steady-state theory does not predict the attenuation suffered by the various frequencies.

Electromagnetic theory provides a familiar example of damped modes, where the loss mechanism, conductivity, is intrinsic to the propagation in the small. We are not concerned with microscopic losses, which induce only slight additional dispersion, but will investigate leakage losses due to coupling of the waveguide to the halfspace. There is no analog in electromagnetic waveguide theory to certain elastic phenomena which are due to the existence of both longitudinal and transverse wave propagation. We do know, however, that the usual definitions of phase and group velocity lose their precise meaning when attenuation occurs.

It has long been felt that leaking modes could be included in the modal transient solution by taking account of the complex roots of the period equation lying on "non-permissible" Riemann surfaces of the integrand. Rosenbaum [1960] accomplished this by a series of contour transformations in the complex s and k planes which enabled him to include modal expressions due to these complex roots. The resulting integrals are then approximated by the saddle

point method in the complex k-plane. The final expressions for the modal solution, save for the introduction of an attenuation factor, are simple generalizations of those obtained in the Pekeris theory. The location of the saddle point which defines the frequency and wave number of the dispersed waves is now in general complex. Group velocity is obtained by an operational definition at the complex saddle point, while phase velocity appears as an auxiliary result. The Rosenbaum solution is distinguished by the following properties:

1. The solution is obtained as the first term of an asymptotic expansion in inverse powers of the time, in contrast to the Pekeris solution in inverse powers of the horizontal distance r. This generalization makes it possible to consider the form of the response at short distances and large times (singing modes).

2. Considered as an equivalent large-r representation for waveguide propagation, the Rosenbaum solution contains as a special case, without damping, the conventional normal mode surface waves.

3. Group velocity, phase velocity, frequency, and wave number, obtain precise operational meaning only by virtue of the form of the solution obtained by the saddle point evaluation. The damping coefficient turns out to depend on the imaginary parts of both ω and k.

4. Intuitive predictions, based on experience with normal mode theory, are not entirely accurate. One is accustomed to speak of waves propagating at a given phase velocity, and would like to know how they are attenuated. The correct representation of transient leaking modes shows that they are to be regarded as a superposition of transient damped oscillations having a characteristic signal, or group, velocity; it is not correct to view them as a superposition of damped harmonic plane waves having a characteristic phase velocity. Were this done, the damping factor would arise from either Im (ω) or Im (k) alone, instead of the correct combination of both. It is valuable, however, to use intuitive plane wave ideas as a check against the final results; there will always be a discrepancy, but it cannot be too great or singular in nature.

Rosenbaum took as an example of his method the leaking modes in a Pekeris liquid waveguide. He found waves with a small group velocity and large phase velocity which are to be observed at times later than the Airy phase. These modes may be considered as due to constructive interference between plane waves incident in the surface layer on the halfspace at angles between normal incidence and the critical angle for compressional waves. One may view this branch of the dispersion curve as due to the normal modes of a liquid

plate bounded by a free surface and an acoustically hard surface. In the limit as the lower halfspace attains infinite acoustic impedance, the Rosenbaum modes become identical with the normal modes for an acoustic plate coupled to a rigid halfspace. Likewise, in the same limit, the Rosenbaum modes become entirely undamped, and the ground wave branch of the dispersion disappears.

Purpose of the Present Paper

We shall now consider leaking modes in the case of a liquid waveguide coupled to an elastic halfspace. This differs from the Rosenbaum problem in that certain leaking modes propagate at signal velocities greater than those of the normal modes. The problem is relevant in both earthquake seismology and explosion seismology and concerns the oscillatory portion of the guided P-wave propagating with the velocity c_2 of P-waves in the halfspace.

It will be necessary to generalize the contour transformations used by Rosenbaum; the passage from a liquid to a solid halfspace introduces an additional branch point in the formal integral solution. This passage is a singular perturbation; an additional (shear) potential is required and another boundary condition is appropriate. It is well-known that the normal mode solutions to this problem are not the analog of the Pekeris normal modes in the liquid bottom case. One obtains instead Rayleigh and shear modes,

which depend strongly on the shear wave velocity structure, and propagate no faster than the shear velocity in the halfspace. The waves which make up the Pekeris modes are no longer totally reflected at the liquid-solid interface, and lose energy into the halfspace by virtue of a transmitted shear wave, even though the compressional wave is totally reflected. Such waves, propagating with a higher signal velocity than the normal modes, but attenuated, due to leakage of energy into the halfspace, are called PL waves or P-modes. The lowest mode may be observed on long period earthquake seismographs as a low amplitude signal preceding the shear wave for epicentral distances of 200 - 2000 km. Higher modes may have some relevance in the propagation of certain crustal earthquake phases such as P_n and P^*. In seismic exploration applications these leaking modes form the oscillatory portion of the refraction arrival. P waves from nuclear explosions would show oscillatory motion because of near surface layering.

We now consider this in a little more detail by going to the imprecise, but helpful, notion of harmonic plane waves bouncing in a layer at different angles of incidence (Fig. 2a and 2b). Between angles corresponding to phase velocities $c = c_2$ and $c = \beta_2$, P waves are totally reflected, while energy leaks into the bottom by P $\rightarrow$ S conversion. One expects that the damping of these waves will be least where the P $\rightarrow$ P reflection coefficient is the greatest.

Referring to Fig. 2b, we see that it is unity for phase velocities less than β_2, giving rise to undamped shear modes at all angles of incidence between grazing (90°) and the critical angle for P→ S transmission. Also, when c is near c_2, the reflection coefficient approaches 1, suggesting that P-modes may propagate most efficiently for that value of phase velocity. This explains qualitatively, at least, why the oceanic PL wave is propagated over unexpectedly great distances [Oliver and Major 1960].

To estimate the dispersion from this simple model, we note that, when $c = c_2$, the phase change on reflection is zero; hence the dispersion should be identical with that in a Pekeris liquid waveguide near cutoff (Fig. 1). Oliver and Major used essentially this method to compute the dispersion. In later sections we will see that this picture is indeed accurate in its gross aspect; in detail it is incorrect. This discrepancy is due to the fundamental inability of harmonic plane waves to describe attenuated transient modes. Physically the discrepancies arise from coupling to the intrinsic long-period vibrations of a free solid halfspace.

The Formal Solution: A Summary

We consider a liquid layer with free upper surface, coupled to a solid halfspace, labeling the former 1 and the latter 2 (Fig. 2a). The layer thickness is H; source and receiver depths are d and z, respectively; densities are given by ρ_i, compressional velocities by c_i, and shear velocities by β_i. The source is considered to be a transient pulse with exponential decay $S(t) = Ae^{-t/\theta}$. The appendix contains a complete list of definitions. For the sake of readability, we also relegate to the appendix all details of the contour transformations which yield the attenuated modal solutions. The following points, however, deserve mention here.

The three expressions denoted α_1, α_2, and α_2', contain square root signs, which generate branch lines in the complex plane. Jardetzky [1953] has shown that α_1 does not generate a relevant branch cut, due to the symmetry of the integrands with respect to this branch point. The integrand then lies upon four Riemann surfaces in the complex k or s plane, which we classify by the following table:

Table 1

		$\mathrm{Re}\alpha_2$	$\mathrm{Re}\alpha_2'$
Riemann surface:	I	+	+
	II	+	-
	III	-	-
	IV	-	+

It is also important to note that all variables are normalized: ρ_1, c_1, and H, are considered equal to one. The unit of time is, then, the vertical travel time of P waves in the layer, and so forth. $s = i\omega$ will be used as the frequency variable for purposes of transforming and evaluating the contour integral, while we speak in terms of ω in discussing the results.

The pressure response of the waveguide to a transient source is given by the double integral:

$$(1)\quad P(r,z,t) = \frac{A}{\pi i}\int_{\lambda-i\infty}^{\lambda+i\infty}\frac{e^{st}\,ds}{s+\theta^{-1}}\int_0^{\infty} J_o(kr)\,k\,\frac{g(\omega,k,z)}{f(\omega,k)}\,dk$$

This expression may be obtained in the usual manner by satisfying the boundary conditions [Ewing, Jardetzky and Press 1957]. f is the period function and g is the response function.

$$f = bs^4\epsilon^4\alpha_2\sinh\alpha_1 + \alpha_1\cosh\alpha_1[(2k^2+\epsilon^2s^2)^2-4k^2\alpha_2\alpha_2']$$

(2)

$$g = \left\{bs^4\epsilon^4\alpha_2\sinh\alpha_1(1-z)+\alpha_1\cosh\left[\alpha_1(1-z)\right][(2k^2+\epsilon^2s^2)^2-4k^2\alpha_2\alpha_2']\right\}\frac{\sinh\alpha_1 D}{\alpha_1}$$

Transformation and evaluation of the formal integral solution at residues lying in the second quadrant of the s-plane yields the following integral expressions in terms of forward propagating modes. We have neglected all non-oscillatory transient response terms.

$$(3)\qquad P = P' + P''$$

$$P' = +4A\mathrm{Re}\sum_{n=0}^{\infty}\int_{S_I} H_o^{(2)}(kr)\,k\,\frac{e^{s_n t}}{s_n+\theta^{-1}}\left\{F_1(s_n,k)\right\}_I\,dk$$

when $r < t/\gamma$. $P' = 0$ otherwise. The integration is over that portion of the real k axis, $k > 0$, whose image $s_n(k)$ lies in the second quadrant of the s-plane, on the I Riemann sheet. This term is the normal mode contribution plus the late-arriving damped modes of the Rosenbaum type. s_n denotes a root of the period equation $f = 0$.

$$(4) \quad P'' = -4A \, \mathrm{Re} \sum_{n=0}^{\infty} \int_{S_{III}} H_o^{(2)}(kr) k \, \frac{e^{s_n t}}{s+\theta^{-1}} \left\{ F_1(s_n, k) \right\}_{III} dk$$

when $r < t/\gamma$. $P'' = 0$ otherwise. The integration is over that portion of the real positive k axis, whose image $s_n(k)$ lies in the second quadrant of the s-plane, on the III Riemann sheet. These roots of the period equation are all complex, and will generate the early-arriving damped oscillations.

Approximate evaluation of integrals of the type (3) and (4) has been thoroughly discussed by Rosenbaum. The method consists of replacing the Hankel function by its asymptotic representation in terms of a wave progressing in the positive direction, obtaining the factor $e^{i(\omega_n t - kr)}$ in the integrand. The k-contour is then considered to be deformed so that it passes through saddle points defined by the condition: $\frac{r}{t} = \frac{d\omega_n}{dk}$. The saddle point approximation yields asymptotic solutions in t^{-1}. Complete evaluation also yields contributions from the end points of the contour and special expressions for the solution at an Airy phase, when $\omega_n'' = 0$. The saddle point representation is then:

$$(5)\quad P(r,t) = \frac{4A}{H\sqrt{rt}} \sum_{n=0}^{\infty} \left| Q_n^c \right| e^{-L_n t} \cos[\mathrm{Re}(\omega_n^c)t - \mathrm{Re}(k_n^c)r + \psi_c]$$

$$\text{where } L_n = I_m(\omega_n^c) - \frac{r}{t} I_m(k_n^c)$$

$$Q_n^c = \frac{F_1(i\omega_n^c,\ k_n^c)k_n^c}{(\theta^{-1} + i\omega_n^c)(\omega_n''^c k_n^c)^{\frac{1}{2}}} = \left| Q_n^c \right| e^{i\psi_c}$$

The procedure for obtaining the dispersion and attenuation curves for damped modes is as follows: solve the period equation $f = 0$ in the complex plane in the neighborhood of the contour S_I or S_{III} (eqs. 3 and 4). Evaluate the complex derivative $\frac{d\omega_n}{dk}$, and iterate this process until one obtains a point which is both a solution of the period equation and satisfies the condition $\frac{r}{t} = \frac{d\omega_n}{dk} \equiv U$ = real. The quantities appearing in the asymptotic representation (5) are then obtained by evaluation at the saddle point indicated by the superscript "c." In general there will exist a family of loci in the complex plane which describe the progress of the saddle point as a function of U, the group velocity.

In point of fact, certain difficulties exist in applying this recipe for obtaining the dispersion curves. One must be able to continuously deform the contour into such a position that it passes over each saddle point along a path of steepest descent. The existence of branch points near the initial contour complicates the issue of locating the steepest

descent contour. Rosenbaum recognized the complexity of the problem, and was able, in his case, to delimit the behavior of the roots of the period equation with enough precision to specify the steepest descent contour with confidence. In the liquid over solid problem, general statements about the analytic properties of the roots $s_n(k)$ are difficult to make, due to the complexity of the period function. One is forced, instead, to generalize from numerical results obtained from a few arbitrary models.

It therefore is advisable to regard any theoretical results as tentative unless corroborative evidence is available. The dispersion curves must resemble those predicted in an examination of the physics of the problem, as we have done in the introduction. Likewise, the computed attenuation coefficient L_n must not deviate too strongly from the behavior predicted on physical grounds. It is helpful to disregard saddle points whose attenuation is so great as to forbid the possibility of observation. In practice one is interested in the least damped wave appropriate to any particular signal velocity U. For the elastic waveguides under discussion, the least damped wave is the normal mode contribution, when $U_A \leq U \leq \beta_2$, where U_A is the Airy phase velocity. Thus it is legitimate to ask after the properties of damped waves only if $U < U_A$ or if $U > \beta_2$.

Numerical Solution of the Problem

The period equation $f = 0$ (2) was solved on an electronic computer, and the derivative $\frac{d\omega_n}{dk}$ evaluated by appropriate formulae in the neighborhood of the III sheet roots $\omega_n(k)$: k real; $k > 0$. In this way the behavior of the aforementioned roots (that is, the initial contour S_{III}) was clearly established, as well as the location of branch points in the neighborhood of S_{III}. Determination of the saddle point loci follows by iteration to the condition $\frac{d\omega_n}{dk}$ real. On the Burroughs 220 Data Processor one pass at the period function f takes 1 second, one root, ω_n, and derivative are obtained in about 9 seconds. Solution of the same problem when the superficial layer is solid will be about 4 times slower.

Dispersion and attenuation curves were computed for the following assumed models:

Table 2

	c_2	β_2	ρ_2
1	5.196	3.000	3.000
2	3.000	1.55	2.5
3	1.667	.909	2.0
4	4.0	2.309	2.5
5	3.0	2.000	2.5
6	3.0	1.732	2.5
7	5.196	2.874	3.0

All layer constants are referred to $c_1 = 1$, $\rho_1 = 1$, $H = 1$.

Case 1 is chosen to represent a simplified model of the oceanic waveguide, with the lower medium a Poisson solid. Cases 4 and 6 represent Poisson solids also, with a reduced propagation velocity in the halfspace. Case 7 is Case 1 with a smaller bottom impedance, accomplished by reducing the shear velocity in the solid slightly. This was chosen to correspond to the reduction in shear velocity believed to occur in the upper mantle. Cases 2 and 5 show the effect of a decrease and an increase, respectively, in the shear velocity of Case 6. The numerical results shown in Figs. 3 through 12 are derived as follows. U is the value of the derivative $\frac{d\omega_n}{dk}$ at a saddle point, and is plotted as a function of frequency, namely the value of $\mathrm{Re}\,\omega_n$ at the saddle point. The phase velocity is plotted to compare with the usual phase velocity plot in normal mode studies; from the form of the solution (Eq. 12) $c = \frac{\mathrm{Re}\,\omega}{\mathrm{Re}\,k}$, at the saddle point. We plot the attenuation constant L_n as a function of the group velocity, which is equivalent to plotting it on a scale of t^{-1}. All quantities plotted in Figs. 3-12 are dimensionless.

Discussion of Numerical Results

The results for the first three modes of Case 1 are plotted in Figures 3 and 4. The associated normal modes and several late-arriving leaky modes are shown for comparison. The points P represent the cutoff of the physically similar Pekeris normal modes. Particularly noteworthy are the following points:

1. At cutoff the group velocity is equal to c_2. This cutoff is imposed by the form of the integral solution (3). The phase velocity at cutoff is slightly greater than c_2. The operational definitions implied by the form of the asymptotic solution (5) do not necessarily require that U follows from c by differentiation, a condition which occurs only when ω_n^c and k_n^c are real. Electromagnetic theory contains examples where a microscopic loss mechanism brings about a similar situation: the group velocity cannot exceed a maximum value, but the phase velocity may suffer possibly extreme increase or decrease determined by the nature of the problem.

2. The frequency of the PL mode near cutoff is somewhat less than that of the analogous acoustic mode (represented by the point P). Mathematically this discrepancy with the prediction of a harmonic plane wave model is due to the essential vagueness of the model with respect to damped oscillations. Physically,

it appears that there is slight coupling to an attenuated long period surface wave which propagates in the solid halfspace. This matter will be discussed in detail in a future paper.

3. The higher modes of Case 1 behave essentially like the first mode. The mode indices n = 1, 2, ... are not arbitrary, but describe the number of nodal surfaces of the wave potential with depth. We may thus think of these as compressional modes, dual to the shear modes. It will turn out that when β_2 is unusually low, the first mode behaves more like a zero mode Rayleigh wave, but the notation selected here is the more natural.

The behavior of the exponential decay constant has strong bearing on the possibility of observing a given damped mode. L_n is plotted as a function of U (Figure 4). The abscissa may also be considered as a non-linear time scale running from right to left. For $U < 3.0$ the curves are dashed, since the shear wave and Rayleigh wave dominate the signal in this range. In the range $3.0 < U < 5.196$, the maximum value of the attenuation increases with increasing mode number, in a ratio roughly 1:3:5 for the three modes computed. The distances to which the modes will propagate can be seen by considering the oblique grid superimposed on Fig. 4, representing the distance at which a wave is attenuated by the factor e^{-1}. We shall call this the decay range, r_o. This

is related to L_n by the formula:

$$r_o = \frac{U}{L_n}$$

r_o is plotted in multiplies of the layer thickness, H. Thus the first mode is seen to propagate without appreciable loss as far as 250 H. At a very great distance, we should see just a small wave packet traveling at a group velocity of 3.9. At a range of 200, the second and third modes would appear at best as a small damped oscillation following the first arrival. For these modes the cusp at which L_n goes to zero occurs later than the shear wave, and is of no practical importance. In order to see the entire second mode, one would have to be at a range of less than 100. Other relations of the same type may be extracted from Fig. 4.

It is important to inquire how readily earthquake data may be inverted to compare with theoretical curves. The first damped mode has a dimensionless mean angular frequency of about 1.4, which implies a dimensionless mean period of roughly 4.5. At a range of 100 H, for example, the time elapsed between the first arrival and the shear wave is just $13.3\frac{H}{c_1}$; we should be able to see only 3 cycles of the PL wave, albeit virtually undamped. Such a signal could not be read to give very accurate or even moderately dense estimates of the dispersion, nor could the fine structure of the damping coefficient be at all evident. Thus the requirement of a reasonably long wave train is in conflict with the

fact that the wave decays at the desirable long ranges. In point of fact, signals of 6 - 10 cycles duration have been observed for oceanic paths. There is no reason why data from many earthquakes cannot be combined to yield sufficiently detailed information. But as regards dispersion, there is some question whether the PL wave will ever be able to more than corroborate Rayleigh wave studies. The decay constant L_n, however, turns out to be quite sensitive to the physical properties of the solid halfspace. Discussion of this matter will follow in a later paragraph.

First mode results for Cases 1, 4, and 6, are plotted in Figs. 5 and 6. These models demonstrate the effect of varying the P-wave velocity in the solid, while keeping Poisson's constant the same. Phase velocity, group velocity, and decay constant show almost identical behavior, save for the scaling of the velocity variable. In particular, the "hump" in the decay factor near cutoff has nearly the same value for all three cases. There is a slight reduction in the value of the cutoff frequency as the cutoff velocity is decreased.

In Figures 7 and 8, Case 6 (the Poisson solid) is compared with Cases 2 and 5, in which the shear velocity of the solid is respectively decreased and increased. Case 5, representing a high bottom impedance, involves less leakage, and the computed curves behave nearly as predicted by analogy with the Pekeris modes. Phase and group velocity

cut off nearly at the Pekeris cutoff, and the damping approaches zero as U and c approach c_2. The opposite extreme, Case 2, entails highly anomalous behavior. There the damping near cutoff is appreciably increased, and the dispersion curves are severely distorted in the direction of lower frequency.

In view of the strong dependence of L_n on the ratio of compressional to shear velocity on the solid, we should look for possible applications to structure determinations in the earth. With this in mind, we have computed Case 7, to simulate, by contrast with Case 1, the decrease in shear velocity which is believed to take place in a zone of the upper mantle. There is no presupposition that the results of this paper have direct numerical correspondence to the nature of actual seismograms due to the simplified models necessarily employed. One would like to know, however, what order of effect this simulated decrease might have on U, c, and L_n, to determine whether calculations for the multilayered model known from Rayleigh wave observations would be appropriate. Figs. 9 and 10 show, as suspected, that L_n suffers a pronounced increase near cutoff, while $U(\omega)$ and $c(\omega)$ are affected only slightly.

The computed group velocity for Cases 1 and 7 has also been plotted in Fig. 13 for the specific oceanic models shown, and compared with data by Oliver and Major for three oceanic paths. The shape of the computed curves agrees

better with the data than did the approximate curve computed by Oliver and Major. Better fit could be achieved in two ways: (1) by varying the layer thickness of the model, we could make the vertical portion of the group velocity curve fit any of the sets of data shown; (2) by introducing an additional crustal (basaltic) layer in our model, it appears that we could "pull" the high velocity end of the theoretical curves down, into better agreement with the data. This is not planned at present for practical reasons. Although the theoretical curve for Case 7 agrees best with the data, the very crudeness of the model forbids us to say anything conclusive. We defer instead to the refined researches now being carried out by means of mantle Rayleigh waves. It is conceivable, however, that the dependence of the attenuation on the Poisson constant in the solid may be utilized to supplement information obtained with Love and Rayleigh waves. It will be necessary first to compute L_n for models in which the solid is generalized to several layers.

Insofar as reliable dispersion data can be collected, we may take advantage of the fact that these P modes have a greater depth of penetration into the mantle than do the Rayleigh waves of similar frequency. Eventually, in terms of multi-layered models of the mantle, the P modes may yield valuable information on regions as deep as 300 km. A long period (60 seconds) P wave has been observed for several

large earthquakes by instruments in Pasadena. This P mode may involve motion as deep as the penetration depth of the P ray and would require theoretical models with several layers. Preliminary examination of records suggests that this wave is the same for oceanic and continental paths.

Another point must be borne in mind regarding the effect of damping. Pronounced variations in layer properties or thicknesses will have a very deleterious effect on the leaking waves, as compared with their effect on Rayleigh waves. The latter propagate undamped, in a relatively wide frequency band which is selected by the dispersion curve. When a change of thickness occurs, such as at a continental margin, each component frequency incident on the boundary merely "feeds" the new propagation modes at the same frequency, but at a new group velocity determined by the local dispersion curves. Thus nearly all of the long-period energy in a Rayleigh wave train is transmitted without loss across structural boundaries, propagating locally as dictated by the local dispersion curves. By contrast, leaking modes traverse appreciable paths only in restricted frequency bands (see Figs. 3 and 13) where the damping is small. When such wave trains encounter a change in the waveguide properties, conditions may then be unfavorable for efficient propagation at the predominant frequency of the signal. Thus propagation along mixed paths, or across major structural discontinuities would tend to destroy the oscillatory

character of the P-arrival.

For the sake of completeness, a model has been considered, in which the shear velocity of the solid is less than the compressional velocity in the liquid layer. In such an instance, no shear modes can exist in the waveguide and the predominant observed guided wave will be the damped P-oscillation. In Case 3, illustrated in Figures 11 and 12, we have chosen $\rho_2 = 2$, $\beta_2 = .91$, and $c_2 = 1.67$, parameters which might describe a semiconsolidated rock basement such as is found in shallow water exploration. The downward frequency shift noted in earlier figures in connection with low shear velocity is the most striking feature of the dispersion.

Pressure and Velocity Distribution

We shall consider further the physical basis for the behavior of the group velocity curves just cited, after examining the distribution of the wave field in the liquid layer. The z-dependence of the pressure, for the trapped portion of the field, is given very nearly by $|\sinh \alpha_1 z|$, provided the remaining factors in the excitation function (eq. 5) do not vary strongly in the range of U that is of interest. This has been evaluated for representative values of U, for Cases 1, 2, 3, 5, and 7, and plotted in Figs. 14 through 18. The reference curve labeled "Pekeris" is the sinusoid which represents the pressure distribution at cutoff of the first mode for the original liquid/liquid problem.

The vertical velocity distribution, u_z, given by the z-derivative of the pressure, has been similarly plotted on the same figures. It will be apparent that the vertical velocity shows most clearly the departure from the reference shape.

We see that leakage into the bottom, which depressed the cutoff frequency, tends to modify the shape of the trapped wave, decreasing the phase difference between the surface and bottom motion. As long as the leakage is relatively small (Cases 1, 5, 7), we may consider the wave as a perturbation from the reference shape. This is not unexpected, since physical grounds have led us to classify the PL modes with the modes of the liquid/liquid case.

The situation becomes more complicated when the damping increases. Cases 2 and 3 show that leakage depresses so much of the waveform into the halfspace that the surface and bottom of the layer are nearly in phase. This, however, is the situation when a long-wavelength Rayleigh wave, for example, is propagated on a solid overlain by a thin liquid; the liquid merely moves in phase with the surface of the solid. We would want to classify these highly damped modes with some sort of surface wave motion in a solid.

Late-arriving Waves

As mentioned previously, the present problem involves late-arriving leaky modes of the type found by Rosenbaum for the liquid/liquid problem. The group velocity curves for these modes have the following two properties: (1) every Airy phase, whether of a normal mode or a leaky mode of the early-arriving type, is associated with a late-arriving branch which "connects" the stationary value of U with U = 0. (2) In the vicinity of U = 0, that is, for arbitrarily large time, the frequencies of the late-arriving modes degenerate to the set of frequencies $\omega = (n - \frac{1}{2})\pi$. This behavior is illustrated in Fig. 3, where three such branches have been computed, which all degenerate near U = 0 to the value $\omega = \frac{1}{2}\pi$. These results have relevance in the analysis of the late-arriving signal from an earthquake, transmitted along an oceanic path. It is a matter of observation that observed oceanic Rayleigh waves do not terminate sharply in a strong Airy phase, but gradually decay, with oscillations near the expected Airy phase frequency observed at very long times after the event. As is seen in Fig. 3, the three different late-arriving modes computed will not differ significantly in frequency for large times. In Fig. 19 we have computed the damping coefficients for these three waves; the least damped for any value of U being represented by the heavy line, which we may take as determining the predominant branch at any

given time. We wish merely to point out this explanation for the observed late-arriving waves; a definitive comparison of data with the theory is not attempted here.

Physically, the late-arriving waves correspond to plane waves multiply reflected in the layer at nearly vertical incidence. In contrast, the early-arriving waves (PL or shear) correspond to an angle of incidence nearly equal to an appropriate critical angle for refraction into the half-space. The high-frequency branch of a normal mode is the result of waves traveling at nearly grazing incidence in the layer.

Rayleigh wave observations for various paths reflect these differences. It is indeed seldom that the high frequency branch is observed, for either continental or oceanic paths. Instead, the Airy phase of the early-arriving (long wave) branch is occasionally followed in time by a weak train of waves at the Airy phase frequency. In view of the physical basis for these waves, it is not surprising that the branch due to grazing waves is destroyed by inhomogeneities or variations in crustal thickness, a mechanism which would not degrade the vertically bouncing waves as severely. A major structural boundary would also tend to destroy the high frequency branch and favor by comparison the late-arriving wave.

Other phenomena related to oceanic seismic wave propagation which are tied in with the leaking modes are briefly:

1. Since a leaking mode is coupled to a body wave, a simple application of reciprocity shows that earthquake body waves may excite a leaky surface wave train. Oliver has applied this to the computation of the long-period waveform associated with the body S phase, which excites a leaky PL mode of phase velocity equal to the local trace velocity of the body wave.

2. We may be concerned with the "complement" of a leaky mode. A leaky mode represents narrow-band energy temporarily stored by the surface portion of the waveguide. Its complement is merely the signal released from the surface and permitted to travel into the bottom as a body wave. The oscillatory portion of the P wave observed at ranges of 25 to 90 degrees (commonly a period of 18 to 28 seconds) is the complement of the late-arriving (vertically incident) mode excited by an earthquake at the base of the crust, propagated in the mantle along the same "ray" as the initial P-motion. Observed P oscillations of around 60 and 150 seconds are of the same type, but, since their wavelength is of the same order as the penetration depth of the P ray, the foregoing remarks become rather imprecise, and it will be necessary to construct a complete wave theory for these oscillations.

3. It is suggested that the late-arriving quasi-standing mode may play a role in the propagation of seismic noise in oceanic regions. Widespread surface pressure variations, whether barometric or due to standing water waves, will excite this mode at least as efficiently as they excite undamped Rayleigh waves. The noise may then leave the source region either by horizontal propagation in the layer or by means of the P waves leaking into the bottom. The former must be regarded as a short range mechanism, while the latter would carry the energy to appreciable distances as body waves. We merely mention these hypotheses, since further consideration will require appropriate experiments.

Conclusions

In the steady state, undamped normal modes are sufficient to describe seismic propagation in the earth's outer layers. When a transient source or a boundary is present, however, it is necessary that the leaking modes be understood in addition. Of particular interest in the transient case is the early-arriving PL wave, in which energy leaves the region of the surface waveguide in the form of body waves. For solids having the properties usually encountered in earth materials the PL wave is the analogue of the normal mode computed by Pekeris for the liquid/liquid

problem. The PL wave dispersion differs, however, from that of the Pekeris normal modes in that the existence of leakage into the solid apparently causes the frequency of the waves to be decreased somewhat. The attenuation factor for PL waves is quite sensitive to the Poisson constant of the underlying solid. Due to the limited ranges of propagation, the extraction of dispersion and attentuation from earthquake records presents considerable difficulty. When models with a high Poisson constant are considered, certain complications arise. It appears that the resulting highly damped wave may be thought of as a long period pseudo-surface wave, an interface wave intrinsic to the solid halfspace, which is in a sense the prograde elliptical dual of the familiar Rayleigh wave. The late-arriving leaky modes appear to be involved in several types of seismic signals, such as P-type body waves, late-arriving surface waves, and microseisms.

The importance of P-modes in shaping the first arrivals from large blasts cannot be too heavily emphasized. In the nuclear detection problem surface layering is responsible for the distortion of the P wave into an oscillatory signal. For P waves from blasts or near earthquakes the frequencies commonly observed may involve higher modes. Pertinent to this, computations are now in progress for models having a solid surface layer.

Exact computation of the dispersion for leaking modes

involves a simple generalization to complex variables of the technique employed in normal mode problems. One computes complex solutions, ω_n, of the period equation for complex k by iteration and looks for the complex loci of this solution along which $\frac{d\omega_n}{dk}$ is also real and positive. Roughly 5 to 10 times more computation time is needed than for the comparable normal mode solution.

Appendix

Definitions and formulae:

A = source amplitude

b = ρ_1/ρ_2

c = phase velocity = $\mathrm{Re}(\omega_n{}^c)/\mathrm{Re}(k_n{}^c)$

c_1 = compressional velocity in liquid layer

c_2 = compressional velocity in solid halfspace

D = source depth in layer

f = period function defined by eq. (2)

g = response function defined by eq. (2)

H = layer thickness

k = complex wave number

L_n = exponential time decay factor for the n^{th} mode

n = mode index

r = horizontal coordinate

r_o = "decay range" for damped modes = U/L_n

s = Laplace transform variable = $i\omega$

t = time

U = group velocity = $d\omega_n/dk$ when this quantity is pure real

u_z = vertical velocity

z = depth coordinate, increasing downward

The subscript n denotes evaluation at a root (n^{th} mode) of the equation $f(\omega_n, k) = 0$. The superscript c in addition denotes evaluation at a saddle point, where $d\omega_n/dk = r/t$.

$$f^* = f(\alpha_2, -\alpha_2'); \quad f^{**} = f(-\alpha_2, -\alpha_2'); \quad f^{***} = f(-\alpha_2, \alpha_2')$$

The subscript I, II, III, or IV, denotes taking the function on the particular Riemann surface defined by Table 1.

Appendix (continued)

$\alpha_1 = (k^2 + s^2)^{\frac{1}{2}}$

$\alpha_2 = (k^2 + \epsilon^2 s^2)^{\frac{1}{2}}$

$\alpha_2' = (k^2 + \gamma^2 s^2)^{\frac{1}{2}}$

β_2 = shear wave velocity in halfspace

$\gamma = c_1/c_2$

$\epsilon = c_1/\beta_2$

θ = decay time of source pulse

ρ_i = density of i^{th} layer

ω = complex frequency = -is

The formal solution in dimensionless variables is a consequence of applying the appropriate boundary conditions and specifying that the source be a point pressure pulse, exponentially damped in time.

$$(1)\quad P(r,z,t) = \frac{A}{\pi i}\int_{\lambda-i\infty}^{\lambda+i\infty} \frac{e^{st}}{s+\theta^{-1}}\, ds \int_0^{\infty} J_0(kr)k\,\frac{g}{f}\, dk$$

where f is the so-called period function and g the response function.

We shall deform the initial contour of integration (Fig. 20) in the s-plane, causing it to lie partly on the II and III Riemann surfaces of the integrand (see table 1). For convenience, auxiliary functions are defined, in order to remove part of the confusion of working with several Riemann sheets. If we wish to take the value of f on the second sheet, we write $f)_{II}$. f* is defined to be the function which is defined on the first sheet to be identical there to $f)_{II}$. Thus

$$f)_{II} = \left\{ bs^4\epsilon^4\alpha_2 \sinh\alpha_1 + \alpha_1 \cosh\alpha_1 [(2k^2+\epsilon^2 s^2)^2 - 4k^2\alpha_2\alpha_2'] \right\}_{II}$$

while

$$f^* = bs^4\epsilon^4\alpha_2 \sinh\alpha_1 + \alpha_1 \cosh\alpha_1 [(2k^2+\epsilon^2 s^2)^2 + 4k^2\alpha_2\alpha_2']$$

That is, $f)_{II} = f^*)_I$

In like fashion, we define $f^{**})_I = f)_{III}$

and $f^{***})_I = f)_{IV}$

Figure 20 shows the original Bromwich contour for evaluation of (1) in the s-plane. Branch points due to $\alpha_2 = 0$ and $\alpha_2' = 0$ are located at $s = \pm \frac{ik}{\gamma}$ and $s = \pm \frac{ik}{\epsilon}$. The familiar roots of the period equation produce poles of the integrand lying on the imaginary s axis between $s = ik$ and $s = ik/\epsilon$ (that would be the real ω axis). The branch cuts are chosen by requiring that Re $\alpha_2 = 0$ and Re $\alpha_2' = 0$ along the two cuts. This conventional choice, while not necessary to this problem, will be followed. The "top" or first Riemann sheet will then be identical with that encountered in the recent literature. We may then make use of theorems that have been proven regarding the disposition of the roots of the period equation.

Since all quantities under the integral sign are real when s is real, then they are complex conjugate at complex conjugate values of s. The positive and negative imaginary halves of the contour in fig. 20 are combined, and we let $\lambda \to 0$, except for indentations at the singularities on the imaginary axis. Then:

$$(A\text{-}1) \qquad P = \frac{2A}{\pi} \operatorname{Im} \int_0^{i\infty} \frac{e^{st}}{s+\theta^{-1}} \, ds \int_0^{\infty} J_0(kr) k \frac{g}{f} \, dk$$

The contour may now be deformed as shown in figure 21. The solution naturally decomposes into the four contributions from the various singularities in the second quadrant. $P = P_1 + P_R + P_{BP} + P_{BS}$. P_1 arises from the line integral along the negative real axis plus the pole contribution from

the source pole at $s = -\theta^{-1}$. The contribution from the infinite arc vanishes as $R \to \infty$. The normal mode poles yield residue contributions which we denote by P_R. P_{BP} and P_{BS} are the two branch line integrals.

Evaluation of P_1

$$(A\text{-}2) \qquad P_1 = \frac{2A}{\pi} \operatorname{Im} \int_0^{\infty} J_0(kr)k\,dk \int_0^{-\infty} \frac{e^{st}}{s+\theta^{-1}} \frac{g}{f}\, ds$$

Except at the indentation at $s = -\theta^{-1}$, the integrand is purely real, giving no contribution. The semicircular indentation is evaluated by residues:

$$(A\text{-}3) \qquad P_1 = 2A\, e^{-t/\theta} \int_0^{\infty} J_0(kr)\, k \left(\frac{g}{f}\right)_{s=-\theta^{-1}} dk$$

This expression, like all others encountered, can be shown to vanish prior to an appropriate arrival time. What is important is that it is a forced non-oscillatory response, and of no interest in the study of modal oscillatory solutions. There is often some ambiguity in taking the contribution from a semicircular arc at a pole; in this case, however, the expression adopted is the only possible correct one. This result would have been obtained if the infinite contour of fig. 20 were deformed into the left half-plane before reducing it to a semi-infinite contour. In that event the pole would contribute by virtue of the residue formula, without ambiguity. With this, we shall drop consideration of P_1.

Evaluation of P_R

P_R is the sum of residue contributions due to roots of $f = 0$ lying on the I sheet imaginary axis between $s = ik$ and $s = \frac{ik}{\epsilon}$. It has been shown that no other roots lie on the top sheet (this is, of course, for k real and > 0). For each mode there exists one root s_n which appears on the I sheet if $k_n \geq k_{n0}$, the cutoff value. For the lowest (Rayleigh) mode, $k_{00} = 0$. For all others (the shear modes) the cutoff is given by:

$$k_{n0} = \frac{(n - \frac{1}{2})\pi}{\beta_2\sqrt{1-\epsilon^2}} \tag{A-4}$$

Proceeding, we perform the residue evaluation:

$$P_R = 2\pi i \sum_n \mathrm{Res}(s_n) = \sum_n 4A\ \mathrm{Re} \int_0^\infty J_0(kr)k \frac{e^{s_n t}}{s_n + \theta^{-1}} F_1(s_n,k)dk \tag{A-5}$$

where:

$$F_1(s_n,k) = \frac{b\, s_n^4\, \epsilon^4\, \alpha_{2n} \sinh(\alpha_{1n} D)\sinh(\alpha_{1n} z)}{\alpha_{1n} \cosh \alpha_{1n} \frac{\partial}{\partial s}(f)_n} \tag{A-6}$$

Branch Line Integrals:

It will be necessary to rewrite the branch line integrals in terms of contours along just one side of the respective branch cuts:

$$P_{BS} = \frac{2A}{\pi} \mathrm{Im} \int_0^\infty J_0(Kr)K\,dk \left\{ \int_{i\infty}^{i\frac{k}{\epsilon}} \frac{e^{st}}{s+\theta^{-1}} \frac{g}{f} ds + \int_{\frac{ik}{\epsilon}}^{i\infty} \frac{e^{st}}{s+\theta^{-1}} \frac{g}{f} ds \right\} \tag{A-7}$$

For the first term in brackets, Im $\alpha_2' > 0$; for the second term, Im $\alpha_2' < 0$.

Combining, we get

$$(A\text{-}8)\quad P_{BS} = -\frac{2A}{\pi}\,\mathrm{Im}\int_0^{\infty} J_o(kr)k\,d\,k\int_{ik/\epsilon}^{i\infty}\frac{e^{st}}{s+\theta^{-1}}F_2(s,k)\,ds$$

where the contour runs along the right side of the cut, and:

$$(A\text{-}9)\quad F_2(s,k) = \frac{8\,bk^2s^4\epsilon^4\alpha_2^2\,\alpha_2'\sinh(\alpha_1 D)\sinh(\alpha_1 z)}{f\cdot f^*}$$

remembering, that using the f* notation implies Re $\alpha_i > 0$.

In like manner, the other branch line integral becomes:

$$(A\text{-}10)\quad P_{BP} = -\frac{2A}{\pi}\,\mathrm{Im}\int_0^{\infty} J_o(kr)k\,d\,k\int_{\frac{ik}{\gamma}}^{i\infty}\frac{e^{st}}{s+\theta^{-1}}F_3(s,k)\,ds$$

where:

$$(A\text{-}11)\quad F_3(s,k) = \frac{2(2k^2+\epsilon^2s^2)^2\,b\,\epsilon^4s^4\alpha_2\sinh(\alpha_1 D)\sinh(\alpha_1 z)}{f\cdot f^{***}}$$

Evaluation of P_{BS}

In the following we shall transform the contour integral A-8 in the complex plane, and will have occasion to break it up into several constituent parts. For clarity, a subscript notation is adopted which, it is hoped, will make it easier to follow the mathematics and suggest the origin of any given term. For example, P_{BS} is decomposed into the sum of two terms; these are denoted P_{BS1} and P_{BS2}. A flow chart is included at the end to summarize the roles of all the subscripted terms.

The contour for eq. A-8, running along the right side of the branch cut, is transformed as indicated in fig. 22. It is deformed into the second quadrant of the s-plane in such a way that it passes through the branch cut and onto the II Riemann sheet. All but a small slice of the second quadrant is enclosed in this manner; all poles of the integrand lying on the II sheet are excluded by small circular contours. The infinite arc contributes nothing, as usual. We then have two contributions to P_{BS}:

P_{BS1}: The line integral from $s = ik/\epsilon$ to $-\infty$.

P_{BS2}: Residue terms due to poles of the integrand lying on the II sheet.

$$(A\text{-}12)\quad P_{BS1} = -\frac{2A}{\pi}\,\mathrm{Im}\int_0^{\infty} J_o(kr)k\,dk\int_{\frac{ik}{\epsilon}}^{-\infty}\frac{e^{st}}{s+\theta^{-1}}\left\{F_2(s,k)\right\}_{II}\,ds$$

$$(A\text{-}13)\quad P_{BS2} = -4A\,\mathrm{Re}\sum_{n=0}^{\infty}\int_{S_{II}}' J_o(kr)k\,\frac{e^{s_n t}}{s_n+\theta^{-1}}\left\{F_2'(s_n,k)\right\}_{II}\,dk$$

where:

$$(A\text{-}14)\quad \left\{F_2'(s_n,k)\right\}_{II} = \frac{-8\,b\,k^2 s^4\,\epsilon^4\alpha_2^2\,\alpha_2'\,\sinh(\alpha_1 D)\sinh(\alpha_1 z)}{f_n\,\frac{\partial}{\partial s}(f^*)_n}$$

The zeros of f* are just the II sheet complex roots of the period equation. We note that f did not have any complex zeroes on the I sheet; thus P_{BS2} arises solely from zeros of f*.

We introduce further notation to simplify the analysis. Let S_{II} denote that portion of the real positive k axis whose root $s_n(k)$ lies in the second quadrant of the II sheet. S_{II} will in general differ for different n. The slightly smaller

set S'_{II} will denote that portion of the real positive k axis which maps into the sector which is enclosed by the dotted contour in fig. 22. We use this notation to represent the range of k for integration until we are able to examine the detailed behavior of the solution $s_n(k)$. S'_{II} is the range of k in eq. A-13.

A-13 may be rewritten by use of the following relations:

(A-15) $$f^* - f = 8\, k^2\, \alpha_1\, \alpha_2\, \alpha'_2 \cosh \alpha_1$$

Thus, when $f^* = 0$, $f_n = -8\, k^2\, \alpha_1\, \alpha_2\, \alpha'_2 \cosh \alpha_1$

and (A-16) $$\left\{F'_2(s_n,k)\right\}_{II} = \frac{b\, s^4\, \epsilon^4\, \alpha_2 \sinh(\alpha_1 D)\sinh(\alpha_1 z)}{\alpha_1 \cosh \alpha_1 \frac{\partial}{\partial s}(f^*)_n} = \left\{F_1(s_n,k)\right\}_{II}$$

hence: (A-17) $$P_{BS2} = -4A\ \mathrm{Re} \sum_{n=0}^{\infty} \int_{S'_{II}} J_o(kr)\, k\, \frac{e^{s_n t}}{s_n + \theta^{-1}} \left\{F_1(s_n,k)\right\}_{II} dk$$

This form, which resembles A-5 closely, is nearly appropriate for evaluating the modal contribution from this sheet. We take this up later.

Resuming consideration of A-12, we note that

$$\left\{F_2(s,k)\right\}_{II} = -F_2(s,k)\ .$$

The object of the following transformations is to obtain an expression which extends the range of integration of A-17 to the set S_{II} corresponding to all II sheet roots lying in the second quadrant of the s-plane. Topologically, this can easily be done by deforming the contour shown in Fig. 22

to circumscribe the entire quadrant. The line integrals remaining, however, are not easily handled, and an estimate of their contribution is difficult. It is therefore necessary to go the long route to accomplish our objective, and several contour deformations and changes of variable will be necessary. Hence, writing as a double integral we get:

$$(A\text{-}18)\quad P_{BS1} = \frac{2A}{\pi} \operatorname{Im} \int_0^{\infty} \int_{\frac{ik}{\epsilon}}^{-\infty} J_o(kr) k \frac{e^{st}}{s+\theta^{-1}} F_2(s,k)\, d\, s\, d\, k$$

q is now introduced as the variable of integration replacing s:

$$q = s - \frac{ik}{\epsilon} \quad ; \quad s = q + \frac{ik}{\epsilon} \quad ; \quad d\, s = d\, q$$

$$(A\text{-}19)\quad P_{BS1} = \frac{2A}{\pi} \operatorname{Im} \int_0^{-\infty} e^{qt} dq \int_0^{\infty} J_o(kr) \frac{k\, F_2(s,k) e^{ikt/\epsilon}}{q + \theta^{-1} + ik/\epsilon}\, dk$$

We now consider this as a contour integral in the complex k-plane (Fig. 23). A pole occurs at $k_p = i\,\epsilon\,(q+\theta^{-1})$. When $-\theta^{-1} < q \leq 0$, the pole lies on the positive imaginary axis. When $-\infty < q < -\theta^{-1}$, the pole lies on the negative imaginary axis. Branch points occur at $k = \pm \frac{1}{2} i\epsilon$ q and $k = \pm \frac{i\gamma\epsilon q}{\epsilon \pm \gamma}$. We may insert branch cuts running to infinity just to the left of the imaginary axis (to avoid the pole).

We now deform the contour of Fig. 23 into a loop enclosing the entire first or fourth quadrant of the k-plane. P_{BS1} now decomposes into three terms:

P_{BS11}: A line integral along an imaginary semi-axis.

P_{BS12}: Contribution from the indentation around the source pole located on the imaginary axis.

P_{BS13}: Modal contributions due to poles in the appropriate quadrant of the k-plane.

The condition that the integral along the infinite arc vanish determines the quadrant into which the contour in the k-plane is deformed. This is a long, but familiar story, which we will only summarize. We represent the Bessel function asymptotically as a sum of outward travelling and inward travelling waves. We shall not be concerned with the latter; a thorough study would double the length of this paper. In general, these inward travelling waves can contribute only non-realizable pulse terms and modal oscillations insignificant compared with those from the outward travelling waves. With respect to the latter, the integrand of A-19 vanishes exponentially in the upper half plane if $t > r\epsilon$ and in the lower half plane if $t < r\epsilon$. We deform the contour in Fig. 23 accordingly. This ensures convergence of the line integral P_{BS11}, as well as vanishing of the infinite arc contribution. To make the details of the contour transformations easier to follow, we shall replace the Bessel function by the Hankel function of the second kind, which

contributes the outward traveling wave solutions. The Hankel function of the first kind, which we have dropped, turns out to be merely excess baggage; this may be shown by a separate but parallel development such as appears here. The restriction of r and t to large positive values is crucial in bringing this about.

If $t > r\epsilon$, we deform the contour into the first quadrant of the k-plane. Then:

(A-20)

$$P_{BS12}=+2A\ \mathrm{Im}\int_{\dot{o}}^{-\theta^{-1}} e^{qt}H_o^{(2)}[i\epsilon(q+\theta^{-1})r]\,\epsilon(q+\theta^{-1})F_2(s,k_p)e^{-(q+\theta^{-1})t}dq$$

If $t < r\epsilon$ then the limits are changed to $-\theta^{-1}$ and $-\infty$. This term represents a non-oscillatory, forced response which we shall not consider further. Proceeding: if $k = i\xi$

$$(A\text{-}21)\quad P_{BS11}=\frac{2A}{\pi}\ \mathrm{Im}\int_o^{-\infty} e^{qt}\,dq\int_o^{\infty} H_o^{(2)}(i\xi r)\,\frac{i\xi\,F_2(s,k)}{q-\xi/\epsilon+\theta^{-1}}\,e^{-\xi t/\epsilon}\,i\,d\xi$$

In the case considered by Rosenbaum, this integral vanished by virtue of the integrand being purely real. We are not so endowed, and must estimate the form and magnitude of the term. The Hankel function is replaced by its far field asymptotic representation; we then estimate the integral by expanding the functions under the integral sign about $q = 0$ and $\xi = 0$. Because of the several factors in F_2 which may be small near this point, we know that, to zero order, the integral will be small; it is therefore necessary to take at least first

order terms in the expansion. The result is an estimate, asymptotic as $r \to \infty$ and $t \to \infty$, of the integral (A-21):

$$P_{BS11} \sim \frac{r^{-1/2}\, t^{-3/2}}{\left| r - t/\epsilon \right|^{8}} \tag{A-22}$$

This expression vanishes strongly except near the arrival time of a pulse traveling in the solid at the shear wave velocity. To the first order of approximation it is a mathematical singularity at the arrival time. Equally of note is the dependence on $r^{-1/2}$ and $t^{-3/2}$, which, for r and t of the same order of magnitude yields a decay of the pulse with distance like r^{-2}. This is the same dependence predicted in the case of a refracted arrival propagating along the interface between two semi-infinite media. The existence of a disturbance prior to the arrival time, suggests that the source pulse has been distorted in transmission, such as occurs when a plane pulse is reflected by a plane discontinuity at greater than the critical angle. We are not in a position to detail the form of the pulse, nor is this sufficiently relevant to the study of the modal oscillations to pursue further.

Evaluation of the modal term: P_{BS13}

When $t > r\epsilon$ we take residues in the k-plane from roots of the period equation lying in the first quadrant(starting with eq. A-19). Thus, in effect, the range of integration in q is now reduced to that set S_q of negative real q whose

image, by virtue of the period equation, lies in the first quadrant (Fig. 24). If $t < r\epsilon$, the same residue formula will obtain, but the q integration will now be over the complementary set S_q' whose map lies in the fourth quadrant. Also, the sign of the result will differ, since the sense of a pole contour in the fourth quadrant differs from that of one in the first quadrant. Since either f or f* may yield poles, we write two terms:

(A-23)

$$P_{BS13} = 4A \text{ Re} \left[\sum_{n=0}^{\infty} \int_{S_{q(II)}} e^{qt} H_o^{(2)}(k_n r) \frac{k_n F_2''(s,k_n)}{q+\theta^{-1}+\frac{ik_n}{\epsilon}} e^{\frac{ik_n t}{\epsilon}} dq \right.$$

$$\left. + \sum_{n=0}^{\infty} \int_{S_{q(I)}} e^{qt} H_o^{(2)}(k_n r) \frac{k_n F_2'''(s,k_n)}{q+\theta^{-1}+\frac{ik_n}{\epsilon}} e^{\frac{ik_n t}{\epsilon}} dq \right] = P_{BS131} + P_{BS132}$$

where: $$F_2'' = \frac{b\, k^2 s^4 \epsilon^4 \alpha_2^2 \alpha_2' \sinh \alpha_1 D \sinh \alpha_1 z}{H f_n \left(\frac{\partial f_n^*}{\partial k} \right)_n}$$

and $$F_2''' = \frac{b\, k^2 s^4 \epsilon^4 \alpha_2^2 \alpha_2' \sinh \alpha_1 D \sinh \alpha_1 z}{H f_n^* \left(\frac{\partial f_n}{\partial k} \right)_n}$$

P_{BS131} is due to roots of f* = 0; P_{BS132} is due to roots of f = 0.

For fixed n, the map of the negative real q axis by virtue of the period equation is shown in Fig. 24. One locus is due to vanishing f, the other due to vanishing f*. When q = 0, the two roots coincide, and lie on the real k axis. As q decreases, one moves into the first quadrant, due to f* = 0, and the other moves into the fourth quadrant, due to f = 0. Both eventually end up in the fourth quadrant as shown. For $t > r\epsilon$, then, A-23 becomes:

$$(A\text{-}24)\quad P_{BS131} = 4A\ \mathrm{Re} \sum_{n=0}^{\infty} \int_{S_q} e^{qt} H_o^{(2)}(k_n r)\, \frac{F_2''(s,k_n)}{q+\theta^{-1}+\frac{ik_n}{\epsilon}}\, e^{ik_n t/\epsilon}\, dq$$

with the zeros of f not contributing anything, and P_{BS132} in A-23 vanishing. The integral over S_q is equivalent to an integral over a certain range in the s-plane (Fig. 25). This is just the segment A'-B' in the s-plane. We shall now make a change of variable from q to k_n, which we call merely k. The integral over S_q is now a contour integral over the arc A-B in Fig. 24. We may deform this contour into the line segment A-B along the real k axis. From the properties of the conformal mapping $s_n = s_n(k)$, it is evident that the image of this segment A-B will be an <u>arc</u> A'-B' in the s-plane. In short, when A-24 is written as an integral along part of the real k axis, with the integrand a function of $s_n(k)$, A-B is the part of the real axis which maps into the strip Re $s < 0$, $\frac{ik}{\epsilon} \geq$ Im $s \geq 0$. Following the notation of eq. A-17, the k integration is over the set $S_{II} - S_{II}'$.

When the appropriate change of variable is made, A-24 becomes

$$(A\text{-}25)\quad P_{BS13} = -4A\ \mathrm{Re} \sum_{n=0}^{\infty} \int_{S_{II}-S_{II}'} H_o^{(2)}(k_n)\, k\, \frac{e^{s_n t}}{s_n+\theta^{-1}} \left\{F_1(s_n,k)\right\}_{II} dk$$

Since we are interested in the outward travelling waves, we may rewrite A-17 using the Hankel function in place of the Bessel function. Thus, combining A-25 and A-17, we get finally:

$$(A\text{-}26)\quad P_{BS2}+P_{BS13} = -4A\ \mathrm{Im} \sum_{n=0}^{\infty} \int_{S_{II}} H_o^{(2)}(kr)\, k\, \frac{e^{s_n t}}{s_n+\theta^{-1}} \left\{F_1(s_n,k)\right\}_{II} dk \qquad t > r\epsilon$$

When $t < r\epsilon$, it is necessary that the contour in the k-plane be transformed into the fourth quadrant. Referring to Fig. 24, we see that the residue contribution from f* is effective over the set complementary to S_q. This we have shown to be equal to S_{II}'. But, as noted previously, the sense of the contour of integration in the fourth quadrant is negative, and the sign of the result differs from that of the pole contributions from the first quadrant. Thus:

$$(A\text{-}27)\quad P_{BS13} = 4A\ \mathrm{Re} \sum_{n=0}^{\infty} \int_{S_{II}'} H_o^{(2)}(kr)\, \frac{k\, e^{s_n t}}{s_n+\theta^{-1}} \left\{F_1(s_n,k)\right\}_{II} dk$$

$$-4A\ \mathrm{Re} \sum_{n=0}^{\infty} \int_{S_I} H_o^{(2)}(kr)\, \frac{k\, e^{s_n t}}{s_n+\theta^{-1}} \left\{F_1(s_n,k)\right\} dk = P_{BS131} + P_{BS132}$$

The first term is due to vanishing of f* as discussed above. Now A-17 as modified is identical with the first term of A-27, except for sign; thus the important result: when $t < r\epsilon$ the complex modes due to roots of the period equation on the II Riemann sheet cancel out and do not contribute to the propagating wave.

The second term of A-27 is due to the roots of the period equation on the I Riemann sheet, the normal mode poles. But here, again, the sign differs from the sign obtained in eq. A-5, with the result that when $t < r\epsilon$, the normal mode poles on the first sheet do not contribute to the propagating wave. This is a familiar result obtained in studies of the real roots of the period equation. It now is shown to be true on topological grounds.

In summary, the first sheet modal contribution is given by eq. A-5; the second sheet modal contribution is given by eq. A-26. When $t < r\epsilon$ both contributions vanish, by cancellation with the two terms in eq. (A-27).

Evaluation of P_{BP}

This term, given by eq. A-10, will be treated in a manner quite analogous to the above detail concerning P_{BS}.

We begin by deforming the s-plane contour into the second quadrant by rotating it 90° counterclockwise. It passes through both branch cuts, effecting changes of sign

in both α_2 and α_2' in the various expressions. It consists of two terms:

P_{BP1}: A line integral from $s = \frac{ik}{r}$ to $s = -\infty$ lying on the III Riemann sheet.

P_{BP2}: Contributions due to poles of the integrand on the III sheet, lying on the sector of the second quadrant bounded by the positive imaginary axis and the contour P_{BP1}.

Eq. A-10 must be altered somewhat to indicate that we are on the III sheet. Since $(f)_{III} = f^{**}$, and $(f^{***})_{III} = f^{*}$, the response term, eq. A-11 must be modified:

(A-28)

$$[F_3(s,k)]_{III} = \frac{-2(2k^2+\epsilon^2 s^2)^2 b\, \epsilon^4 s^4 \alpha_2 \sinh(\alpha_1 D)\sinh(\alpha_1 z)}{f^{*}\, f^{**}} = -F_4(s,k)$$

Then, of course:

$$(A\text{-}29)\quad P_{BP1} = \frac{2A}{\pi}\,\mathrm{Im}\int_0^{\infty} J_0(kr)\, k\, d\, k \int_{\frac{ik}{r}}^{-\infty} \frac{e^{st}}{s+\theta^{-1}}\, F_4(s,k)\, ds$$

and

$$(A\text{-}30)\quad P_{BP2} = 8A\sum_{n=0}^{\infty} Re\left[\int_{S'_{III}} F(s_n k)\frac{e^{s_n t}}{s_n+\theta^{-1}} + \int_{S''_{II}} F(s_n k)\frac{e^{s_n t}}{s_n+\theta^{-1}}\right] k J_0(kr)$$

where S'_{III} is the set of all Re $k \geq 0$, such that $s_n(k)$, by virtue of $f^{**} = 0$, lies in the region Re $s_n < 0$; Im $s_n > k/r$.

S_{II}'' is the similarly defined set with respect to roots of $f^* = 0$. The response functions are given by:

$$(A\text{-}31) \qquad F_{61} = \frac{2(2k^2+\epsilon^2 s^2)^2 b\, \epsilon^4 s^4 \alpha_2 \sinh(\alpha_1 D)\sinh(\alpha_1 z)}{f^*\left(\frac{\partial}{\partial s} f^{**}\right)_n}$$

$$F_{62} = \frac{2(2k^2+\epsilon^2 s^2)^2 b\, \epsilon^4 s^4 \alpha_2 \sinh(\alpha_1 D)\sinh(\alpha_1 z)}{f^{***}\left(\frac{\partial}{\partial s} f^{*}\right)_n}$$

Noting that: $f^* + f^{**} = \alpha_1(2k^2+\epsilon^2 s^2)^2 \cosh \alpha_1$

F_{61} becomes:

$$F_{61} = \frac{b\, \epsilon^4 s^4 \alpha_2 \sinh(\alpha_1 D)\sinh(\alpha_1 z)}{\alpha_1 \cosh \alpha_1 \left(\frac{\partial}{\partial s} f^{**}\right)_n} = -[F_1(s_n,k)]_{III}$$

where the minus sign comes from the change in sign of α_2 when we evaluate it on the III sheet. Similarly, F_{62} becomes: $F_{62} = [F_1(s,k)]_{II}$. The modal term P_{BP2} decomposes into two contributions:

$$(A\text{-}32) \qquad P_{BP21} = 4A \sum \mathrm{Re} \int_{S_{III}'} J_o(kr) k \frac{e^{s_n t}}{s_n + \theta^{-1}} [F_1(s_n,k)]_{III}\, dk$$

$$(A\text{-}33) \qquad P_{BP22} = 4A \sum \mathrm{Re} \int_{S_{II}''} J_o(kr) k \frac{e^{s_n t}}{s_n + \theta^{-1}} [F_1(s_n,k)]_{II}\, dk$$

By operating on the line integral P_{BP1}, we will be able to extend the range of integration of these modal integrals.

As in evaluating eq. A-12, a substitution is in order:

$$q = s - \frac{ik}{\gamma}, \qquad s = q + \frac{ik}{\gamma}, \qquad ds = dq .$$

Consequently:

$$(A\text{-}34) \quad P_{BP1} = \frac{2A}{\pi} \operatorname{Im} \int_0^{-\infty} e^{qt}\, dq \int_0^{\infty} J_o(kr)\, k\, \frac{F_4(s,k)\, e^{\frac{ikt}{r}}}{q+\theta^{-1}+ i\, k/\gamma}\, dk$$

Singularities in the k-plane include a source pole at $k_p = i\gamma(\theta^{-1}+q)$ and branch points along the imaginary axis, which we connect to infinity by cuts along the imaginary axes. The contour in the k-plane is now deformed into the 1st or 4th quadrant, depending on the values of r and t. Considering only the outward travelling wave component, the integral along the infinite quarter-circle vanishes in the first quadrant if $t > r\gamma$; it vanishes in the fourth quadrant if $t < r\gamma$.

P_{BP1} now consists of three terms: P_{BP11}, a line integral along an imaginary semi-axis; P_{BP12}, a contribution from the indentation at the pole located at $k_p = i\gamma(\theta^{-1}+q)$; and P_{BP13}, due to modal contributions from poles of the integrand crossed in deforming the contour. The second of these we shall not consider further; it is a forced pulse term analogous to that obtained in eq. A-20.

If $t > r\gamma$, the contour is deformed into the first quadrant of the k-plane, and we write P_{BP11} from eq. A-34, making the substitution $k = i\xi$. :

(A-35)

$$P_{BP11} = -\frac{4A}{\pi} \operatorname{Im} \int_0^{-\infty} e^{qt} dq \int_0^{\infty} J_0(i\xi r) \frac{\xi F_4(s, i\xi)\, e^{-\xi t/\gamma}}{q + \theta^{-1} - \xi/\gamma} \, d\xi$$

As before, we agree to consider only the outward travelling wave, and replace the Bessel function by the Hankel function of the second kind. The integrand of A-35 is now expanded about the points $q = 0$ and $\xi = 0$, and an asymptotic formula is obtained, valid for large r and large t.:

(A-36)

$$P_{BP11} \sim \frac{r^{-1/2}\, t^{-3/2}}{\left| r - t/\gamma \right|^{8}}$$

When $t < r\gamma$ the same expression occurs, hence the absolute value sign. This term represents a blunt pulse peaking at $t = r\gamma$, with a singularity there, and a $1/r^2$ dependence on range. As the purpose of this paper is to investigate the oscillatory response of the system, we end consideration of eq. A-36.

The modal contribution P_{BP13} decomposes into two terms: P_{BP131}, due to roots of $f^{**} = 0$ and the other, P_{BP132}, due to roots of $f^{*} = 0$. When the modal term P_{BS13} was considered, we obtained pole contributions for $r < t/\epsilon$ only from f^{*} vanishing; the other factor in the denominator, f, did not contribute. Detailed consideration of the two terms; P_{BP131} and P_{BP132}, along the same lines as the analysis previously carried out on P_{BS13} yields analogous results. In

short, P_{BP131} is a modal expression with the same form as P_{BP21} (eq. A-32), but whose range of integration complements that of the earlier results. The two expressions then combine to give the following result:

(A-37)

$$P_{BP131} + P_{BP21} = -4A \sum \mathrm{Re} \int_{S_{III}} H_o^{(2)}(kr)k \frac{e^{s_n t}}{s_n + \theta^{-1}} \left\{ F_1(s_n, k) \right\}_{III} dk$$

where S_{III} is the set of all real positive k whose image, by virtue of f** = 0, lies in the second quadrant of the s-plane. When $t < r\gamma$, the two expressions cancel, rather than complementing each other, and their sum contributes nothing.

P_{BP132} behaves as follows: when $t > r\gamma$ P_{BP132} and P_{BP22} (eq. A-33) add to give a modal contribution integrated over the entire set S_{II}. The resultant expression, however, is positive, while the identical integral appears in eq. A-26 with a negative sign. Thus

(A-38) $P_{BP132} + P_{BP22} + P_{BS2} + P_{BS13} =$

$$= 4A \sum_n \mathrm{Re} \int_{II} H_o^{(2)}(kr)k \frac{e^{s_n t}}{s_n + \theta^{-1}} \left\{ F_i(s_n, k) \right\}_{II} dk \qquad [r\epsilon > t > r\gamma]$$

$$= 0 \qquad [t > r\epsilon > r\gamma]$$

When $t < r\gamma$, P_{BP132} and P_{BP22} cancel, and their sum does not contribute.

We now summarize the oscillatory contributions to the long range, long time pressure signal: the first sheet contribution, eq. A-5, is due to the conventional undamped normal modes, namely the Rayleigh wave and the shear modes. It vanishes prior to $t = r\epsilon$. Late-arriving damped wave trains associated with the normal modes are obtained (it turns out) from this term. The second sheet contribution, eq. A-38, vanishes except in the interval $r\epsilon > t > r\gamma$. When the waveguide, as considered here in detail, is a liquid layer overlying a solid halfspace, S_{II} can be shown to vanish. It may not vanish, however, for multiply layered models, and is in fact significant in the degenerate case of a free solid halfspace. In generalizing to layered structures of greater complexity, it may turn out that the second sheet contributions are significant. The Third sheet contribution, eq. A-37, will, we shall find, give rise to the damped modes coupled to the P-wave velocity in the halfspace and their late-arriving quasi-resonant wave trains.

Our object is now to evaluate the remaining integral in the modal solutions by a saddle point method. At points where $\frac{d\omega_n}{dk}$ = real, this derivative may be placed equal to the group velocity $U \equiv \frac{r}{t}$ of propagating waves whose dispersion and attenuation are functions of ω and k at this saddle point. Eq. 5 is the result obtained by Rosenbaum, valid away from stationary points of the group velocity. It is important for the success of the recipe, that we be

able to continuously deform the initial contour into a position so that it passes through the saddle point on a path of steepest descent. The conditions which determine whether this is possible for a given saddle point are not at all obvious in general, due to the extremely multivalued nature of the mapping of the k-plane into the s-plane (ω plane) induced by the period equation. We have discussed this problem in the main text, with the point of view that physical considerations may provide enough confirmatory information to establish the reality of any computed dispersion curves.

Summary of Modal Terms: P_R, P_{BS2}, P_{BS131}, P_{BS132}, P_{BP21}, P_{BP22}, P_{BP131}, P_{BP132}.

1. $t < r/c_2$:

$$P_{BS2} + P_{BS131} = 0$$

$$P_{BS132} + P_R = 0$$

$$P_{BP132} + P_{BP22} = 0$$

$$P_{BP131} + P_{BP21} = 0$$

2. $\frac{r}{c_2} < t < \frac{r}{\beta_2}$

$$P_{BS132} + P_R = 0$$

$$P_{BP131} + P_{BP21} = \text{III sheet solution (A-37)}$$

$$^{*}\ P_{BP132} + P_{BP22} + P_{BS2} + P_{BS131} = \text{II sheet solution (A-38)}$$

3. $t > \frac{r}{\beta_2}$

$$P_{BP131} + P_{BP21} = \text{III sheet solution (A-37)}$$

$$P_{BS132} = 0$$

$$P_{BP132} + P_{BP22} + P_{BS2} + P_{BS131} = 0$$

$$P_R = \text{I sheet (normal mode) solution (A-5)}$$

* S_{II} appears to vanish for the liquid/solid problem. Here, then, this term = 0 also. The early-arriving pseudo-wave in the Lamb problem may be treated by the method of this paper, and is due to this II sheet contribution.

Flow Chart

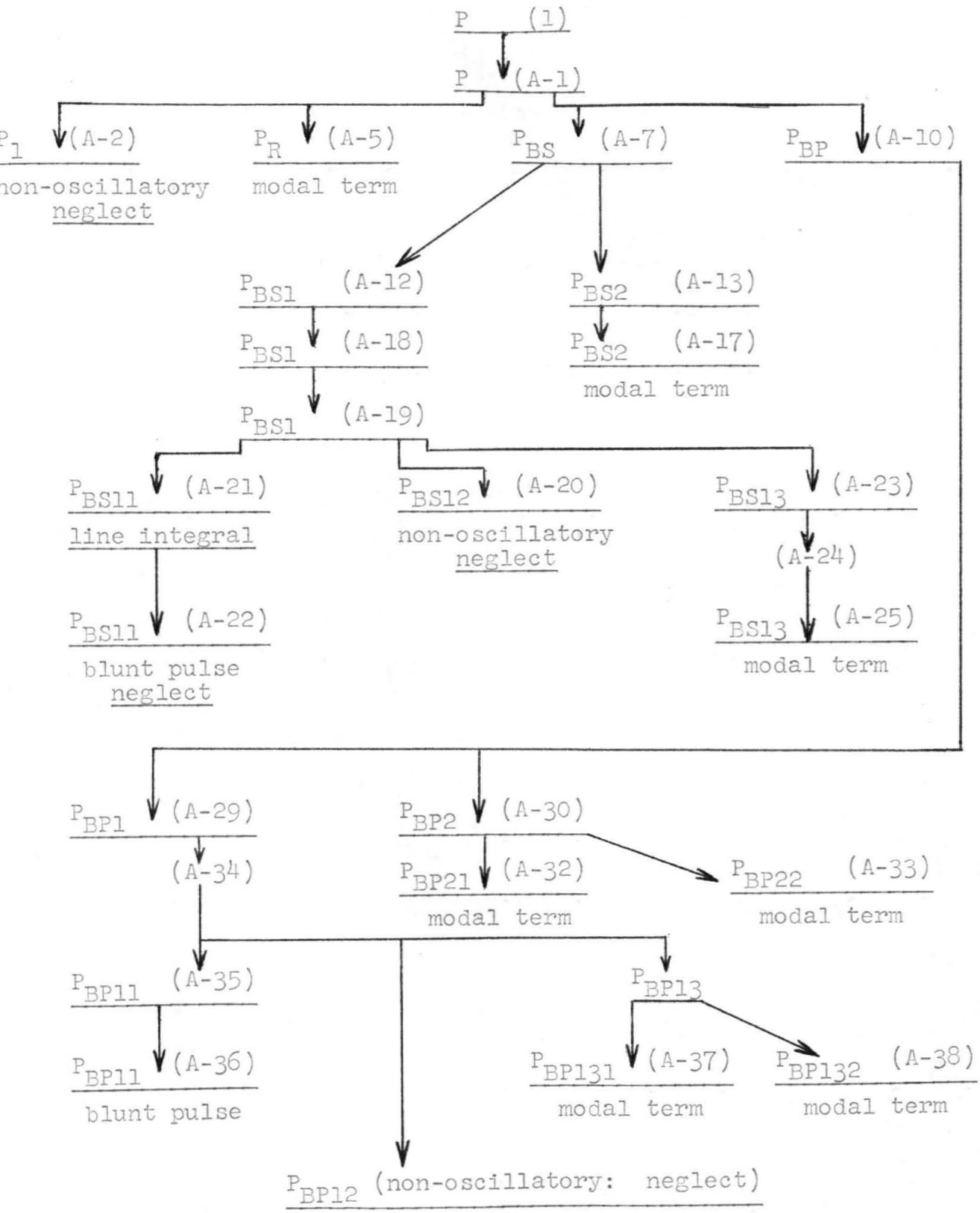
P (1)
P (A-1)
P1 (A-2)
non-oscillatory
neglect
PR (A-5)
modal term
PBS (A-7)
PBP (A-10)
PBS1 (A-12)
PBS2 (A-13)
PBS1 (A-18)
PBS2 (A-17)
modal term
PBS1 (A-19)
PBS11 (A-21)
line integral
PBS12 (A-20)
non-oscillatory
neglect
PBS13 (A-23)
(A-24)
PBS11 (A-22)
blunt pulse
neglect
PBS13 (A-25)
modal term
PBP1 (A-29)
PBP2 (A-30)
(A-34)
PBP21 (A-32)
modal term
PBP22 (A-33)
modal term
PBP11 (A-35)
PBP13
PBP11 (A-36)
blunt pulse
PBP131 (A-37)
modal term
PBP132 (A-38)
modal term
PBP12 (non-oscillatory: neglect)

Acknowledgements

The author wishes to thank Dr. Frank Press for his advice and encouragement throughout this work.

This research was supported in part by Contract No. AF-49 (638) 910 of the Air Force Technical Applications Center as part of the Advanced Research Projects Agency project VELA.

The author is a National Science Foundation predoctoral fellow.

References

Ewing, M., W. S. Jardetzky, and F. Press, Elastic Waves in Layered Media, McGraw-Hill, New York, Ch. 4, 1957.

Jardetzky, W. S., Period equation for an n-layered halfspace and some related questions, Lamont Geol. Obs. Tech. Report 29, 1953.

Oliver, J., and M. Major, Leaking modes and the PL phase, Bull. Seism. Soc. Am., 50, 165-180, 1960.

Pekeris, C. L., Theory of propagation of explosive sound in shallow water, Geol. Soc. Am. Mem. 27, October 15, 1948.

Rosenbaum, J. H., The long-time response of a layered elastic medium to explosive sound, J. Geophys. Research, 65, 1577-1614, 1960.

List of Captions

Fig. 1. Typical behavior of phase and group velocity for a single-layered acoustic waveguide (after Pekeris). $c_2/c_1 = 1.5$

Fig. 2a. Model consisting of a liquid layer overlying a solid halfspace, with typical values for an oceanic crust.

Fig. 2b. Reflection coefficient for P waves incident in water against a solid.

Fig. 3. Phase and Group velocity of first three PL modes: Case 1. Also included are three normal modes and their associated late-arriving leaky modes.

Fig. 4. Exponential Decay constant of first three PL modes: Case 1. Oblique grid represents r_o, the range for e^{-1} decay, in multiples of H.

Fig. 5. Phase and Group velocity of first PL mode: Cases 1, 4, and 6.

Fig. 6. Exponential Decay constant of first PL mode: Cases 1, 4, and 6. Decay range, r_o, in multiples of H.

Fig. 7. Phase and Group velocity of first PL mode: Cases 2, 5, and 6.

Fig. 8. Exponential Decay constant of first PL mode: Cases 2, 5, and 6. Decay range, r_o, in multiples of H.

Fig. 9. Phase and Group velocity of first PL mode: Cases 1 and 7.

Fig. 10. Exponential Decay constant of first PL mode: Cases 1 and 7. Decay range, r_o, in multiples of H.

Figs. 11 & 12. Case 3: Phase and Group velocity of first PL mode. Exponential Decay constant and Decay range.

Fig. 13. Group velocity of first PL mode for two oceanic models represented by Cases 1 and 7. Data by Oliver and Major.

Fig. 14. Pressure and vertical velocity dependence on depth for three values of U/c_1. Case 1.

Fig. 15. Pressure and vertical velocity dependence on depth for three values of U/c_1. Case 7.

Fig. 16. Pressure and vertical velocity dependence on depth for three values of U/c_1. Case 2.

Fig. 17. Pressure and vertical velocity dependence on depth for two values of U/c_1. Case 5.

Fig. 18. Pressure and vertical velocity dependence on depth for three values of U/c_1. Case 3.

Fig. 19. Exponential Decay constant for the first mode late-arriving waves. Case 1.

Fig. 20. Initial Bromwich inversion contour in the s-plane. Branch cuts and first sheet poles.

Fig. 21. Deformation of contour into second quadrant of s-plane.

Fig. 22. Deformation of branch line contour for P_{BS} into second quadrant and onto the II sheet (dashed line).

Fig. 23. k-plane contour for P_{BS1}. Branch cuts and source pole shown.

Fig. 24. Typical mapping of the negative real q axis onto the k-plane induced by solution of the period equation.

Fig. 25. Image of k-plane (Fig. 24) in s-plane obtained by changing variable from k_n to s.

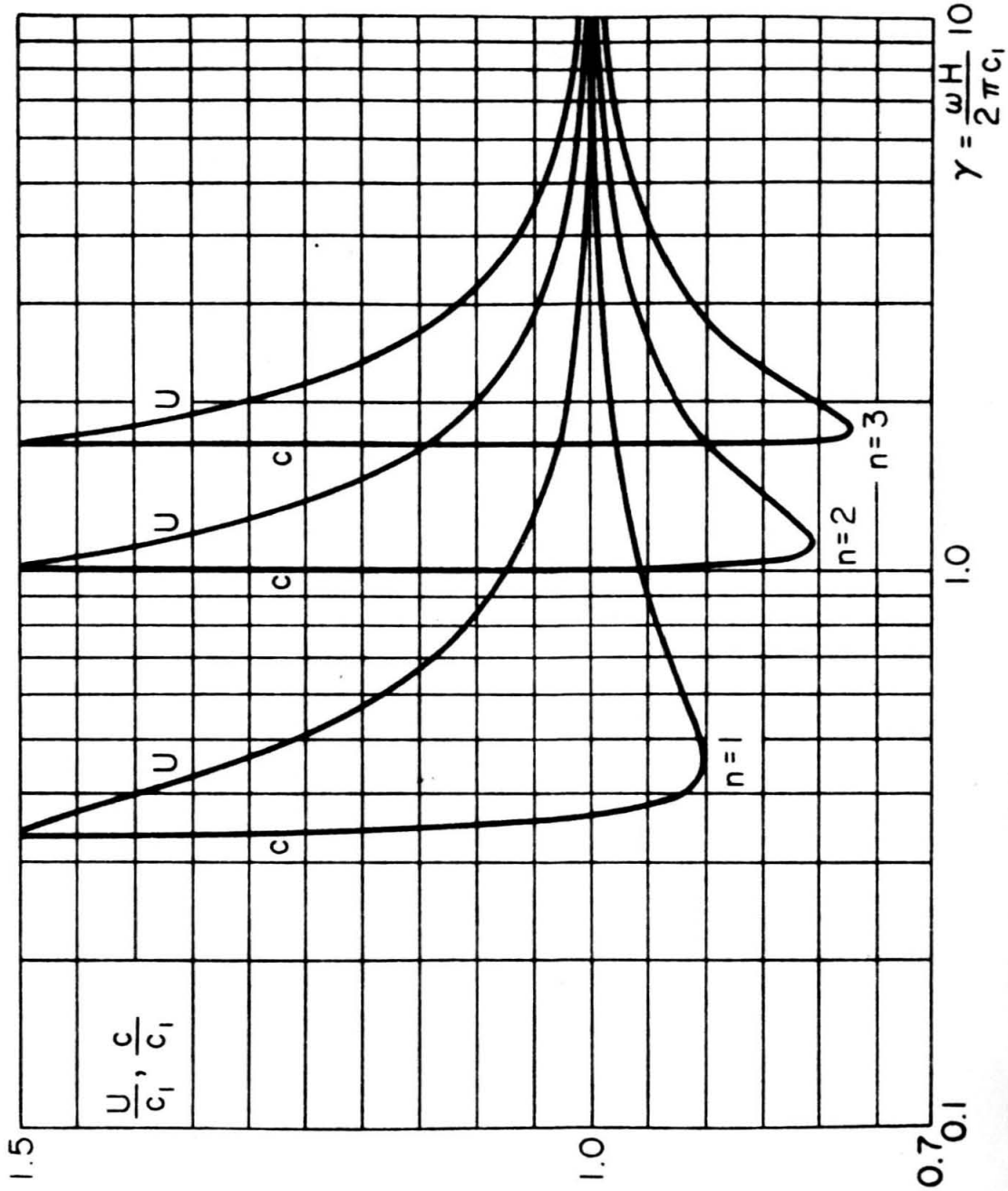
1.5
1.0
0.7
0.1
1.0
10
$\frac{U}{c_1}, \frac{c}{c_1}$
$\gamma = \frac{\omega H}{2\pi c_1}$
U
c
n=1
n=2
n=3

Fig. 1

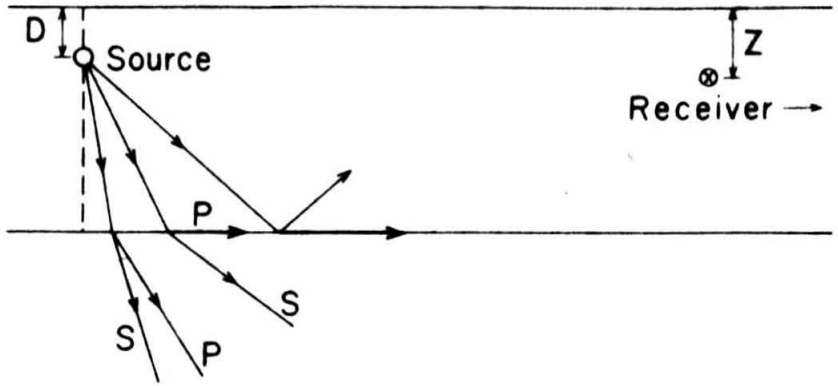

LIQUID: $c_1 = 1.52$ km/sec
$\rho = 1.0$
$H = 5.0$ km

SOLID: $c_2 = 7.88$ km/sec
$\beta_2 = 4.56$ km/sec
$\rho = 3.0$

Fig. 2a

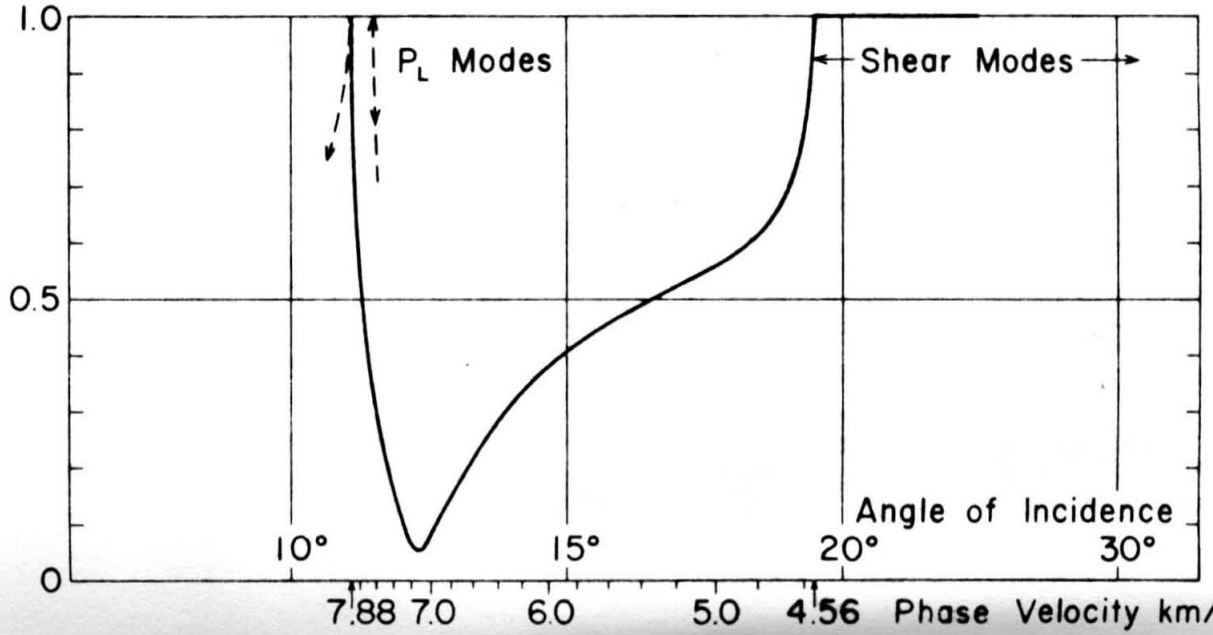

Fig. 2b

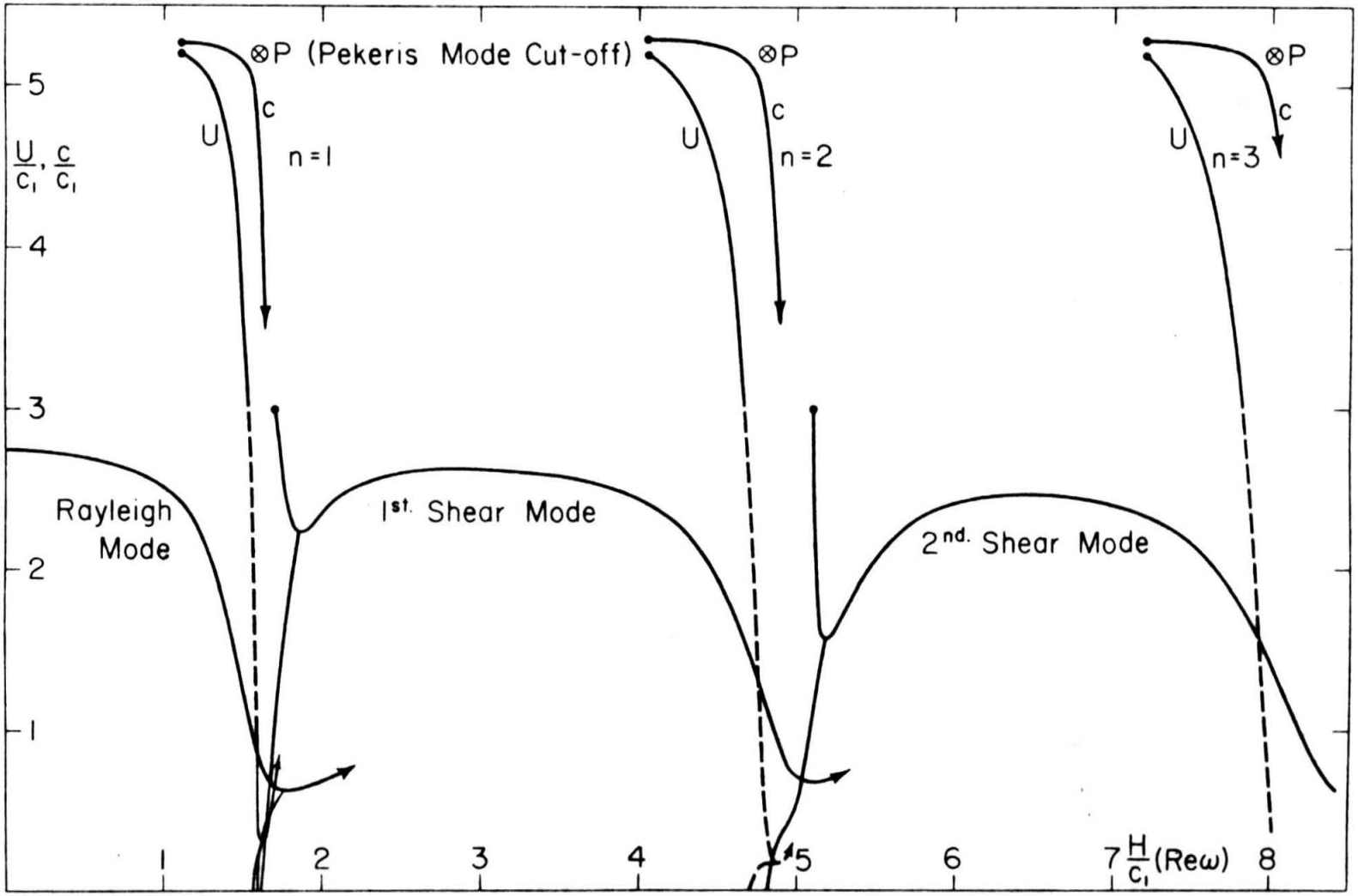
⊗P (Pekeris Mode Cut-off)
⊗P
⊗P
c
c
c
U
U
U
n=1
n=2
n=3
$\frac{U}{c_1}, \frac{c}{c_1}$
5
4
3
2
1
Rayleigh Mode
1st. Shear Mode
2nd. Shear Mode
1
2
3
4
5
6
7
8
$\frac{H}{c_1}(Re\omega)$

Fig. 3

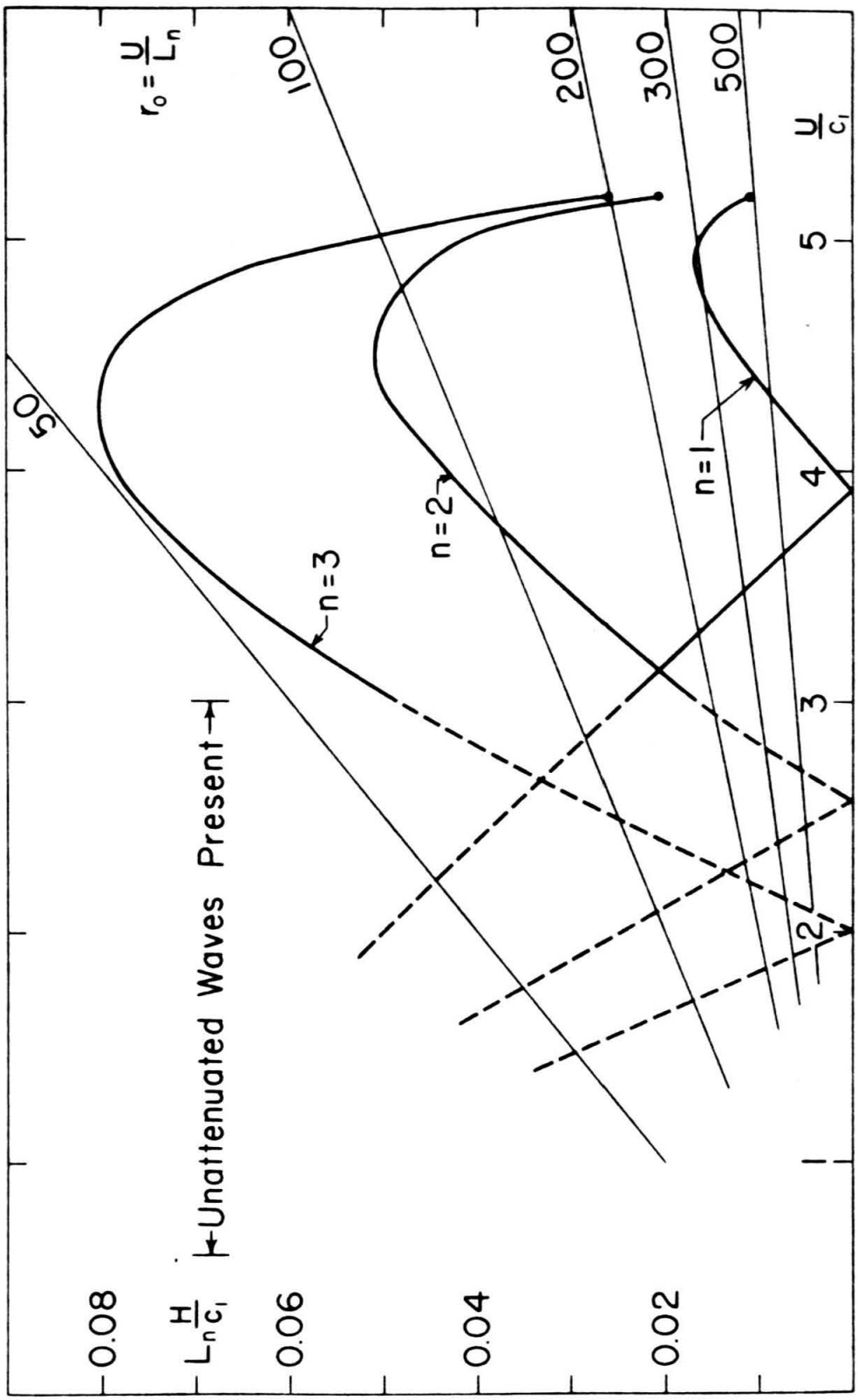
$r_o = \frac{U}{L_n}$
50
100
200
300
500
$\frac{U}{c_1}$
5
4
3
2
n=1
n=2
n=3
Unattenuated Waves Present
$L_n \frac{H}{c_1}$
0.08
0.06
0.04
0.02

Fig. 4

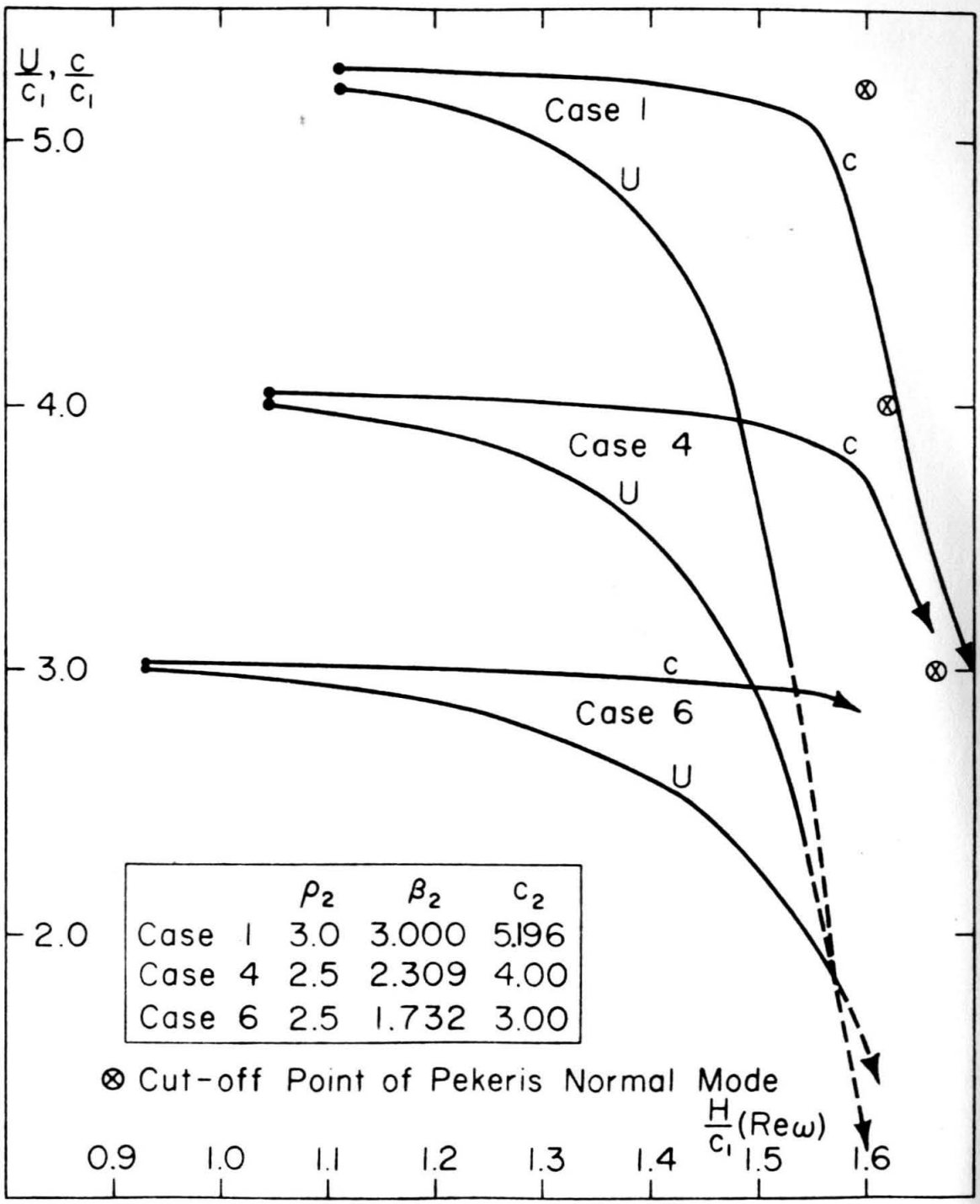

	ρ_2	β_2	c_2
Case 1	3.0	3.000	5.196
Case 4	2.5	2.309	4.00
Case 6	2.5	1.732	3.00

Fig. 5

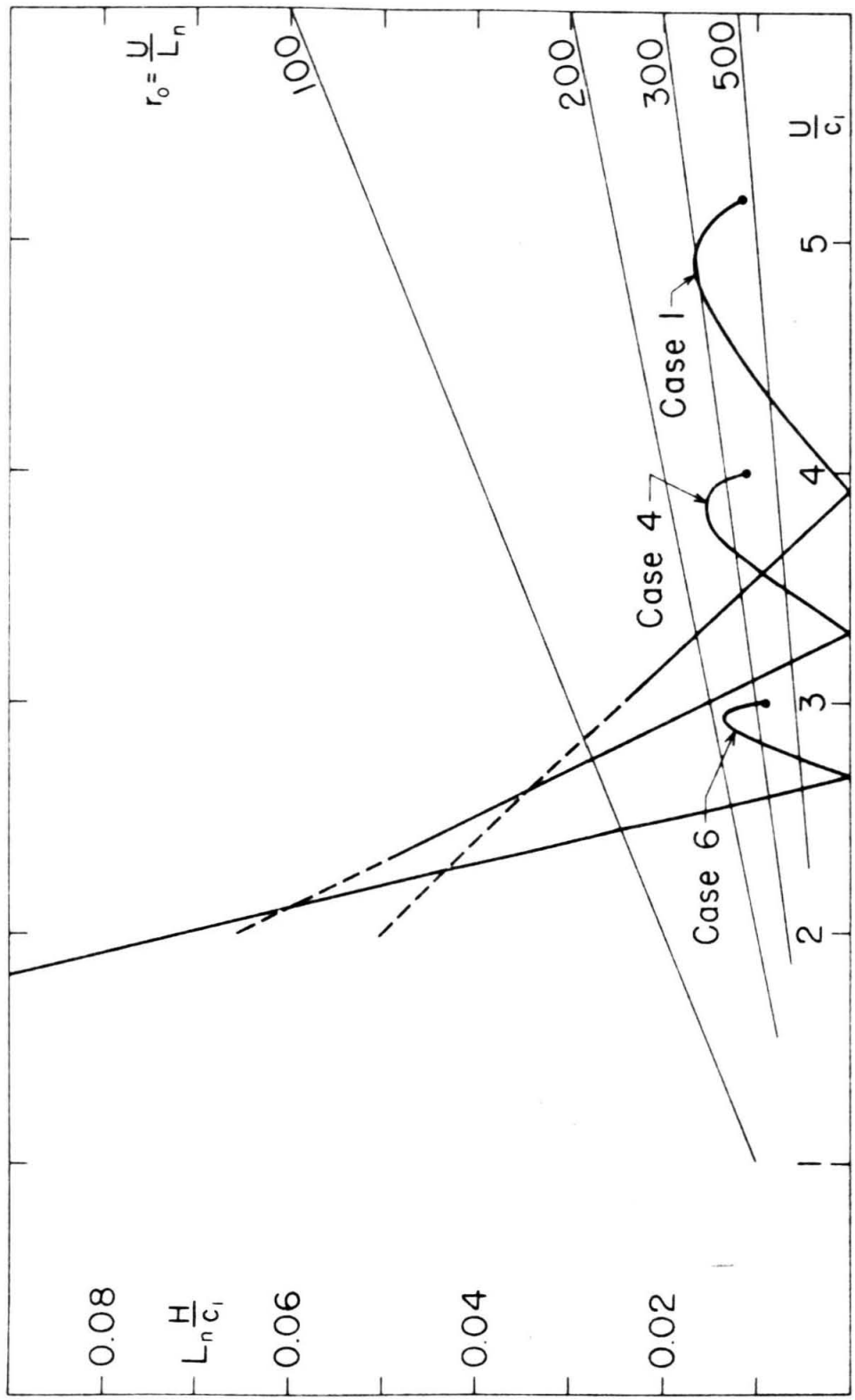
$r_o = \frac{U}{L_n}$
100
200
300
500
$\frac{U}{c_1}$
5
4
3
2
1
Case 1
Case 4
Case 6
$L_n \frac{H}{c_1}$
0.08
0.06
0.04
0.02

Fig. 6

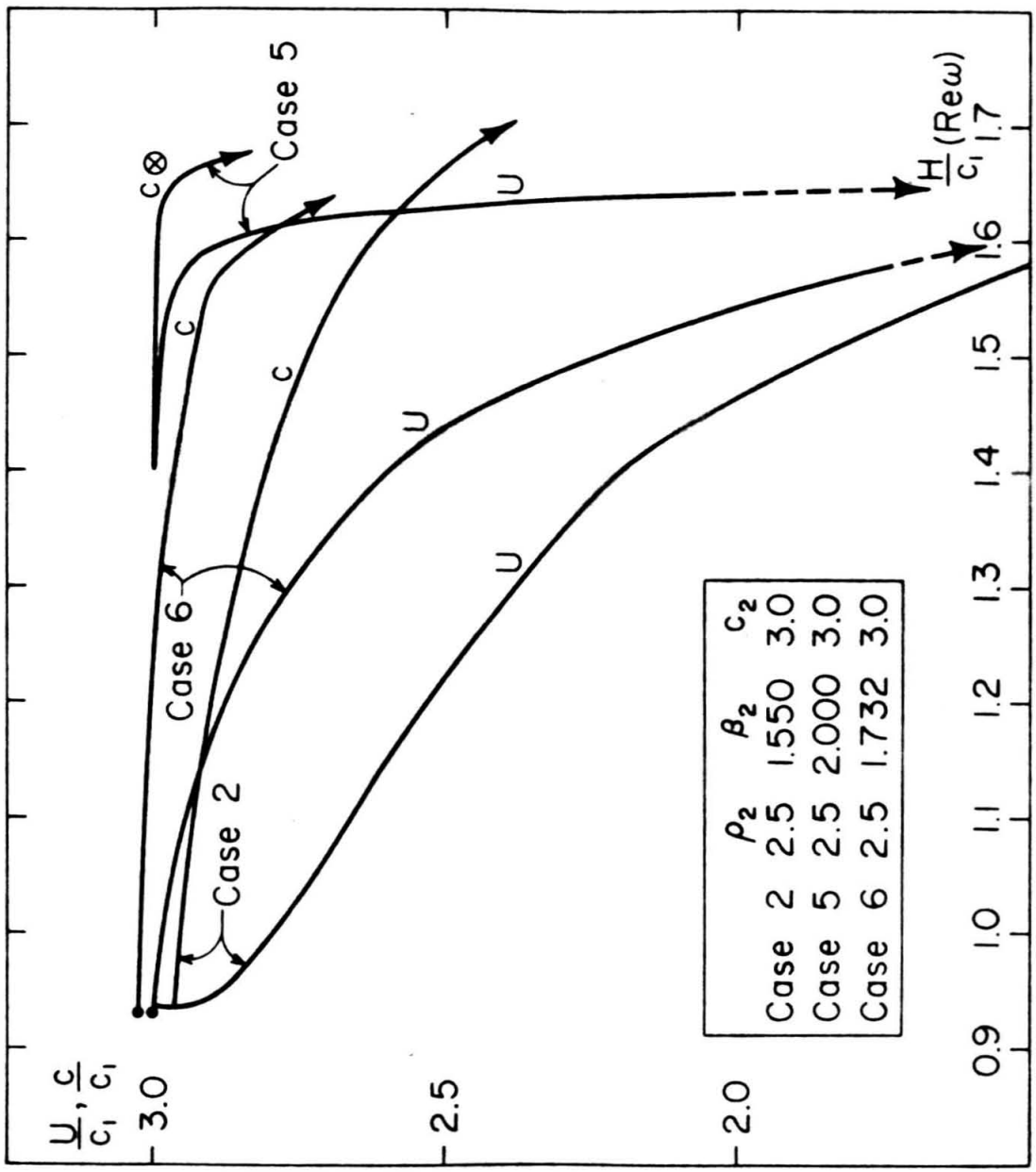
U, c / c1, c1
3.0
2.5
2.0
0.9
1.0
1.1
1.2
1.3
1.4
1.5
1.6
1.7
H/c1 (Reω)
Case 5
Case 6
Case 2
c⊗
c
c
U
U
U
U
ρ2 β2 c2
Case 2 2.5 1.550 3.0
Case 5 2.5 2.000 3.0
Case 6 2.5 1.732 3.0

Fig. 7

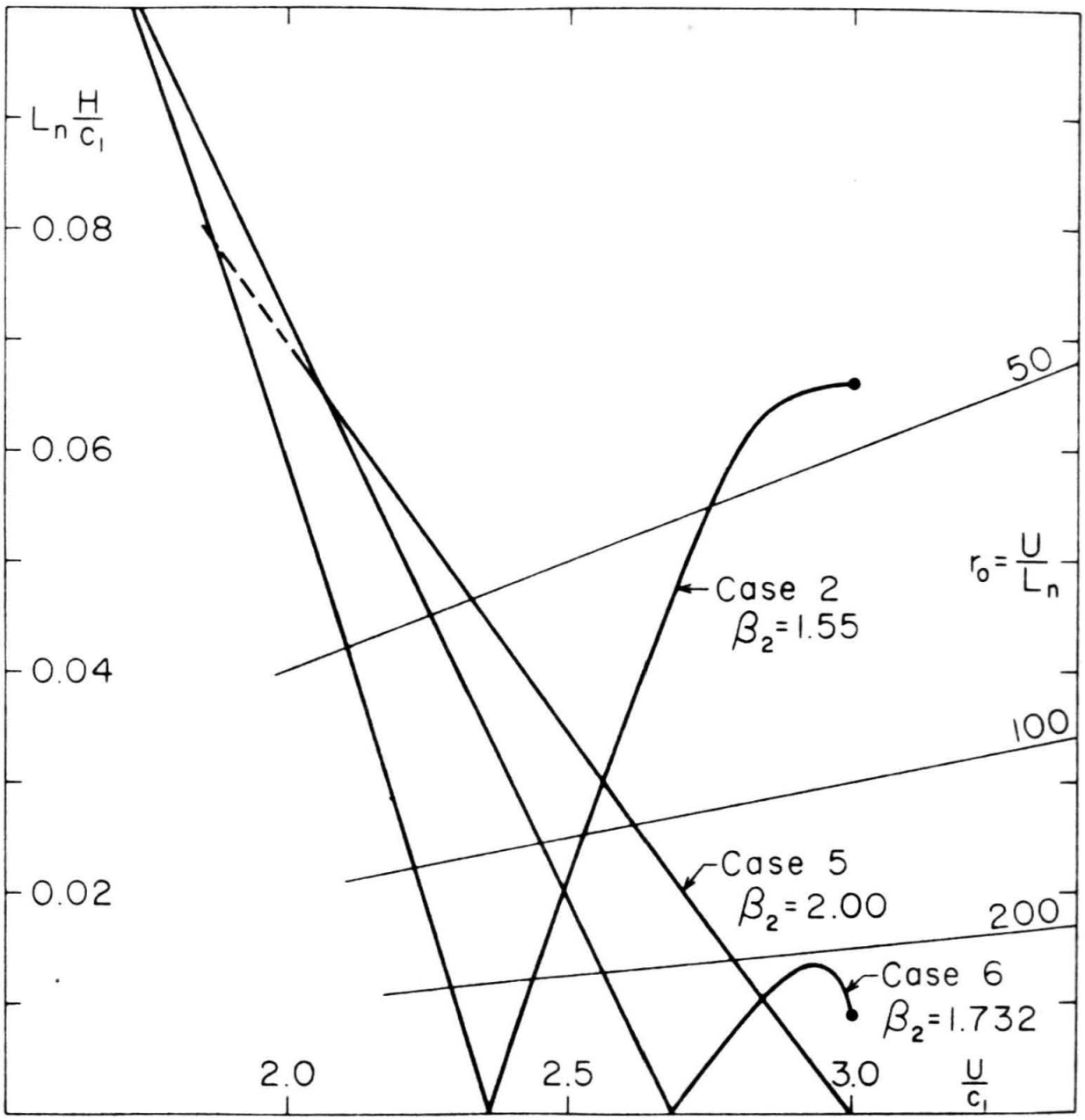
$L_n \frac{H}{c_1}$
0.08
0.06
0.04
0.02
2.0
2.5
3.0
$\frac{U}{c_1}$
50
100
200
$r_o = \frac{U}{L_n}$
Case 2
$\beta_2 = 1.55$
Case 5
$\beta_2 = 2.00$
Case 6
$\beta_2 = 1.732$

Fig. 8

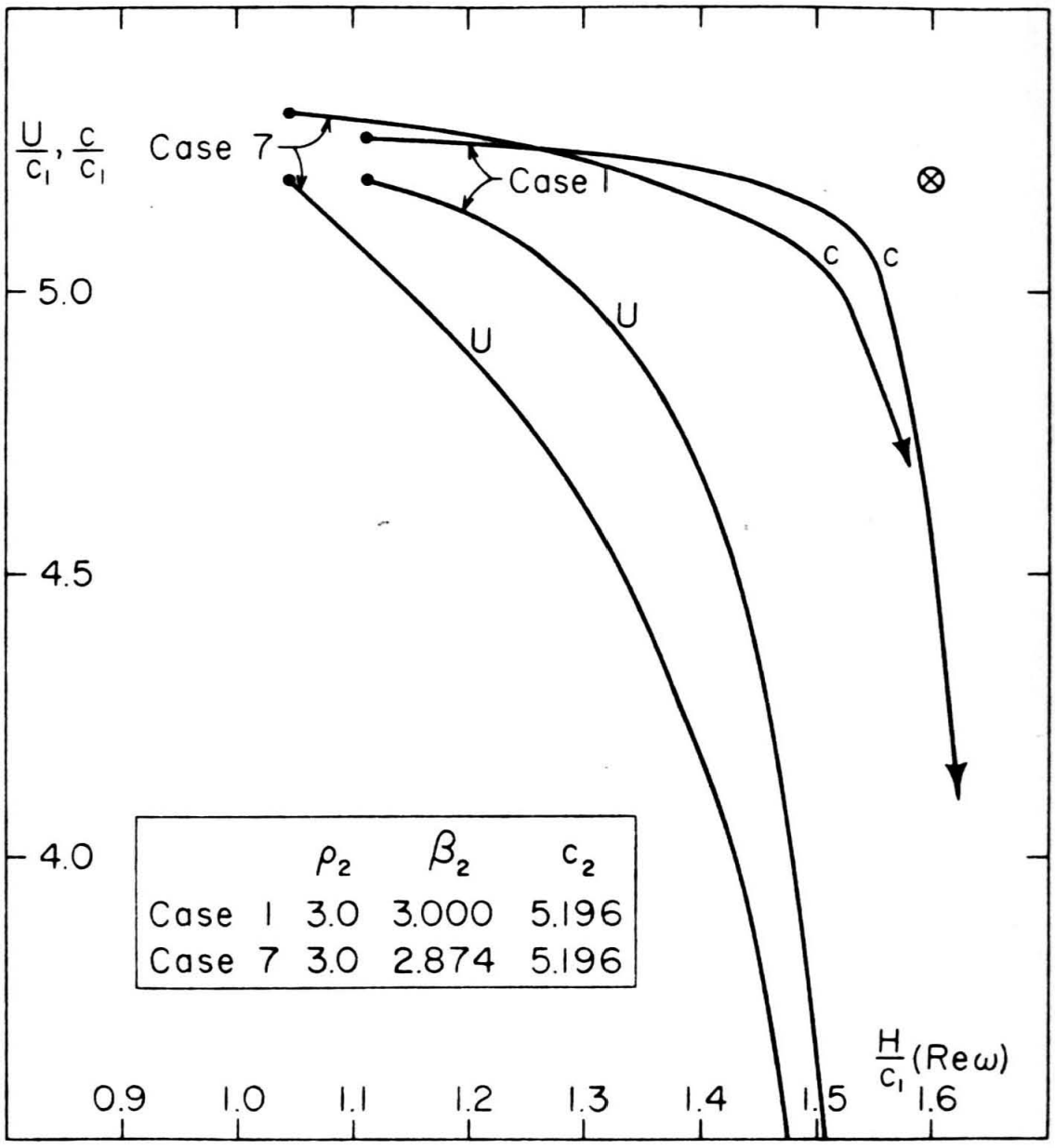
$\frac{U}{c_1}, \frac{c}{c_1}$
Case 7
Case 1
c
c
U
U
5.0
4.5
4.0
ρ_2 β_2 c_2
Case 1 3.0 3.000 5.196
Case 7 3.0 2.874 5.196
$\frac{H}{c_1}(Re\omega)$
0.9 1.0 1.1 1.2 1.3 1.4 1.5 1.6

Fig. 9

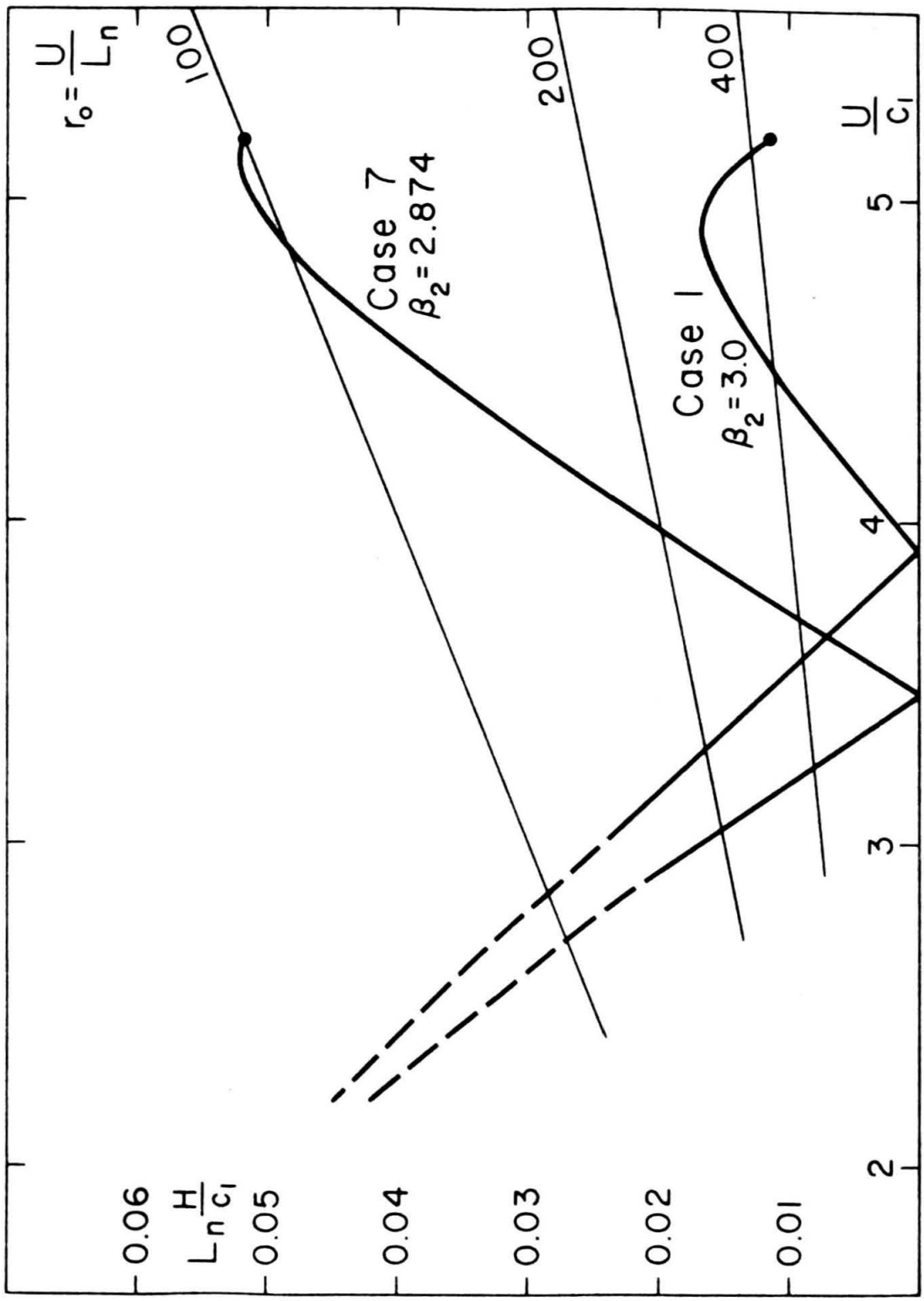
$r_o = \frac{U}{L_n}$
100
200
400
Case 7
$\beta_2 = 2.874$
Case 1
$\beta_2 = 3.0$
$\frac{H}{L_n c_1}$
0.06
0.05
0.04
0.03
0.02
0.01
2
3
4
5
$\frac{U}{c_1}$

Fig. 10

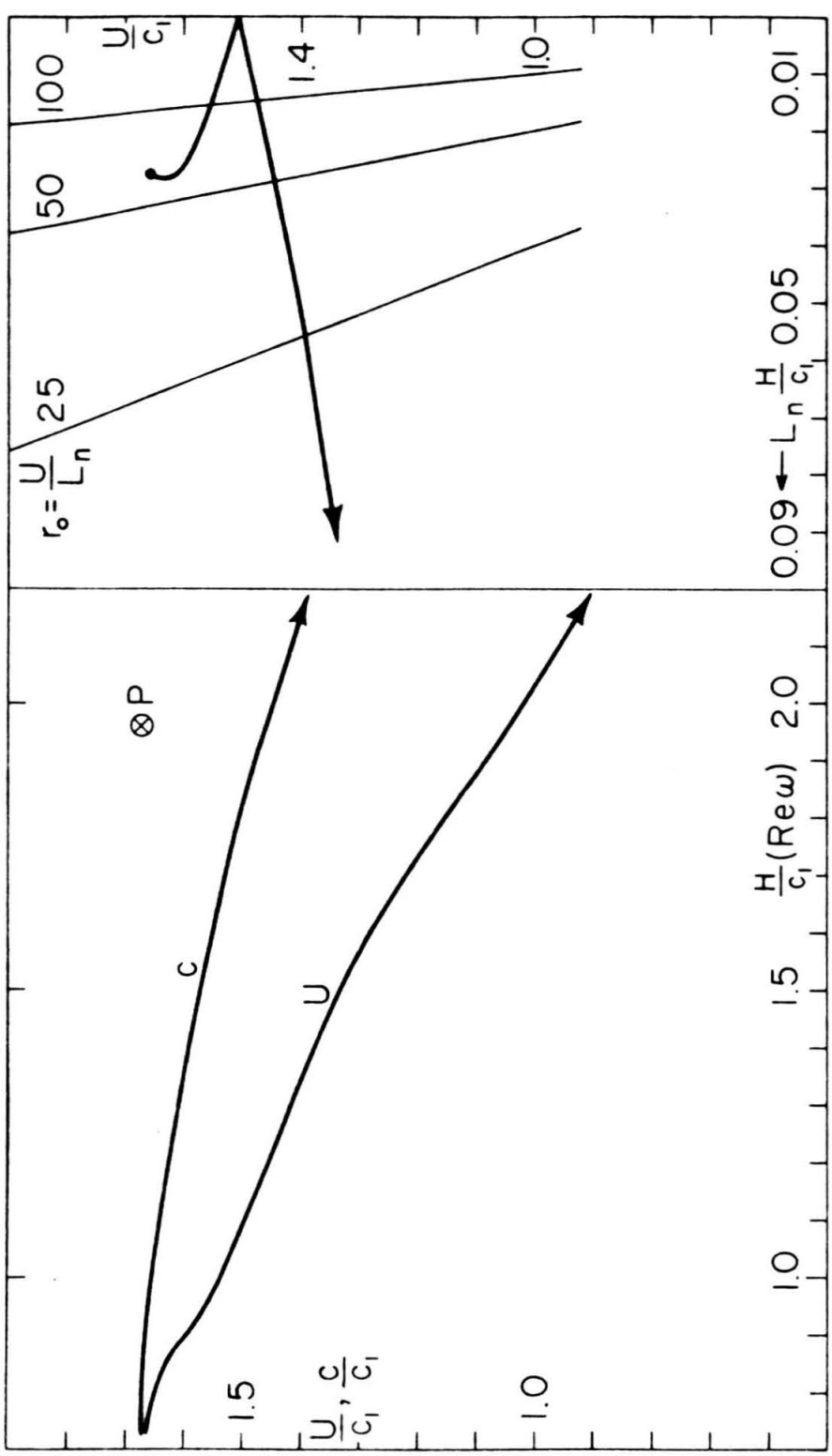
$\frac{U}{c_1}$
100
50
25
$r_o = \frac{U}{L_n}$
1.4
1.0
0.01
0.05
0.09 ← $L_n \frac{H}{c_1}$
⊗P
c
U
1.5
1.0
$\frac{U}{c_1}, \frac{c}{c_1}$
1.0
1.5
2.0
$\frac{H}{c_1}(Re\omega)$

Fig. 11

Fig. 12

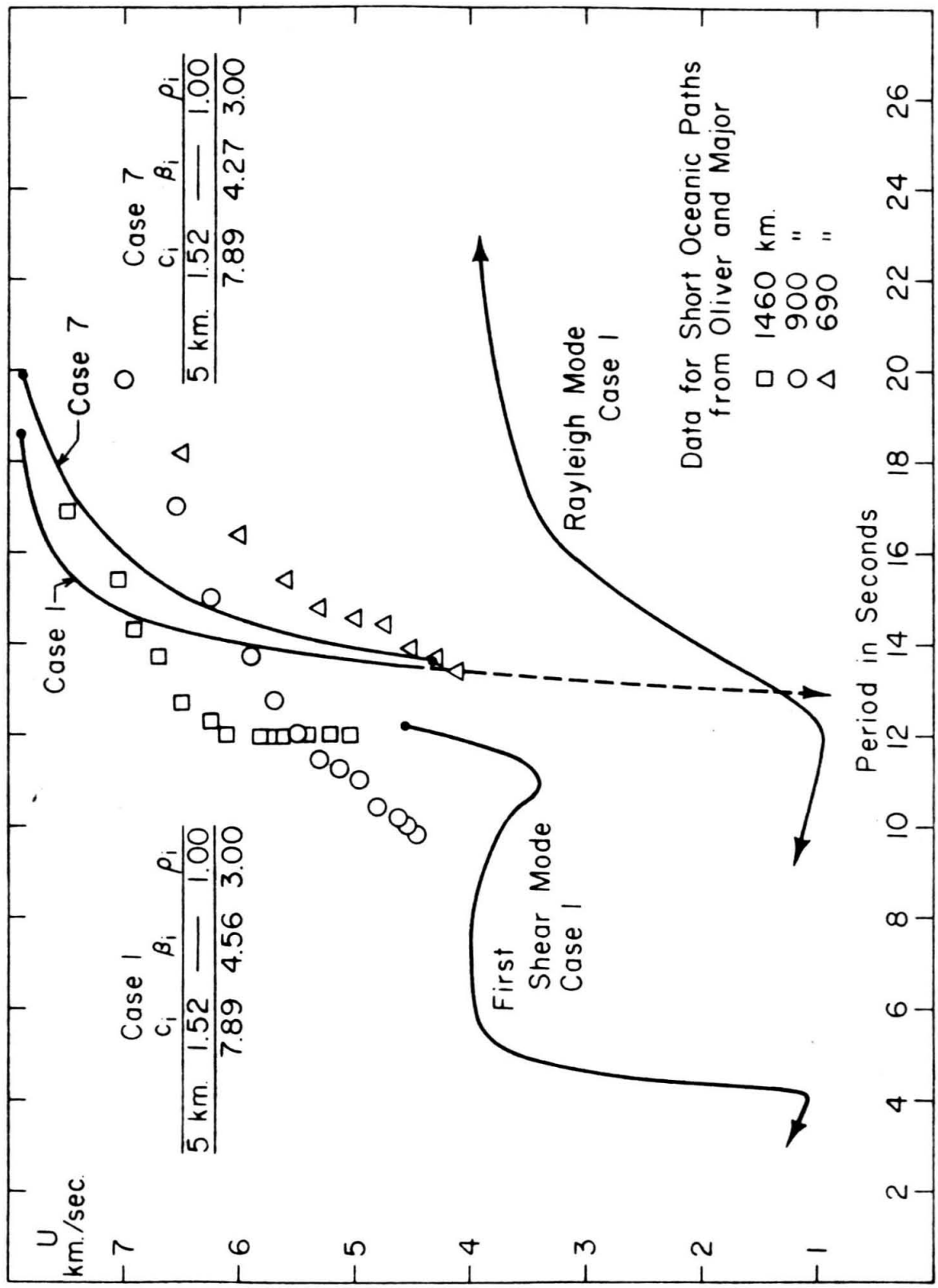
U
km./sec.
7
6
5
4
3
2
1
2
4
6
8
10
12
14
16
18
20
22
24
26
Period in Seconds
Case 1
Case 7
Case 1
c_i β_i ρ_i
5 km. 1.52 — 1.00
7.89 4.56 3.00
Case 7
c_i β_i ρ_i
5 km. 1.52 — 1.00
7.89 4.27 3.00
First
Shear Mode
Case 1
Rayleigh Mode
Case 1
Data for Short Oceanic Paths
from Oliver and Major
□ 1460 km.
○ 900 "
△ 690 "

Fig. 13

Fig. 13

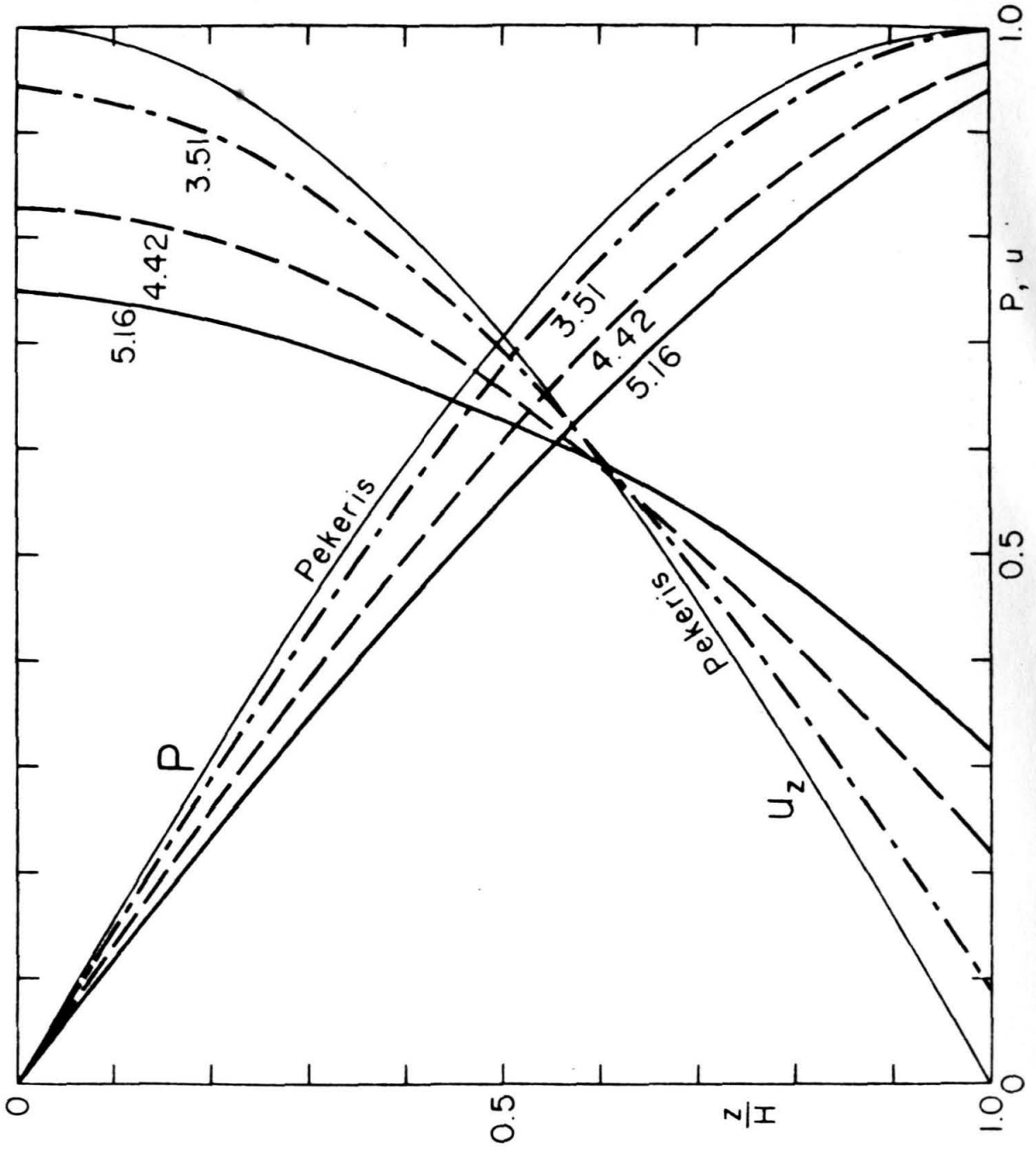

Fig. 14

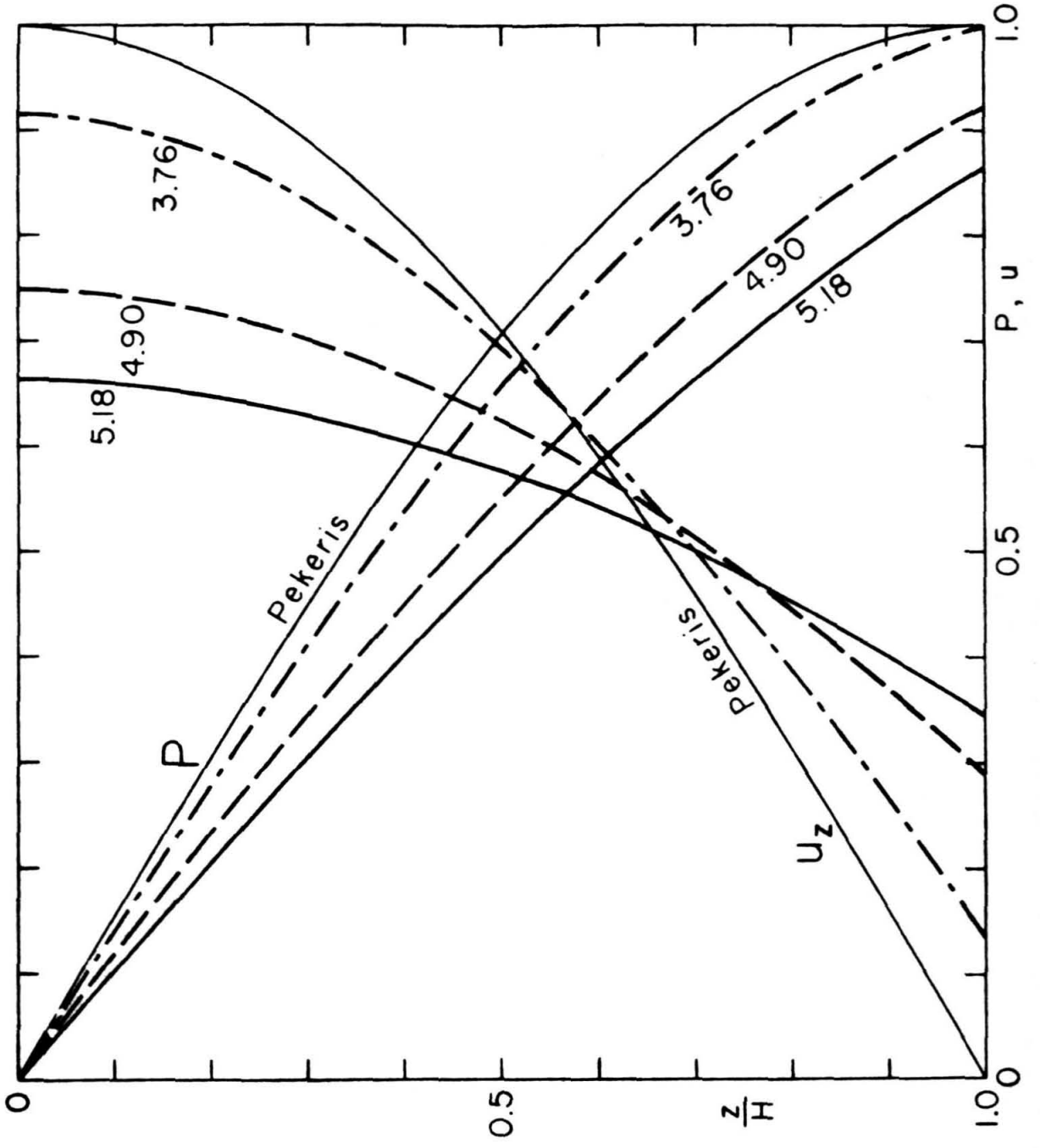

Fig. 15

Fig. 15

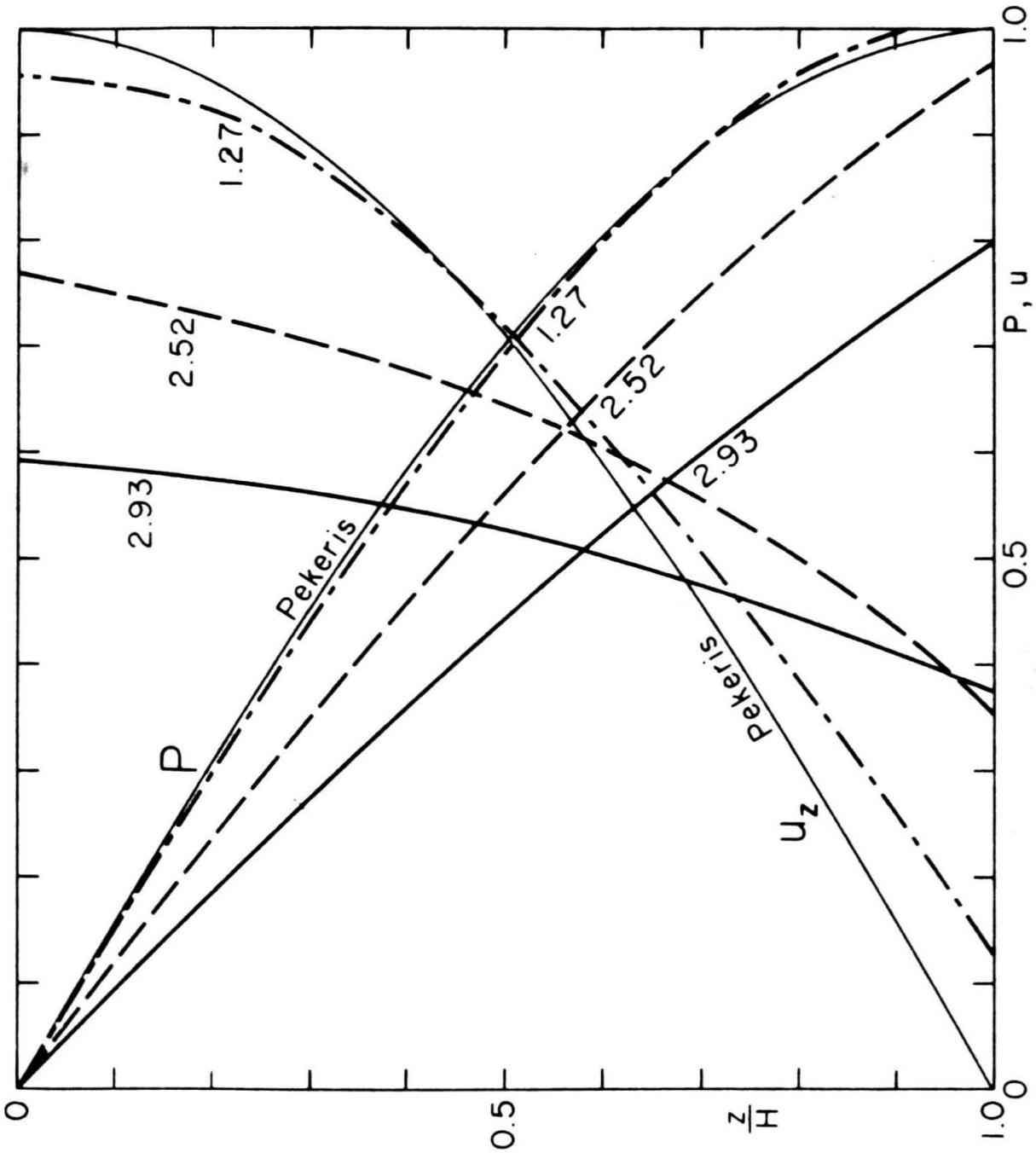

Fig. 16

Fig. 16

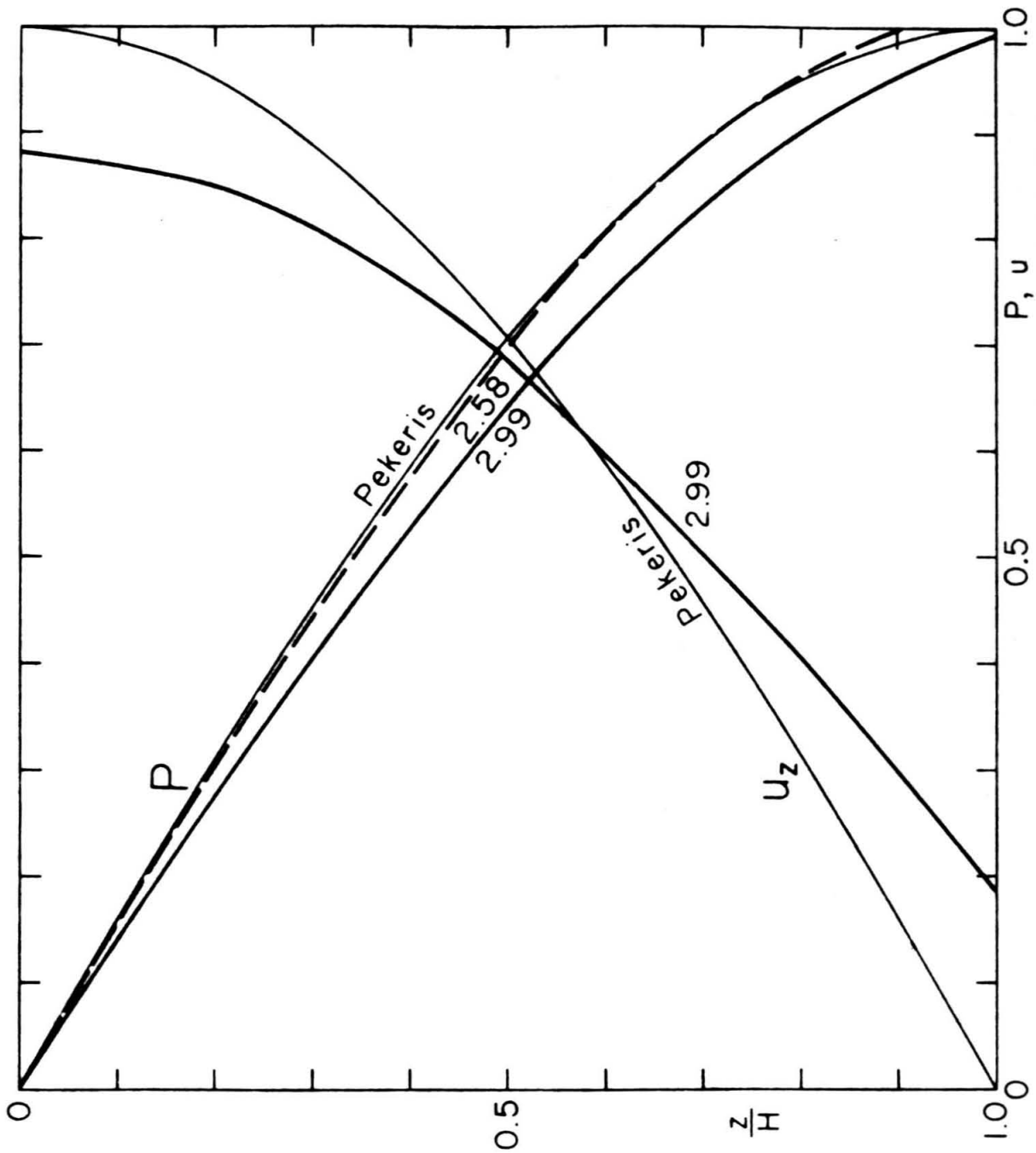

Fig. 17

Fig. 17

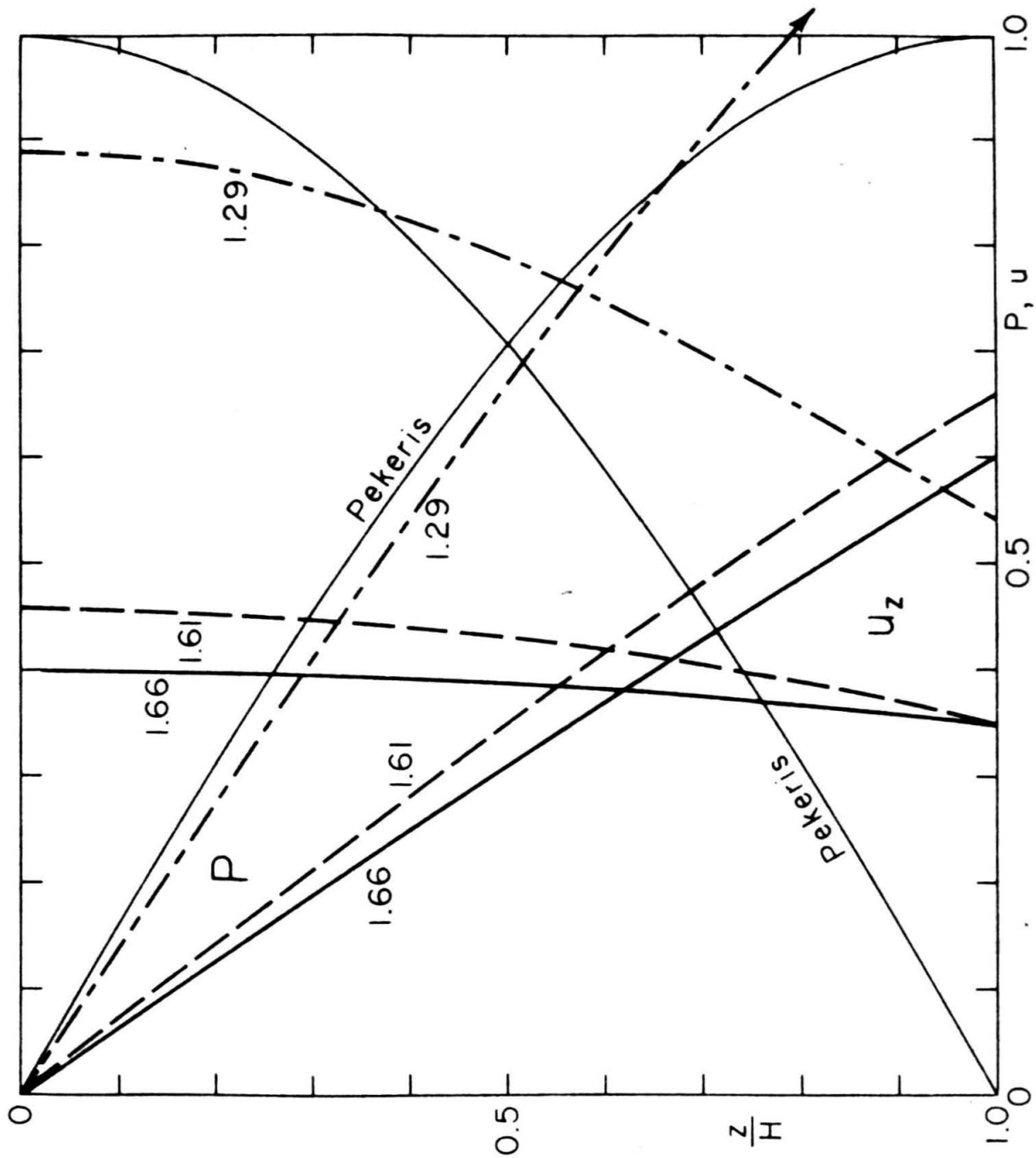
1.29
Pekeris
1.29
1.61
1.66
1.61
P
1.66
Pekeris
U_z
0
0.5
1.0
$\frac{z}{H}$
0
0.5
1.0
P, u

Fig. 18

Fig. 18

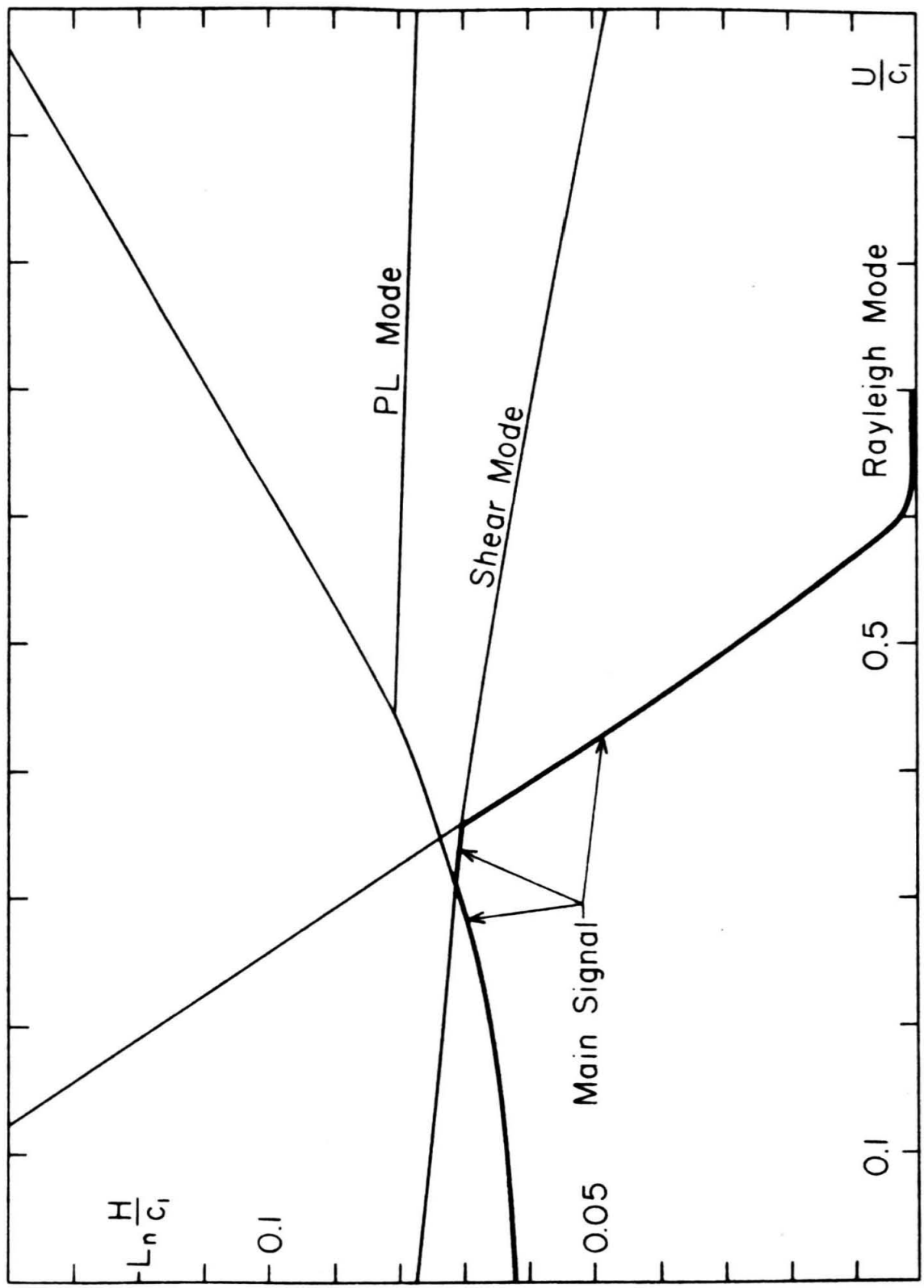
PL Mode
Shear Mode
Rayleigh Mode
Main Signal
$L_n \frac{H}{c_1}$
0.1
0.05
0.1
0.5
$\frac{U}{c_1}$

Fig. 19

Fig. 19

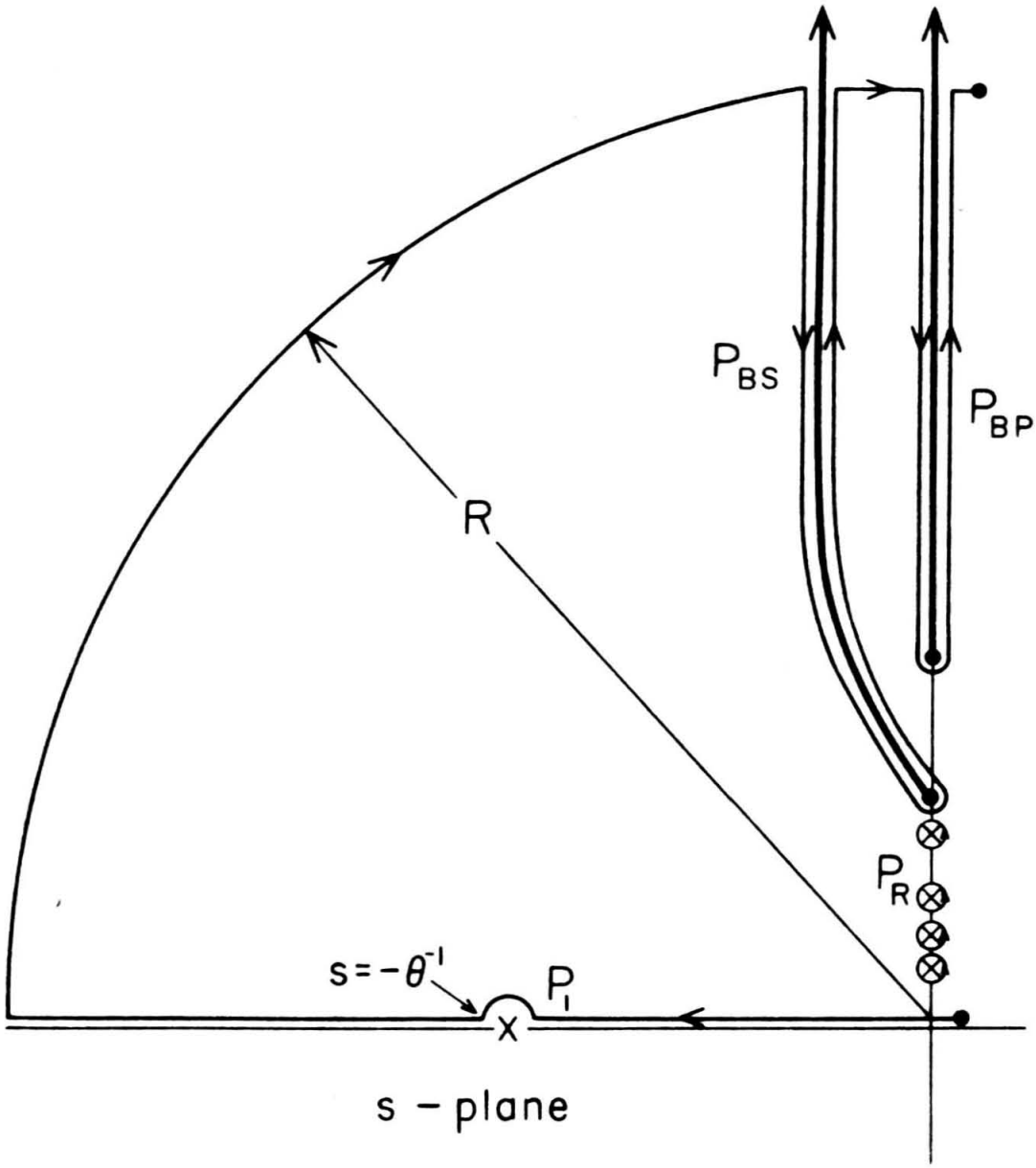

Fig. 21

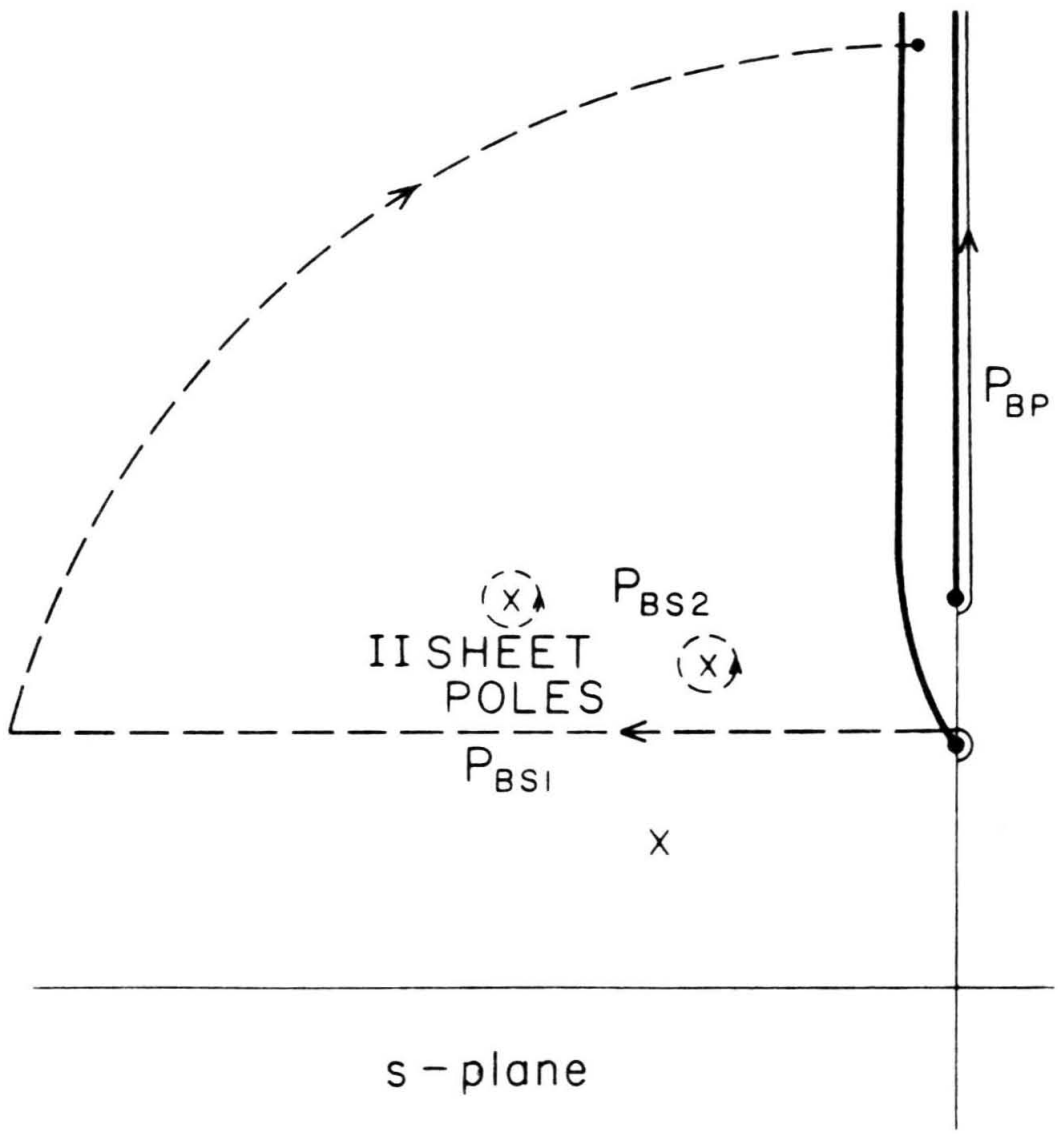

Fig. 22

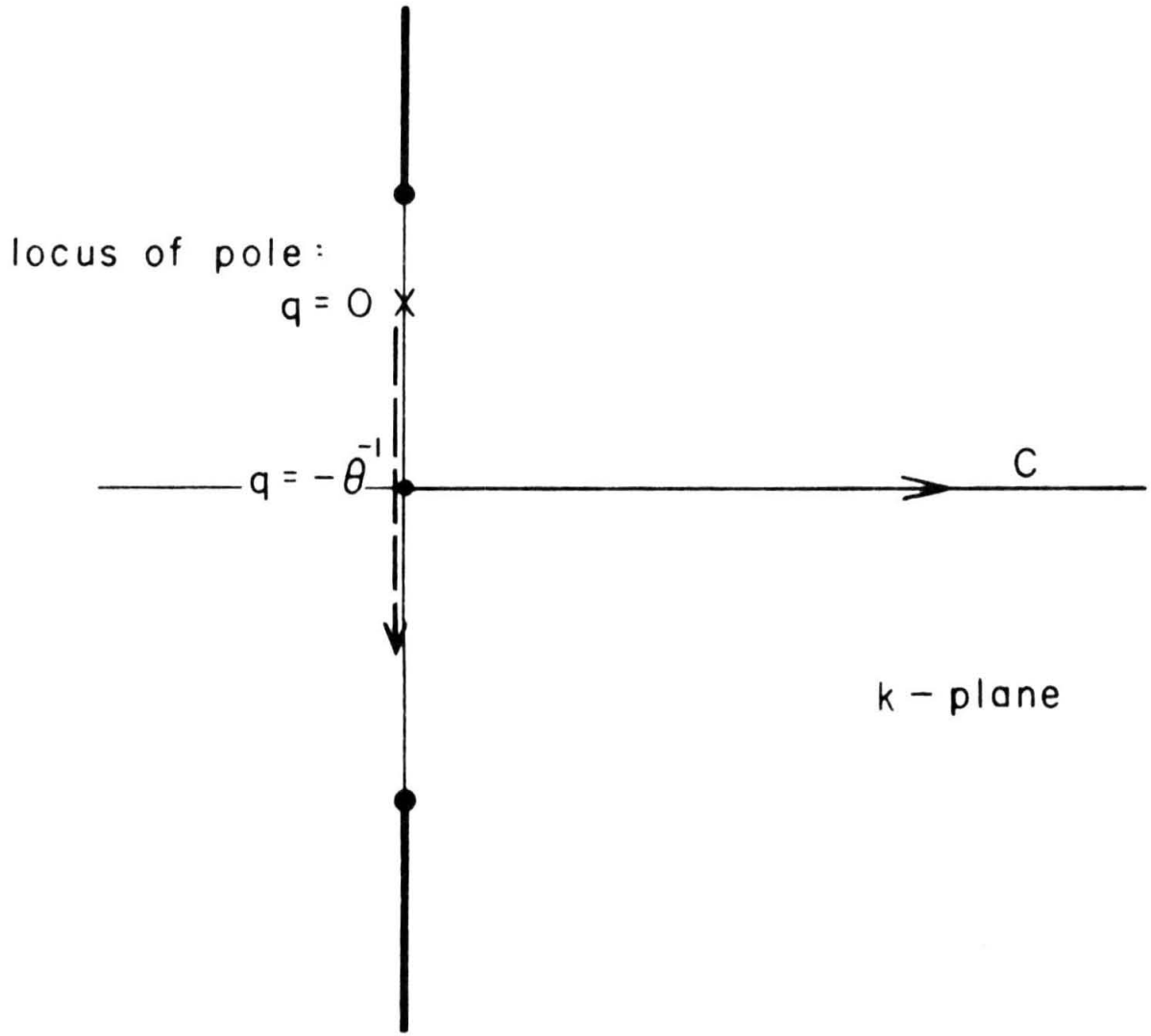

Fig. 23

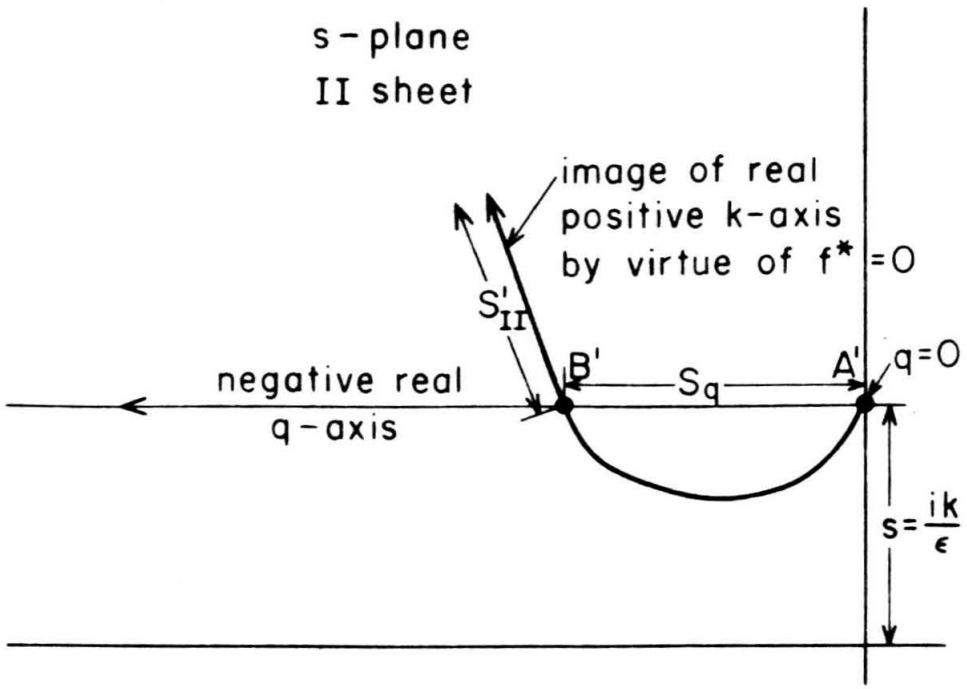
s - plane
II sheet
image of real
positive k-axis
by virtue of f* = 0
S'II
B'
Sq
A'
q=0
negative real
q - axis
s = ik/ε

Fig. 25

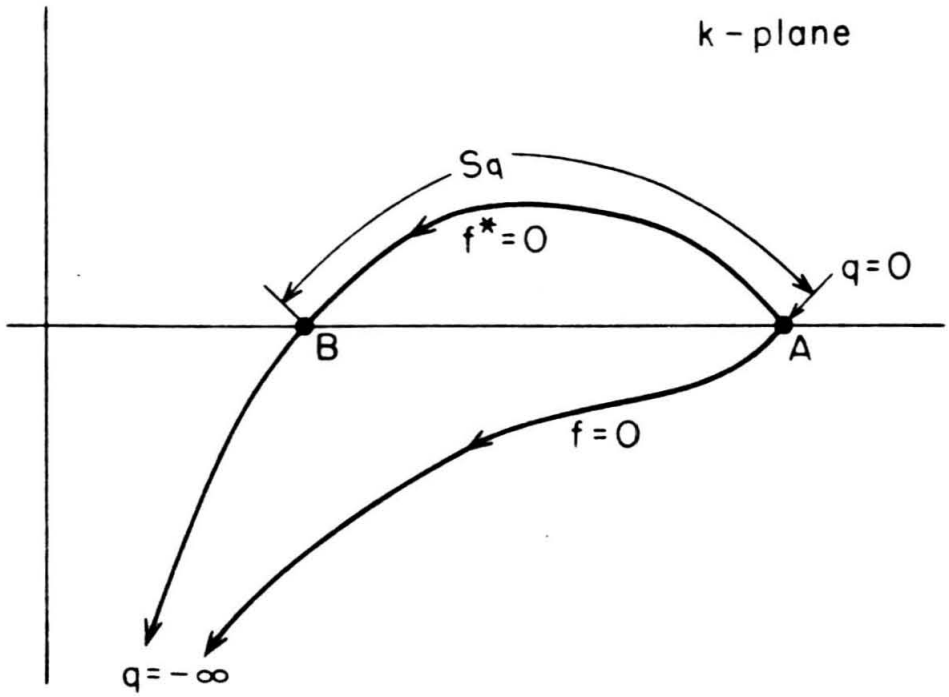
k - plane
Sq
f*=0
q=0
B
A
f=0
q=-∞

Fig. 24

PROPAGATION OF LEAKING INTERFACE WAVES*

Robert A. Phinney

Seismological Laboratory
California Institute of Technology
Pasadena, California

****

Abstract

Using simple generalizations of the method due to Rosenbaum (1961) and Phinney (1961) single integral expressions may be written down for the long range pole contributions to the transient signal in a plane seismic waveguide. This method yields expressions for the leaking, or imperfectly trapped waves, and suffers from no restrictions on the number of layers or the existence of coupling to one or two halfspaces. When applied to the simple interface wave problem of two halfspaces in contact, closed form expressions are obtained, describing the propagation of pulses along the interface due to lower sheet poles. The theory is applied to the Lamb problem, the liquid/solid interface, and the solid/solid interface problems. The leaking wave generali-

---

*Contribution No. 1023, Division of Geological Sciences, California Institute of Technology.

zations of the Rayleigh and Stoneley waves are found, and a new wave, coupled to the P-wave, is demonstrated. The physical importance of leaking interface pulses is shown to be in their coupling to the normal or leaking oscillations of layered structures.

TABLE OF SYMBOLS

Symbol	Definition	Equation Reference
a_i	coefficients in expansion of f	-
A	amplitude of source	1
b_i	coefficients in expansion of g	-
C,C'	contour of integration	Fig. 2
c	any solution of equation (4) where $c = \omega/k$	6
c_i	compressional wave velocity in medium i	Fig. 1
E	energy in delta-function source	9
f	period function	1,4
g	response function	1
h	source-interface separation	7, Fig. 1
k	wave number in horizontal direction	1
L_n	damping constant of modal oscillations (see paper I and Rosenbaum, 1960) $= \mathrm{Im}(\omega_n^c) - (r/t)\mathrm{Im}(k_n^c)$	3
m	index of halfspace = number of media in layered structure	-
m(c)	excitation function for interface wave problem	7
n	subscript indicating evaluation at a root of the period equation	2
N	2 + homogeneous degree of (g/f)	7,14

Symbol	Definition	Equation Reference
p	order of Bessel function in expression for field variable	5
q_o	horizontal displacement on surface of free halfspace	19
Q	$r - ct + ih\gamma(c)$	10
Q_n^c	excitation function of saddle point formula; usage conforms to paper I--occurs here only once	3
r	horizontal coordinate in circular cylindrical coordinates	1
s	$= i\omega$: Laplace transform variable	1
t	time	1
v	Re(c)	15
v_i	body wave velocity defined by $v_i < v_{i+1}$, equals some particular c_j or β_j	Table 2
w_o	vertical displacement on surface of free halfspace	20
$x(t)$	field variable, such as pressure, displacement, stress, etc.	1
γ_1	Re $\gamma(c)$	15
γ_2	Im $\gamma(c)$	15
z	axial coordinate in circular cylindrical coordinates	-

Symbol	Definition	Equation Reference
α_i	$\sqrt{k^2 - \omega^2/c_i^2} = \sqrt{k^2 + s^2/c_i^2}$	Introduction
α_i'	$\sqrt{k^2 - \omega^2/\beta_i^2} = \sqrt{k^2 + s^2/\beta_i^2}$	Introduction
β_i	shear velocity in medium i	-
$\gamma(c)$	$\sqrt{1 - c^2/c_i^2}$	9
δ	rotation angle between k-plane and ξ-plane	10
ξ	$k\, e^{-i\delta}$	10
η	Im(c)	9
θ	time decay constant of source	1
υ_i	$\sqrt{k^2 - \omega^2/v_i^2}$	Table 2
ρ_i	density of medium i	-
σ_i	Poisson constant of medium i	-
$\psi(c)$	phase of m(c)	13
ϕ_o, ϕ	_____	14
ω	angular frequency: = - is	-

INTRODUCTION

In this paper we make it possible to apply recent developments in leaking mode theory to a fairly broad class of seismic waveguides. What is desired is a simple technique for investigating the complex roots of the period equation and interpreting them in light of an appropriate representation of the solution. We shall first state two generalizations which make it possible to use formulae obtained in an earlier paper for this purpose. In the body of the paper we treat the interface wave problem of two halfspaces in contact on a plane boundary. This is done by reducing the single integral obtained by general considerations to a closed expression representing propagation of a leaking interface pulse. The complex roots of the appropriate period equation may now be numerically evaluated, and the velocity and shape of the pulse then follow.

In a previous paper (Phinney, 1961), which we designate as I, we have deduced the leaking, or attenuated, modes of a seismic waveguide consisting of a liquid layer coupled to a solid halfspace. The method (Rosenbaum, 1960) consists of writing the response to a transient point source ($x_0(t) = e^{-t/\theta}$) as a double integral.

$$(1) \quad \chi(t) = \frac{A}{\pi i} \int_{\lambda - i\infty}^{\lambda + i\infty} \frac{e^{st}}{s + \theta^{-1}} \, ds \int_0^{\infty} J_0(kr) \, k \, \frac{g(s,k)}{f(s,k)} \, dk$$

The Laplace transform variable is s, k is the wave number in the horizontal coordinate, x(t) is some field variable such as pressure or displacement. We determine g(s,k) and f(s,k) by applying boundary conditions at the plane interfaces bounding the media.

Letting the index m refer to the halfspace, then $\alpha_m = \sqrt{k^2 + s^2/c_m^2}$ and $\alpha'_m = \sqrt{k^2 + s^2/\beta_m^2}$, which occur in g and f, give rise to branch points in the s-plane. Cuts are introduced, joining the branch points to $i\infty$ along the imaginary s-axis. The s-integration in (1) may be performed by rewriting it as a set of residue contributions from poles lying on the sheet of integration and two branch line integrals arising from integration around the cuts. By deformation of the branch line contours onto lower Riemann surfaces, the branch line integrals decompose into (a) residue contributions from complex zeros of f and (b) pulse terms which are interpreted as ray arrivals at the body wave velocities. All the residue contributions from both the top sheet and the relevant lower sheets have the same form and may be written symbolically as a single integral.

$$(2) \quad x(t) = 4A \sum_{n=0}^{\infty} \int_{S_{I,II,III}} J_0(kr)\, k\, \frac{e^{s_n t}}{s_n + \theta^{-1}} \left\{ \frac{g}{\frac{\partial f}{\partial s}} \right\}_n dk$$

$S_{I,II,III}$ are contours on three Riemann sheets. When this expression is evaluated by a saddle point method in the k-plane, a representation of the solution at long ranges may be

written down (3). It expresses the oscillatory contributions at long range in terms of a cosine term and a damped exponential. The subscript n denotes evaluation at a root $s_n(k)$ of the period equation $f(s_n,k) = 0$. The superscript c denotes evaluation at a saddle point where $r/t = d\omega_n/dk$. $(s = i\omega)$

$$(3) \quad \chi(t) = Q_n^c e^{-L_n t} \cos\left[(Re\,\omega_n^c)t - (Re\,k_n^c)r + \Omega\right]$$

Generalizations of the theory

We now summarize two results which may be obtained by generalizing the analysis in I.

(1) The liquid layer/solid halfspace problem of I differs from the liquid layer/liquid halfspace problem done by Rosenbaum (1960) in that the integrand g/f contains two branch cuts instead of one. More general surface waveguides consisting of a stack of solid and liquid layers overlying a solid halfspace still only involve two branch cuts. We may write f and g in the form: $f = a_0 + a_1\alpha_m + a_2\alpha_m' + a_3\alpha_m\alpha_m'$; $g = b_0 + b_1\alpha_m + b_2\alpha_m' + b_3\alpha_m\alpha_m'$, where the a_i and b_i do not involve the branch points. If this form is used in the analysis in I, it follows that all quantities transform exactly as they did in the particular case in I. The single integral (2) now expresses the pole contributions from all sheets. The saddle point solution (3) now may be applied to this general layered problem, provided only that a saddle point exists and is "accessible" to the initial contour of (2).

(2) If the waveguide under consideration is bounded by halfspaces on both top and bottom, the integrand in (1) will involve up to 4 branch lines. In I we obtained the following result, which states the values of time for which each Riemann sheet is appropriate:

TABLE I

	Re α_2	Re α_2'
$t > r/\beta_2$	+	+
$r/\beta_2 > t > r/c_2$	+	-
$0 > t > r/c_2$	-	-

To generalize to 3 or 4 branch lines it is necessary to trace the way in which the period function, f, is transformed as the branch line integrals in I are manipulated. The essence of the matter is that each branch line integral is deformed in the s-plane in such a way that the line integral converges most rapidly. When this is done, the resulting line integral and pole contributions are found on some particular "lower" Riemann sheet. Each branch line integral, consisting of two terms, gives rise in this way to pole contributions from two lower sheets; analysis of the conditions which ensure convergence on an arc at ∞ gives the range of t which is appropriate to the poles from each sheet, as illustrated in the table above for the two branch line problem. The result for

four branch lines is stated in Table 2. In connection with the interface wave problem we shall write the restrictions of Table 2 in more specific form. In general, we find that when the signal velocity (r/t) lies between two body wave velocities, the relevant Riemann sheet is "upper" for all faster body waves and "lower" for all slower body waves. In all cases, the signal is constrained to vanish prior to the earliest body wave, and the signal after the slowest body wave is determined by the conventional "top sheet" for all variables.

TABLE 2

Two halfspaces in contact, having four body wave velocities: $v_1 < v_2 < v_3 < v_4$, without specification as to type. Setting $\nu_i = \sqrt{k^2 - \omega^2/v_i^2}$, specification of the sign of the real part of each of the ν_i specifies the Riemann surface appropriate to any given signal velocity according to this table.

	$\mathrm{Re}\,\nu_1$	$\mathrm{Re}\,\nu_2$	$\mathrm{Re}\,\nu_3$	$\mathrm{Re}\,\nu_4$
$0 < r/t < v_1$	+	+	+	+
$v_1 < r/t < v_2$	-	+	+	+
$v_2 < r/t < v_3$	-	-	+	+
$v_3 < r/t < v_4$	-	-	-	+
$0 < r/t < v_4$	-	-	-	-

The first sheet root is real, when it exists. Roots of the period equation lying on lower sheets must be complex with a positive imaginary part if they are to contribute to the signal. (This refers to a complex root $\omega_n(k)$, when k is real and positive.)

The general interface wave problem

We now restrict ourselves to the case of two halfspaces in contact on a plane interface. Three types of problem may be considered:

(A) A solid halfspace with vanishing stresses on the surface (Lamb's problem).

(B) A solid halfspace in contact with a liquid halfspace.

(C) Two solid halfspaces in welded contact.

Excitation functions and period equations for these problems are well known, since they may be derived from steady-state considerations. A fairly complete collection of results for various types of source is found in Ewing, Jardetzky, and Press (1957). In this paper we consider a point source near the interface, and use results given in the reference. Period equations for the three cases are as follows:

(A) $$f_A = \left(2k^2 - \frac{\omega^2}{\beta_2^2}\right)^2 - 4k^2\alpha_2\alpha_2'$$

(4) (B) $$f_B = \frac{\rho_1 \omega^4 \alpha_2}{\rho_2 \beta_2^4} + \alpha_1 f_A$$

(C) $$f_C = k^2\left[\frac{\mu_2}{\mu_1}\left(\frac{\omega^2}{\beta_2^2} - 2k^2\right) + \left(2k^2 - \frac{\omega^2}{\beta_1^2}\right)\right]^2 - \alpha_1\alpha_1'\left[2k^2\left(1 - \frac{\mu_2}{\mu_1}\right) + \frac{\mu_2}{\mu_1}\frac{\omega^2}{\beta_2^2}\right]^2 -$$

$$- \alpha_2\alpha_2'\left[2k^2\left(\frac{\mu_2}{\mu_1} - 1\right) + \frac{\omega^2}{\beta_1^2}\right]^2 - \left(\alpha_1\alpha_2' + \alpha_2\alpha_1'\right)\frac{\omega^4\mu_2}{\beta_1^2\beta_2^2\mu_1} + 4k^2\left(\frac{\mu_2}{\mu_1} - 1\right)^2\alpha_1\alpha_2\alpha_1'\alpha_2'$$

If a transient point source, $x_0(t) = Ae^{-t/\theta}$, is excited at a distance h from the interface, then the solution is represented as the double integral:

$$(5)\quad \chi = \frac{2A}{\pi i}\int_{\lambda-i\infty}^{\lambda+i\infty} \frac{e^{st}}{s+\theta^{-1}}\,ds \int_0^\infty \frac{g(s,k)}{f(s,k)}\,k\,J_p(kr)\,dk$$

p is zero or one depending on the field variable of interest. f is one of the period functions (4), and g contains the dependence on h and z.

By a method due to Cagniard it is possible to obtain an exact closed form solution for all ranges. Cagniard (1939) investigated the solid/solid problem, Garvin (1956) and Gilbert (1956) solved the Lamb problem, and Cagniard (1939) and Strick (1959) treated the liquid/solid interface problem. These authors found the various waves long known from asymptotic evaluation of the solution in the steady state. P and S waves arise from integration near a branch point, while the familiar surface waves are due to a pole lying on the sheet of integration. As is customary, this sheet is defined by the condition that $\mathrm{Re}\,\zeta_i > 0$ for all the radicals ζ_i; this is brought about by the requirement that the steady state solution die off exponentially away from the interface. Surface waves, due to "top sheet" poles, may be categorized as follows: (A) the Rayleigh wave, having a velocity between $.86\beta_2$ and $.96\beta_2$, (B) the Stoneley wave, having a velocity near $.99c_1$ for typical models, and (C) the Stoneley wave, with a velocity less than either β_1 or β_2, but greater than the Rayleigh velocity in the faster medium.

The Stoneley wave (C) exists only for a very restricted class of models. These remarks are not intended to be complete, but only to characterize. For a complete discussion of the Stoneley wave for (B) and (C), the list of references should be consulted.

Various investigators have suggested the existence of partially trapped interface waves, representing a generalization of the Rayleigh and Stoneley waves cited. Strick (1959) demonstrated a generalized Rayleigh wave for case (B), with a velocity equal to that of the comparable undamped Rayleigh wave (A), but decaying in time by coupling to P-waves in the liquid. Gilbert and Laster (1961) have found a partially trapped wave in the Lamb problem, existing in solids with a high Poisson constant. They have also identified a leaking Stoneley wave for case (C) when the model parameters do not permit a true Stoneley wave to exist. All of these pseudo-waves are caused by poles of the integrand which lie on Riemann sheets other than the principal sheet of integration. By their proximity to the branch cuts (in the Cagniard formulation) they affect the form of the solution obtained by evaluation near the cuts, thus generating a contribution to the signal, despite their location on a lower sheet. Investigations of the sort cited are equipped to delineate exact seismogram shapes, but prove tedious in many cases without shedding proportionate light on the physical nature of the

signals. In this paper we treat the interface wave problem in a more traditional way, obtaining asymptotic formulae for the pulse shape by direct attack on the double integral solution (5). The results cited in the introduction make it possible to do so with a precision which brings the lower sheet contributions into sharp focus, instead of leaving them implicit in the branch line integrals as has been the practice up to now.

Our starting point is the single integral formula (2), a rather general tool which is easily applied to the cases we are considering. An asymptotic representation of the pulse due to each lower sheet pole arises directly from (2) by exact evaluation of the integral resulting from the long distance approximation to the Bessel function. In this approximation each wave has a constant velocity, given by the real part of the root $\underline{c}$ of the period equation. We may now view the leaking interface waves as free vibrations of the interface in a more general sense than that which describes ordinary undamped surface waves. Arising from so-called extraneous roots of the period equation, the pseudo-waves make sense physically in terms of plane wave reflection and transmission coefficients. The attractiveness of this method lies in its simplicity; for a given set of layer parameters the complex roots of the period equation may be easily obtained, enabling one to predict the velocity, pulse

width, attenuation, and existence of all the trapped or partially trapped free waves.

For each pole of the integrand which lies on a permissible sheet (Tables 1 - 2) we may write down the single integral obtained from (2):

$$(6)\quad \chi = 4A\,Re\int_0^\infty J_r(kr)\,\frac{e^{ikct}}{ikc+\theta^{-1}}\left(\frac{g_i}{\frac{\partial f}{\partial \omega}}\right)_{\omega=kc} k\,dk$$

Since the period equation (4) is homogeneous in ω and k, it is possible to write $f = f(\omega,k) = f(kc,k) = k^a f(c,1) = 0$. Thus roots of the period equation may be regarded as single complex numbers c, rather than functions $\omega_n(k)$. Henceforth, appearance of the letter c implies that it is a root of the period equation. The integrand in (6) is the result of the substitution $\omega = kc$. Since g is also homogeneous, the expression in parentheses in (6) reduces to the form $k^{N-1}m(c)$, where m(c) is a complex function of complex c. If the source or receiver are not on the interface, exponential factors of the form:

$$e^{-\left(k^2-\frac{\omega^2}{c_i^2}\right)^{\frac{1}{2}}|z|} \qquad \text{or} \qquad e^{-\left(k^2-\frac{\omega^2}{c_i^2}\right)^{\frac{1}{2}}h}$$

will also result (from the function g). It is sufficiently general for our purposes to assume that z is zero and h positive, with the source compressional in nature, lying in medium i. (6) may now be written:

$$(7)\quad \chi = 4A\ \mathrm{Re}\left\{ m(c) \int_0^\infty k^N J_p(kr)\, \frac{e^{ikct}}{ikc + \theta^{-1}}\, e^{-kh\sqrt{1-\frac{c^2}{c_i^2}}}\, dk \right\}$$

We now make the only approximation in the analysis. It is the conventional long distance representation of the Bessel function, under the assumption of no sources at infinity:

$$J_p(kr) = H_p^{(1)}(kr) + H_p^{(2)}(kr) \longrightarrow H_p^{(2)}(kr) \sim$$

$$\sim \sqrt{\frac{2}{\pi kr}}\ \exp\left[-i\left(kr - \frac{\pi}{4} - \frac{p\pi}{2}\right)\right]$$

Then:

$$(8)\quad \chi = 4A\ \mathrm{Re}\left\{ \sqrt{\frac{2}{\pi r}}\, m(c)\, e^{i\frac{\pi}{2}(p+\frac{1}{2})} \int_0^\infty k^{N-\frac{1}{2}}\, \frac{e^{-ik(r-ct-ih\sqrt{1-\frac{c^2}{c_i^2}}}}{ikc + \theta^{-1}}\, dk \right\}$$

If we assume the source function to be a delta-function in time, then $\theta^{-1} \longrightarrow \infty$. We let the source amplitude $A \longrightarrow \infty$ as well, so that the source pulse still has finite energy. Setting $E = A\theta$ and $\gamma(c) = \sqrt{1 - c^2/c_i^2}$:

$$(9)\quad \chi = 4E\sqrt{\frac{2}{\pi r}}\ \mathrm{Re}\left\{ m(c)\, e^{i\frac{\pi}{2}(p+\frac{1}{2})} \int_0^\infty k^{N-\frac{1}{2}} e^{-ik(r-ct-ih\gamma(c))}\, dk \right\}$$

Consider the integral alone:

$$(10)\quad Y = \int_0^\infty k^{N-\frac{1}{2}} e^{-ikQ}\, dk \qquad \text{where} \quad Q = r - ct - ih\gamma(c)$$

This integral is easily evaluated if the variable k is replaced by $\xi = k\, e^{-i\delta}$. The effect is a rotation of the k-plane. (Figure 2).

The original contour C in the k-plane maps into C in the ξ -plane. We distort C into C' along the real ξ -axis and along an arc at infinity. δ is chosen so that C' is a steepest descent path, as follows:

$$Q = Q_1 + iQ_2$$

$$\exp(-ikQ) = \exp(-ikQ_1)\exp(kQ_2) =$$

$$\exp\left[-i\xi Q_1(\cos\delta + i\sin\delta)\right]\exp\left[\xi Q_2(\cos\delta + i\sin\delta)\right] =$$

$$\exp\left[-i\xi(Q_1\cos\delta - Q_2\sin\delta)\right]\exp\left[-\xi(-Q_1\sin\delta - Q_2\cos\delta)\right]$$

For a steepest descent path δ is chosen so that $Q_1\cos\delta = Q_2\sin\delta$. In other words: $\sin\delta = -Q_1/|Q|$; $\cos\delta = -Q_2/|Q|$ where the minus sign is necessary to make the integral converge. Thus: $\exp(-ikQ) = \exp\left[-\xi\,\frac{Q_1^2+Q_2^2}{|Q|}\right] = \exp\left[-\xi|Q|\right]$

Therefore: $Y = \int_0^\infty (\xi e^{i\delta})^{N-\frac{1}{2}} e^{-\xi|Q|} d(\xi e^{i\delta})$

$$= e^{i\delta(N+\frac{1}{2})}\int_0^\infty \xi^{N-\frac{1}{2}} e^{-\xi|Q|}\,d\xi$$

This integral may be evaluated in terms of the gamma function:

(11) $$Y = \frac{e^{i\delta(N+\frac{1}{2})}\Gamma(N+\frac{1}{2})}{|Q|^{N+\frac{1}{2}}} \equiv \frac{e^{i\delta(N+\frac{1}{2})}\lambda(N)\sqrt{\pi}}{|Q|^{N+\frac{1}{2}}}$$

Substituting in (9), we get:

(12) $$\chi = 4E\sqrt{\frac{2}{\pi r}}\,\mathrm{Re}\left\{m(c)\,e^{i\delta(N+\frac{1}{2})}\,e^{i\frac{\pi}{2}(p+\frac{1}{2})}\lambda(N)\sqrt{\pi}\;|Q|^{-(N+\frac{1}{2})}\right\}$$

If m(c) is cast in polar form: $= |m(c)|\,e^{i\psi(c)}$ then

(13) $$\chi = \frac{4E\sqrt{2}}{r^{\frac{1}{2}}|Q_{r,t}|^{N+\frac{1}{2}}}\,|m(c)|\,\lambda(N)\cos\left[\psi(c) + \frac{\pi}{2}(p+\tfrac{1}{2}) + (N+\tfrac{1}{2})\delta_{r,t}\right]$$

where:

$\delta = \frac{3}{2}\pi$ - phase (Q)

$Q = (r-ct)^2 - ih\gamma(c)$ where c is in general complex

$\lambda(N) = \frac{\Gamma(N+\frac{1}{2})}{\sqrt{\pi}}$

N = 2 + homogeneous degree of g/f

p = order of Bessel function

m(c) = excitation function depending on model and source

By subscripts r, t it is suggested that Q and δ are functions of the time and horizontal range. It is this dependence, in fact, which shapes the pulse. (13) may be cast in a more convenient form depending explicitly on the phase of Q (which we denote by ϕ).

$$(14) \quad \chi = \frac{4E\sqrt{2}}{r^{\frac{1}{2}}|Q_{r,t}|^{N+\frac{1}{2}}} |m(c)| \lambda(N) \cos\left[\phi_0 - (N+\tfrac{1}{2})\phi_{r,t}\right]$$

where $\phi_0 = \psi(c) + \pi + (p-N)\frac{\pi}{2}$

We shall use (14) to describe the shape of the pulse propagated along an interface due to complex poles, c, of the period equation. It is, therefore, necessary at this point to write down in tabular form the restrictions on the Riemann sheets for various values of t. These are taken from Table 2, or a similar table for two or three branch lines.

For all three problems the "lower" sheet for all variables (last line in Table 2) is identical to the "top" sheet. This is seen by inspection of the period equations (4). It is, therefore, not relevant to the description of the pole contributions.

(A) Free solid halfspace: $\beta_2 < c_2$

	Re α_2	Re α_2'
$0 < r/t < \beta_2$	+	+
$\beta_2 < r/t < c_2$	-	+

(B) Liquid halfspace/solid halfspace:

$$c_1 < \beta_2 < c_2$$

		Re α_1	Re α_2'	Re α_2
$0 < r/t < c_1$	(Stoneley wave)	+	+	+
$c_1 < r/t < \beta_2$	(Pseudo-Rayleigh)	-	+	+
$\beta_2 < r/t < c_2$	(Pseudo-P wave)	-	-	+

$$\beta_2 < c_1 < c_2$$

$0 < r/t < \beta_2$	+	+	+
$\beta_2 < r/t < c_1$	+	-	+
$c_1 < r/t < c_2$	-	-	+

$$\beta_2 < c_2 < c_1$$

$0 < r/t < \beta_2$	+	+	+
$\beta_2 < r/t < c_2$	+	-	+
$c_2 < r/t < c_1$	+	-	-

(C) Solid halfspace/solid halfspace:

$$\beta_1 < c_1 < \beta_2 < c_2$$

	Re α_1'	Re α_1	Re α_2	Re α_2'
$0 < r/t < \beta_1$	+	+	+	+
$\beta_1 < r/t < c_1$	-	+	+	+
$c_1 < r/t < \beta_2$	-	-	+	+
$\beta_2 < r/t < c_2$	-	-	-	+

$$\beta_1 < \beta_2 < c_1 < c_2$$

$0 < r/t < \beta_1$	+	+	+	+
$\beta_1 < r/t < \beta_2$	-	+	+	+
$\beta_2 < r/t < c_1$	-	+	-	+
$c_1 < r/t < c_2$	-	-	-	+

$$\beta_1 < \beta_2 < c_2 < c_1$$

$0 < r/t < \beta_1$	+	+	+	+
$\beta_1 < r/t < \beta_2$	-	+	+	+
$\beta_2 < r/t < c_2$	-	+	-	+
$c_2 < r/t < c_1$	-	+	-	-

All other combinations of body velocities are either trivial or physically inadmissable. Henceforth, we refer to a Riemann sheet by a sequence of +'s and -'s: e.g. (-+), (-++), or (-+-+).

Typical pulse shapes predicted by (14)

We now inspect the pulse representation (14) in enough detail to show its relation to the physics of the problem and demonstrate its agreement with known results for undamped surface waves. Written in terms of real quantities, Q has the form:

$$(15) \qquad Q = (r - vt + hy_2) - i\,(\eta t + hy_1)$$

where: $v = \mathrm{Re}\ c$ $\qquad y_1 = \mathrm{Re}\ \left(1 - c^2/c_1^2\right)^{\frac{1}{2}}$

$\eta = \mathrm{Im}\ c$ $\qquad y_2 = \mathrm{Im}\ \left(1 - c^2/c_1^2\right)^{\frac{1}{2}}$

Case (B) is taken as representative. We take a model typical of water in contact with a solid, with the source located in the water layer: $c_1 = 1.0$, $c_2 = 3.0$, $\beta_2 = 1.732$, and $\rho_2 = 2\rho_1$ (a Poisson solid):

sheet	v	η	type of wave
(+++)	.9860	-	Stoneley
(-++)	1.6151	.0980	Pseudo-Rayleigh
(--+)	3.036	-	Trivial pseudo-P
(--+)	3.917	-	

When Poisson's constant is taken to be .355, the situation is slightly different: $c_1 = 1.0$, $c_2 = 3.0$, $\beta_2 = 1.41$, and $\rho_2 = 2\rho_1$:

(+++)	.966	-	Stoneley
(-++)	1.348	.0917	Pseudo-Rayleigh
(--+)	2.768	.492	Pseudo-P

These results are taken from a later section, where the complex phase velocities for a representative class of models have been computed and presented in the form of arrival-time diagrams.

The pulse is shaped by (14) as follows. A cylindrical spreading term, $r^{-\frac{1}{2}}$, which multiplies the pulse amplitude, is identical with that obtained for point source excitation of true surface waves. If we were considering a line source problem this factor would be missing. The factor $|Q|^{-(N+\frac{1}{2})}$ determines the pulse envelope, and $(N + \frac{1}{2})\phi$, as an argument of a cosine function, determines oscillation of the signal within the pulse envelope. For all the cases considered in this paper, N = 2. Higher N corresponds to a field variable obtained by one or more spatial or time derivatives; its appearance in the phase factor makes sense from this point of view.

Stoneley wave: h = 0, $\eta = 0$. Q vanishes when t = r/v, namely at the arrival time of the wave whose velocity = Re c. There is, therefore, a singularity at the arrival time of the Stoneley wave. Also, m(c) is real, therefore $\psi(c) = 0$; for the pressure signal in the water, p = 0. Thus $\phi_0 = \pi + 0 + 0 + 3\pi = 4\pi \rightarrow 0$. When $t < r/v$, $\phi = 0$; when $t = r/v$, $\phi = -\frac{1}{2}\pi$ (assuming a small + imaginary η); when $t > r/v$, $\phi = -\pi$. Figure 3 shows: (1) Q as a function of t (in the complex plane), (2) a polar diagram of phase, (3) and the consequent pulse

shape, obtained by applying the envelope function and the cosine operation.

The singularity is, of course, a result of taking a delta function source in the first place, and is suggestive of the fact that the Stoneley wave is perfectly trapped and that the high frequencies are preserved in transmission. (The pulse shape shown is just that due to the Stoneley pole; when considered as part of an actual seismogram, we must "gate" the pulse on at $t = r/c_1$, and superimpose the contribution from the direct body wave. A similar qualification holds for all the pulse shapes we shall derive.)

When we take into account the separation of the source and interface, $h \neq 0$, $\eta = 0$, and $y_2 = 0$ (since $c = v < c_1$). Figure 4 shows the variation (with t) of Q, $(\phi_0 - (5/2)\phi)$, and x(t). The effect of removing the source from the interface is to remove the high frequencies from the interface wave. The source preferentially excites longer wavelengths; in the same way, a receiver not on the interface does not "see" shorter waves due to their greater localization near the interface.

The preceding has been to demonstrate the use of the representation (14), since the Stoneley wave is no newcomer, and has been thoroughly described in the literature. We now demonstrate its applicability to leaking interface waves. The results to be derived for the pseudo-Rayleigh wave will

bear out some of the properties discussed by Strick (1959) in his exact treatment. This is just a Rayleigh wave on the solid which loses energy by conversion into compressional waves radiating into the liquid. It, therefore, looks like an interface wave with respect to the solid, but has the properties of a critically refracted ray in the liquid. Its velocity is essentially that of a Rayleigh wave on a free halfspace. We set $h = 0$ in order to isolate the effect of η on the pulse shape. Then:

$$x \sim r^{-\frac{1}{2}} \left| (r - vt) - i\eta t \right|^{-5/2} \cos\left(\phi_0 - (5/2)\phi_{r,t}\right)$$

To ease the computation slightly, we set $\Psi(c) = 0$, an assumption which affects the phase of the wavelet, but not the point we wish to make. Figure 5 shows the construction of the waveform as before. The existence of $\mathrm{Im}\ c = \eta$ manifests itself in a smoothing of the waveform and a reduction of the maximum amplitude. In other words, the higher frequencies attenuate more rapidly than the lower frequencies. This is as it must be: The absence of a characteristic dimension in the geometry implies, by a similarity argument, that the decay range of a given frequency must be proportional to its wavelength.

For $h \neq 0$, we must take into account $y_1 + iy_2 = \sqrt{1 - c^2/c_1^2}$. c is nearly real, and $\mathrm{Re}\ c > c_1$. y_1 is, therefore, small and negative, while y_2 is large and positive. The sign choice is due to the fact that we are on the sheet where $\mathrm{Re}\ c_1 < 0$.

Then:

$$x \sim r^{-\frac{1}{2}} \left| (r - vt + hy_2) - i(\eta t - hy_1) \right|^{-5/2} \cos\left(\phi_0 - \tfrac{5}{2}\phi\right)$$

In harmonic wave theory, y_1 describes a wave increasing exponentially away from the interface. Here, its only effect is to decrease the bluntness of the pulse by counteracting the ηt term. Alternatively, we may say that the existence of a ray path into the liquid permits the source to communicate the high frequencies to the interface more efficiently than was possible for the wholly trapped Stoneley wave (and reciprocally). y_2 is responsible for a term which delays the peak amplitude of the pulse a time equal to the time required for the signal to reach the interface along the critical ray feeding the Rayleigh wave in the solid. Thus, while roots of the characteristic equation lying on lower Riemann sheets yield physically impermissible steady-state waves, the result of superposition in the time domain is physically quite reasonable.

The pseudo-P wave, which we shall discuss later in detail, is an intrinsic leaky vibration of a solid halfspace which does not "see" the liquid halfspace in a significant way. Energy is radiated away from the interface as shear energy into the solid and as P waves into the liquid. When $\sigma_2 = .355$, for example, the maximum pulse amplitude propagates at a velocity slower than c_2. The high imaginary part of c suggests that this pulse is very much blunted in comparison with the

Pseudo-Rayleigh wave. This pulse is identically zero prior to $t = r/c_2$, and "gates" on only with the arrival of the initial P phase. When $\sigma = .25$, the pair of roots which were complex conjugate for $\sigma = .355$ have degenerated to a pair of unequal real roots whose real parts exceed c_2. The main body of the corresponding pulse never exists, because the signal is constrained to vanish prior to $t = r/c_2$; at times shortly after the P-wave these poles may affect the signal slightly, giving the P-wave a slight tail.

Summary: The solution (14) is an asymptotic representation of a pulse propagated along a plane interface, due to complex roots of the period equation (4). The results are subject to the constraints of Tables 1 and 2, which denote the permitted Riemann sheets for any r, t. As pointed out by Strick (1959), these quasi-surface waves are not always physically separable on experimental or exact theoretical records due to their close association with body phases. The purpose of our demonstration has been to generalize the familiar long range expression of free surface waves to describe partially trapped waves in the same framework. A harmonic theory is not possible; we may, however, cast the real and complex roots of the period equation in the same framework. We interpret the complex roots as modes of motion which involve less coupling to body waves (radiation away from the interface) than neighboring motions (in a variational sense).

Having a single framework for both true surface waves

and complex surface waves, we hope that the nomenclature may become standardized. The resemblance between the true Rayleigh wave, the Stoneley wave for a liquid/solid interface, and the Stoneley wave for a solid/solid interface is superficial, since they arise by coupling to the lowest body wave velocity in the system, which is different in each case. We may now identify corresponding wave types for the 3 types of system; Strick (1959) has already established, for example, the correspondence of the true Rayleigh wave (A) with the pseudo-Rayleigh wave (B)

Mathematically, the solution has the following properties:

1. It was not necessary to approximate the second integral beyond using the long range representation of the Bessel function. If desired we could write out further terms in the asymptotic series for $J_p(kr)$ and obtain a more precise estimate of the pulse shape. As this is not our object, we defer to the exact solution by the method of Cagniard, should theoretical seismograms be desired.

2. The existence of characteristic roots on lower Riemann sheets is physically permissible. The only effect of $\mathrm{Re}\,\nu_i$ (be it + or -) is to modify the pulse shape slightly. $\mathrm{Im}\,\nu_i$, which is connected with radiating body waves, appears in a time delay due to the source-interface separation.

3. Reciprocity enables us to make the same remarks about a receiver at distance z from the interface as we have made concerning a source at h. By superposition we may consider both

simultaneously.

4. A pseudo-surface pulse will travel faster than certain of the body velocities and slower than the remainder. The former group will couple to the pulse as body waves in the relevant medium. The latter velocities cause the trapped portion of the energy. An instrument sensitive to body potentials with velocities $v_j > \mathrm{Re}\ c$ will see an exponential decrease away from the interface. One sensitive to wave potentials whose velocities $v_j < \mathrm{Re}\ c$ will see body waves feeding (or leaving) the interface at a critical angle θ: $\sin\theta = v_j/v$.

In what follows we shall display the complex roots of the period equation in a manner which is suggestive of the form of the pulse expression (14). $\underline{h}$ has the effect of modifying and delaying the pulse arrival; since propagation along the interface is of interest, we set $h = 0$. $\underline{v}$ is the velocity of the maximum pulse amplitude, and causes a broadening and weakening of the pulse. A rough measure of the pulse broadening may be obtained: We express the envelope function $|Q|^{-(N+\frac{1}{2})}$ in terms of the arrival time of the pulse and solve for the time where the envelope is down by some factor. It is assumed that $(\eta/v) < .3$, so that $(\eta/v)^2$ may be neglected in the result.

$$(16)\quad |\chi| \sim r^{-\frac{1}{2}} \left|(r-vt) - i\eta t\right|^{-(N+\frac{1}{2})} = r^{-\frac{1}{2}} r^{-(N+\frac{1}{2})} \left|(1-\frac{vt}{r}) - i\frac{\eta t}{r}\right|^{-(N+\frac{1}{2})} =$$

$$= r^{-(N+1)} \left|1 - t' - i\frac{\eta}{v}t'\right|^{-(N+\frac{1}{2})} = r^{-(N+1)} |P|^{-(N+\frac{1}{2})}$$

$t' = 1$ corresponds to the pulse maximum.

When $t' = 1$, $|P| = \eta/v$

When $t' = 1 + \tau$, $|P| = \sqrt{\tau^2 + \left(\frac{\eta}{v}\right)^2(1+\tau)^2}$ which we set equal to $m|P(1)| = m\eta/v$. Solving for τ and dropping $(\eta/v)^2$ in the result, we have an estimate of the half-width of the pulse in terms of its arrival time:

(17) $\tau \sim \sqrt{\left(\frac{\eta}{v}\right)^2(m^2-1)}$

If $n = 2$, $m = 2$ suffices to describe the point at which the pulse has about 1/6 peak amplitude. Using the formula $\tau = 1.7\ (\eta/v)$, we indicate the half-width in Figures 6-13 by the shading.

Another measure of pulse width in this case is the peak to trough time for the oscillatory center of the pulse. Under assumptions like those given above, $0.7(\eta/v)$ is an equivalent estimate, which we shall not use.

Setting $t' = 1$ in (16), we get an expression for the decay of the peak amplitude with distance.

(18) $\chi \sim r^{-(N+1)}\left(\frac{\eta}{v}\right)^{-(N+\frac{1}{2})} = r^{-\frac{1}{2}}\left(\frac{r\eta}{v}\right)^{-(N+\frac{1}{2})}$

Numerical results: These are plotted in the form of an arrival-time diagram. The horizontal axis is the time, normalized to the arrival of one of the body waves in the system. The vertical coordinate represents the variation of some function of the densities and body velocities; in this way we are able to show the behavior of the interface waves for a representative class of models. The arrival of the various body waves and true interface waves is represented by solid

lines, and the pseudo-waves are indicated by the arrival of the pulse maximum. Shading indicates the pulse width of the pseudo-waves according to (17). The areas between the body waves are labeled with the (-+++) notation to denote the relevant Riemann sheet for interface wave propagation.

The Lamb Problem

From equations (2-86) in Ewing, Jardetzky, and Press (1957), we may write the surface response to a compressional point source at depth. Generalized to a pulse, the horizontal and vertical displacements become (with a slight notational change):

$$(19)\quad q_o = \frac{4A}{\pi i}\int_{\lambda-i\infty}^{\lambda+i\infty} \frac{e^{st}}{s+\theta^{-1}}\,ds \int_0^\infty \frac{\left(-\alpha_2' k^2 \frac{s^2}{\beta_2^2}\right)}{f_A(k)}\, e^{-\alpha_2 h}\, J_1(kr)\,dk$$

$$(20)\quad w_o = \frac{2A}{\pi i}\int_{\lambda-i\infty}^{\lambda+i\infty} \frac{e^{st}}{s+\theta^{-1}}\,ds \int_0^\infty \frac{k\frac{s^2}{\beta_2^2}\left(2k^2+\frac{s^2}{\beta_2^2}\right)}{f_A(k)}\, e^{-\alpha_2 h}\, J_0(kr)\,dk$$

where $f_A(s,k)$ is the Rayleigh function in (4). These expressions have the form of (1). (14) results immediately, with:

	q_o	w_o
p	1	0
N	2	2

There are two relevant Riemann sheets. When $t > r/\beta_2$, we consider the sheet (++). When $r/\beta_2 > t > r/c_2$, we consider the sheet (-+). For all nontrivial values of ρ_2, β_2, c_2, a real root of $f_A(c)$ exists on the (++) sheet with a velocity near .92 β_2, the familiar Rayleigh wave. A pair of roots exists on the (-+) sheet. When β_2/c_2 is less than .52, these roots are real, unequal, and their velocities greater than

c_2; hence they do not contribute to the observed signal. For small values of β_2, the roots become complex conjugates, with velocities less than c_2 and greater than β_2. Since only roots with positive imaginary parts (on the lower sheets) are pertinent to our solution, a single pulse is predicted, arriving between the P and S waves. Since this pulse is trapped with respect to compressional motion and appears shortly after the P wave, we call it the Pseudo-P wave. Fig. 6 is the arrival-time diagram for Pseudo-P and the Rayleigh pulse, normalized to the arrival of the shear wave.

The shaded area on the figure represents roughly the extent of the Pseudo-P pulse. When $.3 < \sigma_2 < .45$ it appears as an appendage to the P-wave. When $\sigma_2 > .45$ it becomes distinct from both P and S; as $\sigma_2 \rightarrow .50$ (variable β_2, fixed c_2), the amplitude of Pseudo-P approaches zero, due to the very great time of arrival relative to the P-wave. When $\sigma_2 < .30$ no pulse occurs, although the images of the root are plotted using a dashed line. A familiar result states that, when $\sigma_2 = .25$, two "extraneous" real roots are found on the lower Riemann sheet. These have been interpreted as describing the angles at which shear waves are converted wholly into P-waves upon reflection by the free surface (or vice versa). We may generalize this interpretation: when $\sigma_2 > .30$, a shear wave incident on the free surface with a certain "complex angle of incidence" is converted entirely into a compressional motion critically refracted along the interface.

Conversely, a signal moving along the interface with velocity near c_2 (making it largely a P-wave) continually feeds a shear wave radiating into the solid. If we assume a pulse moving along the surface at a velocity between β_2 and c_2, then only radiating shear waves are possible. The particular velocity of Pseudo-P is that velocity which minimizes the loss by conversion to shear waves.

Gilbert and Laster have found Pseudo-P by evaluating the exact (Cagniard) closed form solution of Lamb's problem. In that framework the signal at times between the arrival of P and S is obtained by evaluating a certain function at a point near the branch cut. When $\sigma_2 > .30$, a pole lying on the lower sheet becomes so disposed with respect to the branch cut that it affects the value of the solution for certain values of time. The authors have reported a broad, ill-defined pulse coming after the P-wave, a result in agreement with the calculations reported here (Fig. 6). The method described in the present paper is valid only at long ranges and lacks the precision of the Cagniard method, but it gives us a simple tool for investigating the physical importance of the complex poles.

We do not claim that Pseudo-P would be an observed phase in field problems. It should be observed in model experiments, if sufficient control of the physical properties is possible. The physical importance of this wave is in its effect on leaking mode propagation in more elaborate wave-

guides. In a recent paper (Phinney, 1961), the leaking modes of a liquid layer coupled to a solid halfspace were determined. It was then noticed that the frequency of the first PL mode is somewhat less than expected on the basis of a simple ray theory. This effect becomes more pronounced as the shear velocity of the solid decreases. At the time it was hypothesized that this was due to coupling of the channel wave to an intrinsic long-period vibration of the halfspace. In this paper we have already shown that such a vibration does exist and that it propagates at velocities in common with the PL group velocity ($\beta_2 < c < c_2$).

The coupling effect is demonstrated by computing PL wave dispersion for several cases, whose properties resemble those permitting propagation of Pseudo-P. The following models are presented in Fig. 7.

Case	σ_2	β_2/c_2	
5	.10	.667	
6	.25	.577	$\rho_2 = 2\rho_1$
2	.32	.517	
8	.405	.400	$c_2 = 3c_1$
9	.45	.300	

The equivalent Lamb problems are indicated on Fig. 6 by case number. On Fig. 7 the arrows labeled (2), (8), and (9) represent the velocity of Pseudo-P in the halfspace, according to Fig. 6. For cases 5 and 6 the Pseudo-P root is degenerate and is not plotted; although the peak does not propagate in such cases, the tail of the pulse falls in the range ($\beta_2 < r/t < c_2$) and the corresponding PL mode is affected in

the immediate neighborhood of the P arrival. Since all systems of geophysical interest are layered (or worse), we conclude that Pseudo-P manifests itself indirectly, by coupling to leaking modal oscillations of a layered system.

We may test the physical meaning of waves such as Pseudo-P in another way. This wave is presumably coupled to shear waves radiating into the halfspace; it therefore loses energy by leakage. If this is correct, then we may stop the leakage by putting a perfectly reflecting bottom on the structure to trap the downward radiating shear waves. The perfectly trapped (normal) modes of a free elastic plate should then show coupling to the Pseudo-P wave of an elastic halfspace. At long wavelengths the appropriate wave is the extensional, or plate wave, whose velocity of propagation is given by the formula:

$$(21) \qquad \frac{c_P}{\beta_2} = 2\sqrt{1 - \frac{\beta_2^2}{c_2^2}}$$

This has been evaluated for various Poisson constants and plotted as a normalized arrival time in Fig. 6. The agreement of the plate wave with the Pseudo-P wave is very good, in the range where the latter exists.

Recent work on early-arriving waves, which are usually leaking waves, has tended to associate them with progressive elliptical surface motion as contrasted with the retrograde motion of Rayleigh waves. Oceanic and continental PL waves,

as well as the plate wave just cited, fall into this class. Typical numerical results pertinent to the Pseudo-P have been applied to (14) with the object of estimating the sense of the orbital ellipse. A rather flat prograde ellipse is found, having its major axis tipped backward about 45 degrees from the vertical. We may thus think of Pseudo-P as the basic progressive elliptical motion of a halfspace, dual to the Rayleigh motion. It manifests itself chiefly in similar motions of more complicated layered waveguides.

The liquid/solid interface problem

Having introduced the pseudo-P pulse, we are in a position to consider more complicated problems; we expect to find generalizations of the Pseudo-P and Rayleigh waves, as well as encountering the familiar Stoneley wave. In an earlier section, numerical data for this problem were used in a discussion of the behavior of (14). A complete physical discussion as well as representative numerical results are now offered.

The Stoneley wave, which has a velocity less than the least body wave velocity (usually the liquid velocity), propagates as a trapped wave with respect to all modes of motion. As is well known, the Stoneley wave exists for all non-trivial values of the wave velocities, and has been verified experimentally in recent model work (Roever and Vining, 1959; and Osborne and Hart, 1945). If we perturb Lamb's problem by imposing a liquid halfspace on the surface, the Rayleigh wave velocity will, for a great many cases, be greater than the compressional wave velocity in the liquid. The Rayleigh wave thus excites a radiating P-wave in the liquid, which serves to abstract energy from the interface. This leaking Rayleigh wave, or Pseudo-Rayleigh wave, has been discussed by Strick (1959) in the context of the closed algebraic solution (Cagniard). In our earlier discussion of the pulse solution (14) we have verified most of the properties discussed by Strick. The Pseudo-Rayleigh wave is the least

damped, and hence the most observable, of all the leaking wave types which arise from lower sheet roots of the period equation. In the numerical results schematically shown in Figs. 8 - 13, the Pseudo-Rayleigh wave is shown arriving directly after the S-wave, with a pulse width which involves the initial S motion. When the shear velocity is nearly the same as the liquid velocity, the Pseudo-Rayleigh wave ceases to exist. If $c_1 > \beta_2$ the Rayleigh motion is manifest in the Stoneley wave.

It is to be noted that seeming disagreement exists with a result in Strick's paper. We show that the Pseudo-Rayleigh velocity is nearly equal to the true Rayleigh velocity (Fig. 6) as $\beta_2 \rightarrow .707 c_2$, with considerable disagreement as $\beta_2 \rightarrow c_1$. Strick showed that the two velocities were always the same. We have defined the pulse velocity by the velocity of the pulse envelope maximum, while Strick computed the velocity of a zero-crossing in the pulse. Thus no contradiction actually exists. Details about the signal as $\beta_2 \rightarrow c_1$ must be resolved by numerical evaluation of the closed form solution.

The generalization, for the liquid/solid interface, of the Pseudo-P pulse is shown in Figs. 8 - 13. The pole is on the Riemann sheet appropriate to radiation as shear waves and as P-waves in the liquid, but describing trapped P-waves in the solid, namely the sheet (--+). The figures show that Pseudo-P is little affected by the liquid when a poor impedance match occurs between the media. When one or both

of the solid velocities is near to or less than c_1, Pseudo-P differs considerably in breadth and velocity from the "standard" in Lamb's problem.

If $\beta_2 < c_1$, the sheet (+-+) is relevant to the motion when $r/\beta_2 > t > r/c_1$. It is seen in the figures that a root occurs with a velocity roughly 1.4 - 1.5 times the shear velocity. The pulse breadth (17) is so great that we can hardly regard this wave as easily observable. Its amplitude must be quite small in view of the long times at which it arrives. We suggest that it may be a manifestation of Pseudo-P motion, much as the Rayleigh motion is described by two different branches, depending as $c_1 < \beta_2$, or vice versa. This is probably the same root encountered by Strick, by a zero-crossing formula, with a velocity $\sqrt{2}$ times the shear velocity.

Figure 12 deserves special comment. It shows the effect on the Pseudo-P and Pseudo-Rayleigh waves of varying the density ratio. $\beta_2/c_2 = .43$ is chosen to insure that Pseudo-P is not degenerate. When ρ_1 becomes greater than ρ_2, the increased impedance of the liquid rapidly suppresses the free motion of the solid. The effect is less drastic on Pseudo-P than on Pseudo-Rayleigh, since the former is largely a compressional motion parallel to the interface and involves less coupling from solid to liquid.

The solid/solid interface problem:

Numerical results for this problem will be reported in a separate paper. Due to the increased number of parameters involved, many figures will be required to even outline the general behavior of the pseudo-waves. The following general results may be mentioned here.

If the slow halfspace is viewed as a perturbation of the faster medium, we find pseudo-P and pseudo-Rayleigh coupled to the P and S waves of the faster medium, with radiation into the slower material. If the faster medium is viewed as a perturbation of the slower, we find that it suppresses the pseudo-waves in the slower material, although roots may be found which are trivial in the sense that they do not contribute appreciably to the signal. The true Stoneley wave for this problem appears as a very special case of the pseudo-Rayleigh wave in the faster medium, when its velocity turns out to be slower than all four body wave velocities. Gilbert and Laster have treated this problem from the point of view of the exact (Cagniard) solution, and our numerical results should provide a valuable complement to their detailed discussion.

Appendix 1

In this appendix we provide a little more detail regarding the assertions in the introduction. We claimed that equations (2) and (3) may be applied to the deduction of leaking mode dispersion in plane seismic waveguides with any number of layers. We also stated that problems involving two halfspaces (and any number of layers) are susceptible to the same equations if the results regarding permissible Riemann surfaces are generalized. This latter point, in particular, formed an integral part of the discussion on leaking interface waves. Enough steps will be demonstrated to enable the reader familiar with the author's previous paper (Phinney, 1961), denoted by I, to derive the results stated.

Generalization to multilayered waveguides:

If we assume a structure consisting of m - 1 solid layers bounded above by a free surface and bounded below by a solid halfspace, we may write the response as a ratio of two determinants of order $4m - 2$.

(B-1) $$g_j/f = \Delta_j/\Delta$$

Both expressions are even in the variables α_i, α_i' $(i < m)$. Only the variables α_m, α_m' generate branch cuts in the s $(=i\omega)$ plane. As these quantities occur in only two wave potentials, they appear in only two columns of either determinant. Inspection of equation (4-276) in Ewing, Jardetzky, and Press, (1957), showing the form of the determinant, shows that we may write:

(B-2) $$\Delta = a_0 + a_1\alpha_m + a_2\alpha_m' + a_3\alpha_m\alpha_m' = f$$

$$\Delta_j = b_0 + b_1\alpha_m + b_2\alpha_m' + b_3\alpha_m\alpha_m' = g$$

The expressions (B-2) may now be substituted into (1) and the development of paper I carried out. We refer to equations A-1, A-2, . . which are located in the appendix to I.

Equations A-1 through A-3 remain unchanged under the use of (B-2), and (A-4) may be deleted. The first sheet modal contribution to the signal is described by (A-5). A generalization of the response factor (A-6) yields:

(B-3) $$F_1(s_n,k) = \left(\frac{g}{\frac{\partial f}{\partial s}}\right)_{s=s_n} = \left[\frac{b_0 + b_1\alpha_m + b_2\alpha_m' + b_3\alpha_m\alpha_m'}{\frac{\partial f}{\partial s}}\right]_{s=s_n}$$

The development in I continues; if α_m and α_m' are considered where α_2 and α_2' appear in I, we need only to rewrite the expressions for the response factors as they are transformed. (A-9) becomes:

(B-4) $$F_2(s_n,k) = \frac{g^*}{f^*} - \frac{g}{f} = \frac{b_0+b_1\alpha_m-b_2\alpha_m'-b_3\alpha_m\alpha_m'}{f^*} - \frac{b_0+b_1\alpha_m+b_2\alpha_m'+b_3\alpha_m\alpha_m'}{f}$$

$$= \frac{2\alpha_m'}{ff^*}\left\{(b_0+b_1\alpha_m)(a_2+a_3\alpha_m) - (b_2+b_3\alpha_m)(a_0+a_1\alpha_m)\right\}$$

(A-11) now takes the form:

(B-5) $$F_3(s_n,k) = \frac{g^{***}}{f^{***}} - \frac{g}{f} = \frac{2\alpha_m}{ff^{***}}\left\{(b_0+b_2\alpha_m')(a_1+a_3\alpha_m') - (b_1+b_3\alpha_m')(a_0+a_2\alpha_m')\right\}$$

(A-14) becomes:

(B-6) $$F_2'(s_n,k)\Big]_{II} = \left\{\frac{2\alpha_m'}{f\frac{2f^*}{2s}}\left[(b_0+b_1\alpha_m)(a_2+a_3\alpha_m) - (b_2+b_3\alpha_m)(a_0+a_1\alpha_m)\right]\right\}_{s=s_n}$$

which is evaluated (subscript n) at the roots of f^*.

Now: $f^* - f = -2\alpha_m'(a_2 + a_3\alpha_m)$. When $f^* = 0$, $f_n = 2\alpha_m'(a_2 + a_3\alpha_m)$. Also: $a_0 + a_1\alpha_m = \alpha_m'(a_2 + a_3\alpha_m)$. (B-6) thus reduces to:

$$(B\text{-}7)\quad \left[F_2'(s_n,k)\right]_{II} = \frac{\left[b_0 + b_1 d_m - d_m'(b_2 + b_3 d_m)\right]_n}{\left(\frac{\partial f}{\partial s}\right)_n} = \left[F_1(s_n,k)\right]_{II}$$

which is the same result obtained in I (eq. A-16). F_2'' and F_2''' may be treated in the same manner, yielding the analogous result, which is stated in equations (A-25) and (A-26). Evaluation of the contribution P_{BP} follows the same lines, yielding equations (A-37) and (A-38) as written.

We conclude that the results of paper I may be taken over with only minor alterations. The exact functional dependence of the a_i and the b_i on ω and k differs from case to case and therefore defines an $F_1(s_n,k)$ and a Q_n^c which carry all the specific information about the model not given directly by the period equation $f = 0$.

Generalization to two halfspaces (three or four branch cuts).

Two solid halfspaces or one solid halfspace and one liquid halfspace are considered as bounding a plane layered seismic waveguide. Medium 1 occupies $z < 0$ and medium 2 occupies $z > D > 0$. One or more layers occupy the region $D > z > 0$. Since the existence of these finite layers does not increase the number of branch points, it is unnecessary to acknowledge their existence in the following discussion.

Using the development of paper I, we may locate the singularities in the complex s-plane. It is sufficient to restrict consideration to the upper half plane. There will be four branch points in the upper half plane, joined by cuts to $s = i\infty$. Since the layer velocities c_1, β_1, c_2, β_2, may satisfy various inequalities among themselves, we merely call them v_1, v_2, v_3, v_4, where $v_1 < v_2 < v_3 < v_4$. The radicals generating the branch cuts will be of the form $\nu_i = \sqrt{k^2 + s^2/v_i^2} \quad = \sqrt{k^2 - \omega^2/v_i^2}$; the branch points will consequently lie at $s = ikv_i$ (Figure 15).

We denote a Riemann sheet by a sequence of p's and m's. For example, (pmmp) denotes the sheet where $\mathrm{Re}\,\nu_1 > 0$, $\mathrm{Re}\,\nu_2 < 0$, $\mathrm{Re}\,\nu_3 < 0$, and $\mathrm{Re}\,\nu_4 > 0$. This notation refers to the velocities arranged in increasing order of magnitude, and differs from the (+--+) notation used in the main text, which refers to specific velocities. The single integral solution (2) will be represented by the symbol X. The appropriate Riemann sheet will be designated by the symbol, e.g. (pmmp), as an argument of the symbol X. For example:

$$(B\text{-}8)\quad 4A \sum_{n=0}^{\infty} \int_{S_{II}} J_0(kr)\, k\, \frac{e^{s_n t}}{s_n + \theta^{-1}} \left[F_1(s_n, k)\right]_{II}\, dk \quad = X_{II} = X(mp)$$

An algebraic sign is also necessary to specify the result.

In I the individual branch line and pole contributions behaved as follows:

Top sheet poles: $P_R = X_I = X(pp)$: all r,t

First branch line: $P_{BS} = -X_I = -X(pp)$: $t > r/\beta_2 \equiv r/v_1$

$-X_{II} = -X(mp)$: $t > r/v_1$

Second branch line: $P_{BP} = X_{II} = X(mp)$: $t > r/c_2 \equiv r/v_2$

$-X_{III} = -X(mm)$: $t > r/v_2$

When all contributions are summed, we find:

X(pp) contributes when $t > r/v_1$

X(mp) contributes when $r/v_1 > t > r/v_2$

-X(mm) contributes when $t > r/v_2$

subject to the restriction that roots on the lower two sheets contribute only over the range of k such that $\mathrm{Im}[\omega_n(k)] > 0$, k being real and positive (or with a very small negative imaginary part).

The evaluation of P_{BP} was typical of the result to be obtained if one of several branch cuts is evaluated. Suppose that there are four branch cuts; consider the way in which P_{B3} will transform under the contour deformations of I (Fig. 16). The original branch line integral on the top sheet will have f(pppp) and f(ppmp) as factors in the denominator, after the two sides of the branch line contour have been algebraically combined into a single contour on the right side of the cut. If this contour is deformed into the second quadrant by a 90° counterclockwise rotation, all the quantities in the integrand go onto the lower sheet with respect to $\sqrt{}_1$, $\sqrt{}_2$, and $\sqrt{}_3$. I. e., f(pppp) $\longrightarrow$ f(mmmp) and f(ppmp) $\longrightarrow$

f(mmpp). Since the contour did not cross the fourth branch cut in being deformed, the fourth index remains unchanged.

Following the technique employed in I, it may be eventually concluded that when $t > r/v_3$, modal contributions result, in the form of the terms X(mmpp) and -X(mmmp). When $t < r/v_3$, the contour integrals in the s-plane converge only if they are transformed in a way which causes both terms to vanish. In general, P_{B1} will transform like P_{BS}; P_{B2} will behave like P_{BP}; P_{B3} and P_{B4} behave similarly, as we have outlined above. A table of all modal contributions may then be constructed:

Top sheet poles:	$P_R =$ X(pppp)	all r,t
First branch line:	$P_{B1} =$ -X(pppp)	$t > r/v_1$
	-X(mppp)	$t > r/v_1$
Second branch line:	$P_{B2} =$ X(mppp)	$t > r/v_2$
	-X(mmpp)	$t > r/v_2$
Third branch line:	$P_{B3} =$ X(mmpp)	$t > r/v_3$
	-X(mmmp)	$t > r/v_3$
Fourth branch line:	$P_{B4} =$ X(mmmp)	$t > r/v_4$
	-X(mmmm)	$t > r/v_4$

Summation of the terms in this table yields the following statements defining the permissible Riemann sheets for different values of time.

X(pppp)	$t > r/v_1$
X(mppp)	$r/v_1 > t > r/v_2$
X(mmpp)	$r/v_2 > t > r/v_3$
X(mmmp)	$r/v_3 > t > r/v_4$
-X(mmmm)	$t > r/v_4$

These results are subject to the restriction that roots on the lower four sheets contribute only over the range of k such that $\mathrm{Im}[\omega_n(k)] > 0$, where k lies on a contour running from 0 to ∞ just below the real positive k-axis.

Appendix 2

It is easily shown that the exact closed form solution by Cagniard's method yields restrictions on pole contributions from the lower Riemann sheets analogous to those found by the more traditional analysis. To simplify the algebra, we set $h = z = 0$. This method is, of course, applicable only to the unlayered, simple interface problem.

The Fourier transform of $x(t)$ may be reduced to a one-sided transform by virtue of $x(t)$ vanishing prior to $t = 0$:

$$\overline{x} = \int_{-\infty}^{\infty} x(t)\, e^{-i\omega t} dt = \int_{0}^{\infty} x(t)\, e^{-i\omega t} dt$$

Setting up steady state solutions of the wave equation which satisfy the boundary conditions on the interface, we obtain:

$$\overline{x} = A\, S(\omega) \int_{0}^{\infty} \frac{g(\omega,k)}{f(\omega,k)}\, k\, J_p(kr)\, dk$$

where $S(\omega)$ is the Fourier transform of the source time dependence.

We now consider the solution at sufficiently long range that we may approximate the Bessel function and drop the inward traveling wave.

$$J_p(kr) = H_p^{(1)}(kr) + H_p^{(2)}(kr) \longrightarrow H_p^{(2)}(kr) \sim \sqrt{\frac{2}{\pi kr}} \exp\left[-i(kr - \pi/4 - p\pi/2)\right]$$

Then:

$$\overline{x} = A\, S(\omega)\, e^{\frac{1}{2}\pi i(p + \frac{1}{2})} \sqrt{\frac{2}{\pi r}} \int_{0}^{\infty} \frac{g(\omega,k)}{f(\omega,k)}\, k^{\frac{1}{2}}\, e^{-ikr}\, dk$$

If we set $u = k/\omega$, then $dk = \omega\, du$ and:

$$\bar{x} = A\, S(\omega)\, e^{\frac{1}{2}\pi i(p+\frac{1}{2})}\sqrt{\frac{2}{\pi r}} \int_0^\infty \frac{g(\omega,u\omega)}{f(\omega,u\omega)}(u\omega)^{\frac{1}{2}}\, e^{-iu\omega r}\omega\, du$$

Now set $\tau = ur$: $du = d\tau/r$:

$$\bar{x} = A\, S(\omega)\, e^{\frac{1}{2}\pi i(p+\frac{1}{2})}\sqrt{\frac{2}{\pi r}} \int_0^\infty \frac{g(\omega,\omega\tau/r)}{f(\omega,\omega\tau/r)}\left(\frac{\omega}{r}\right)^{\frac{3}{2}}\tau^{\frac{1}{2}}\, e^{-i\omega\tau}\, d\tau$$

For solvable cases (simple interface problem) g and f are homogeneous in ω. If f and g are now factored, the resulting power of ω will just be the difference in homogeneous degree of f and g. We set this equal to N - 2 to conform with the convention used in the main text.

$$\bar{x} = A\, S(\omega)\, e^{\frac{1}{2}\pi i(p+\frac{1}{2})}\sqrt{2/\pi}\ \omega^{N-2}\ \omega^{\frac{3}{2}} r^{-2} \int_0^\infty \frac{g(1,\tau/r)}{f(1,\tau/r)}\ \tau^{\frac{1}{2}}\, e^{-i\omega\tau} \cdot d\tau$$

When $S(\omega) = 1$, the source is a delta function; when $S(\omega) = 1/i\omega$, the source is a unit step. By taking $S(\omega) = 1/\sqrt{i\omega}$, we simplify the analysis as well as represent a source somewhere between the step and delta function.

$$\bar{x} = A\sqrt{2/\pi}\, e^{\frac{1}{2}p\pi i}\ \omega^{N-1}\ r^{-2} \int_0^\infty \frac{g(1,\tau/r)}{f(1,\tau/r)}\ \tau^{\frac{1}{2}}\, e^{-i\omega\tau}\, d\tau$$

The time function corresponding to $\bar{x}$ is now obtained by inspection:

$$x = A\sqrt{2/\pi}\, e^{\frac{1}{2}p\pi i} r^{-2}\, e^{-\frac{1}{2}(N-1)\pi i}\, \frac{d^{N-1}}{dt^{N-1}}\left\{ t^{\frac{1}{2}}\, \frac{g(1,t/r)}{f(1,t/r)}\right\}$$

where the variable t runs from 0 to ∞ along the real τ-axis.

The radicals ν_i which generate branch cuts must be expressed in terms of τ.

$$\nu_i = \sqrt{k^2 - \frac{\omega^2}{v_i^2}} = \omega \sqrt{\frac{t^2}{r^2} - \frac{1}{v_i^2}} = \omega \nu_i^+$$

If the Riemann sheets are defined as before, with Re $\nu_i = 0$ defining the cuts, we may locate the singularities in the τ-plane.(Fig. 17). We assume t to lie along the bottom bank of the cut.

When t lies between two of the branch points in the τ-plane, the value of g/f is affected by any poles near $\tau = t$. There are none on the top sheet except the surface wave pole lying on the real axis at $t > r/v_1$. There may be poles on lower sheets, however, and one which is contiguous to the point t will affect the signal in that range. This is made clear by redrawing the branch cuts so as to expose those portions of the lower sheets which represent a continuation of the real τ-axis into the first quadrant. Portions of the τ-plane (Fig. 18) so cut which do not lie on the first sheet are indicated by the conventional notation (mppp), (mmpp), . . etc. Note that for the interface wave problem (mmmm) and (pppp) have the same poles.

The result demonstrated in the previous appendix and used in the main text is now apparent from inspection of the figure. When t lies between the arrival times of two body waves, the signal may be influenced by zeroes of f

lying on the Riemann sheet contiguous to t. This is the same conclusion obtained by the longer analysis based on the straightforward evaluation of the double integral form of the solution. Table 2 in the main text will be seen to be equivalent to the results demonstrated graphically in Figure 18.

We might write down a formula which isolates the effect of such a lower sheet pole in the τ-plane and attempt a close comparison with the pulse expression (14) obtained in the main text. The difference between the two representations is too great, however: In the τ-plane, proximity of the branch point manifests itself by multiplying the effect of the pole. The analysis in this paper leaking up to (14) separates the pole contributions from the body waves in such a way that they <u>add</u> to give the total signal.

Acknowledgements

The author wishes to thank Dr. Frank Press for his advice and encouragement throughout this work.

This research was partially supported by Contract No. DA-04-495 Ord. 1808 (Model Seismology) of the Office of Ordnance Research, U. S. Army.

The author is a National Science Foundation predoctoral fellow.

REFERENCES

Cagniard, L.

1939. Reflexion et Refraction des ondes Seismique Progressives, Gauthier-Villars, Paris. 255 pp.

Ewing, W. M., W. S. Jardetzky, and F. Press

1957. Elastic Waves in Layered Media, McGraw-Hill, New York. 379 pp.

Garvin, W. W.

1956. "Exact Transient Solution of the Buried Line Source Problem," Proc. Roy. Soc. A., 234: 528-541.

Gilbert, F.

1956. "Seismic Wave Propagation in a Two-Layer Half-Space," Ph.D. thesis, Massachusetts Institute of Technology.

Gilbert, F., and S. L. Laster

1961. unpublished report

Ginzbarg, A. S., and E. Strick

1958. "Stoneley-Wave Velocities for a Solid-Solid Interface," Bull. Seism. Soc. Am., 48: 51.

Osborne, M. F. M., and S. O. Hart

1945. "Transmission, Reflection, and Guiding of an Exponential Pulse by a Steel Plate in Water, I Theory," Jour. Acoust. Soc. Am., 17: 1-18.

REFERENCES (cont'd)

Phinney, R. A.

1961. "Leaking Modes in the Crustal Waveguide Part I: The Oceanic PL Wave," Jour. Geophys. Res., (in press).

Roever, W. L., and T. F. Vining

1959. "Propagation of Elastic Wave Motion from an Impulsive Source Along a Fluid-Solid Interface. I, Experimental Pressure Response," Phil. Trans. Roy. Soc. A., 251: 455-465.

Rosenbaum, J. H.

1960. "The Long-Time Response of a Layered Elastic Medium to Explosive Sound," Jour. Geophys. Res. 65: 1577-1614.

Scholte, J. G.

1949. "On True and Pseudo-Rayleigh Waves," Proc. Kon. Ned. Akad. Wetensch. Amst., 52: 652-653.

Stoneley, R.

1924 "Elastic Waves at the Surface of Separation of Two Solids," Proc. Roy. Soc. A., 106: 416-428.

Strick, E.

1959. "Propagation of Elastic Wave Motion from an Impulsive Source Along a Fluid-Solid Interface. Parts II and III," Phil. Trans. Roy. Soc. Lon. A, 25: 465-523.

Strick, E., and A. S. Ginsbarg

1956. "Stoneley-Wave Velocities for a Fluid-Solid Interface," Bull. Seism. Soc. Am., 46: 281.

List of Captions

Figure Number

1. Three classes of interface wave problem.

2. k-plane and ξ-plane for integration of (10).

3. Q-plane, $[\phi_0 - (5/2)\phi]$, and x as functions of t. Stoneley wave: $h = 0$, $\eta = 0$.

4. Q-plane, $[\phi_0 - (5/2)\phi]$, and x as functions of t. Stoneley wave: $h \neq 0$, $\eta = 0$.

5. Q-plane, $[\phi_0 - (5/2)\phi]$, and x as functions of t. Pseudo-Rayleigh wave: $h = 0$, $\eta \neq 0$.

6. Normalized arrival time diagram for Lamb's problem. Effect of variable β_2/c_2.

7. Coupling of Pseudo-P to group velocity of first PL mode: liquid layer overlying a solid half-space. Effect of variable β_2/c_2. Pseudo-P velocities for Cases 2, 8, 9 shown by arrows.

8. Normalized arrival time diagram for liquid/solid interface. Effect of variable β_2/c_2. $c_2/c_1 = 5$.

9. Normalized arrival time diagram for liquid/solid interface. Effect of variable β_2/c_2. $c_2/c_1 = 3$.

10. Arrival time diagram of Fig. 9 renormalized to arrival of the shear wave.

11. Normalized arrival time diagram for variable c_2.

12. Normalized arrival time diagram for variable density contrast.

13. Normalized arrival time diagram for liquid/solid interface. Effect of variable β_2/c_2. $c_2/c_1 = 1.20$.

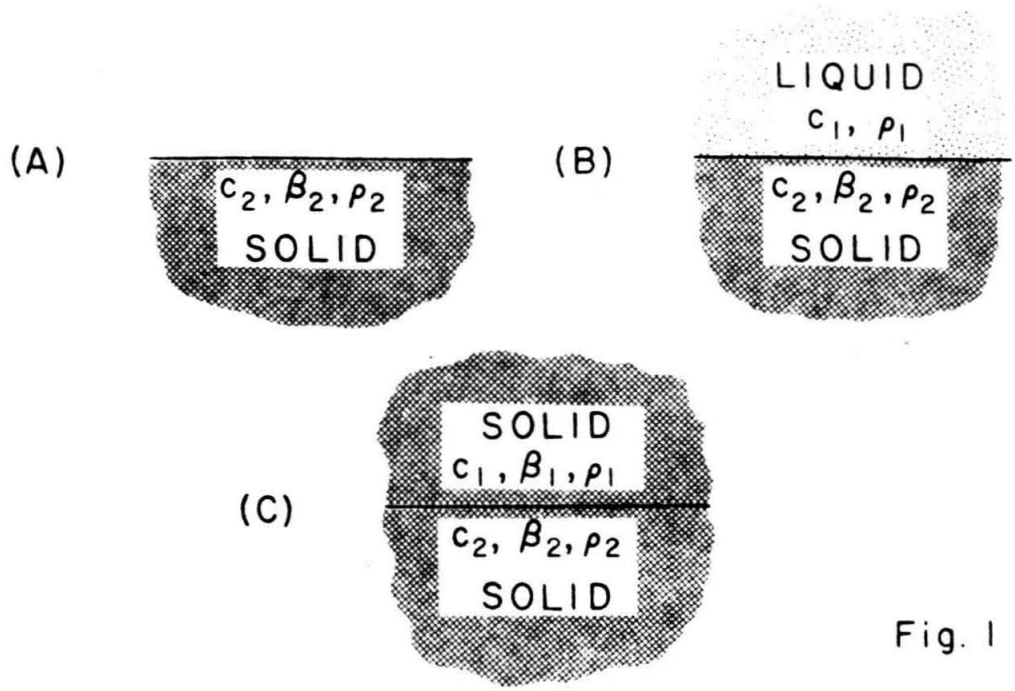
(A)
c_2, β_2, ρ_2
SOLID
(B)
LIQUID
c_1, ρ_1
c_2, β_2, ρ_2
SOLID
(C)
SOLID
c_1, β_1, ρ_1
c_2, β_2, ρ_2
SOLID

Fig. 1

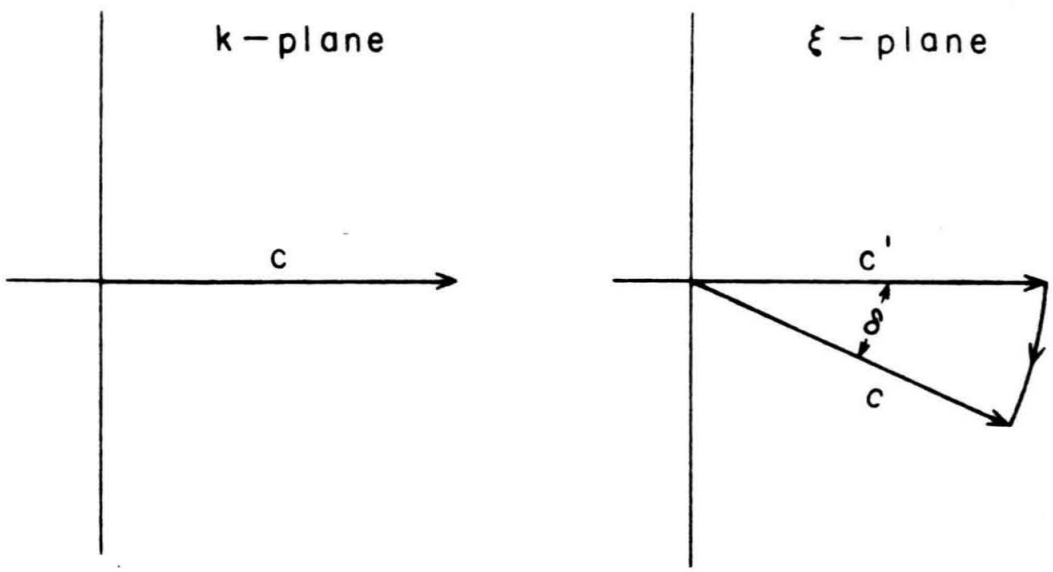
k – plane
c
ξ – plane
c'
δ
c

Fig. 2

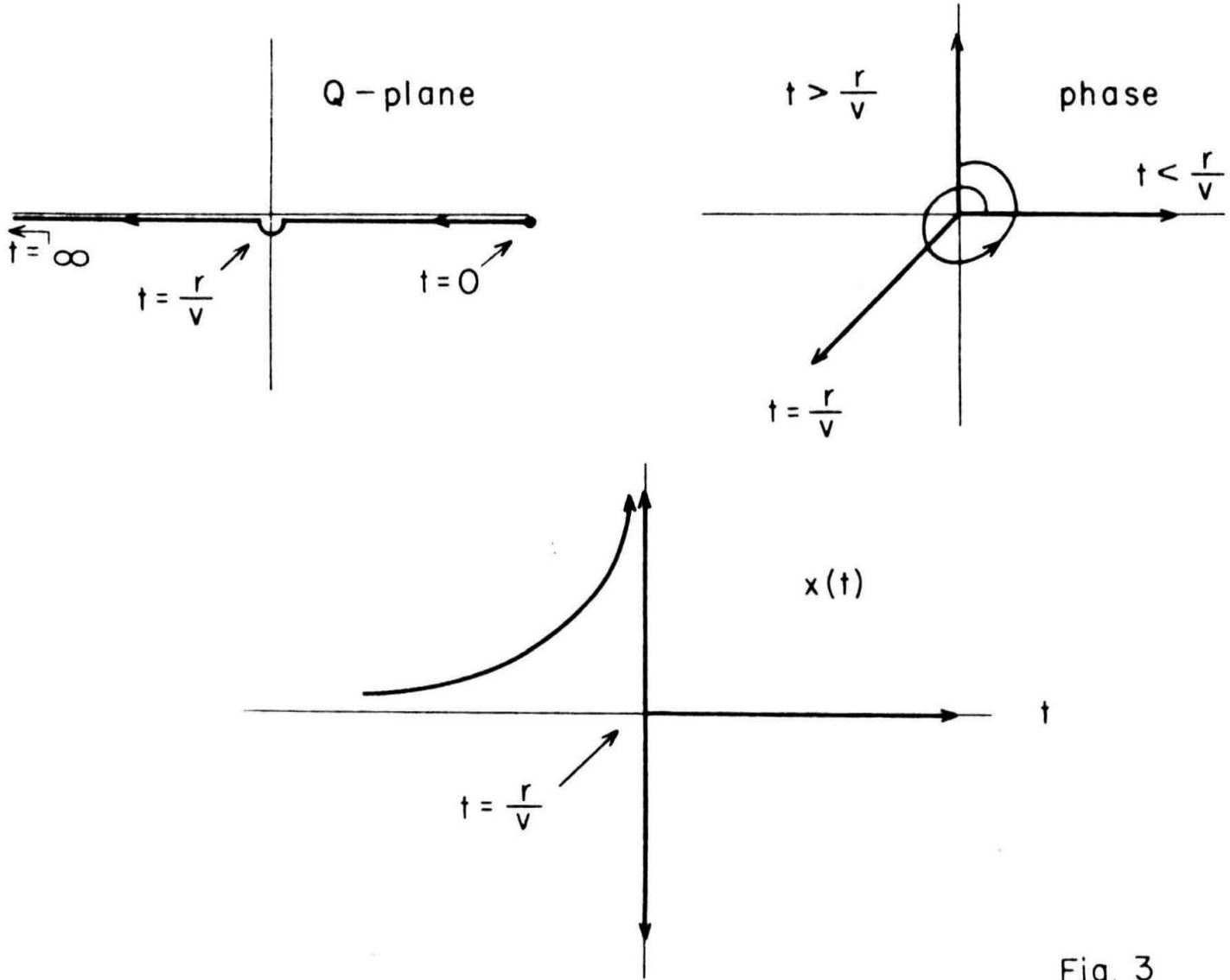

Fig. 3

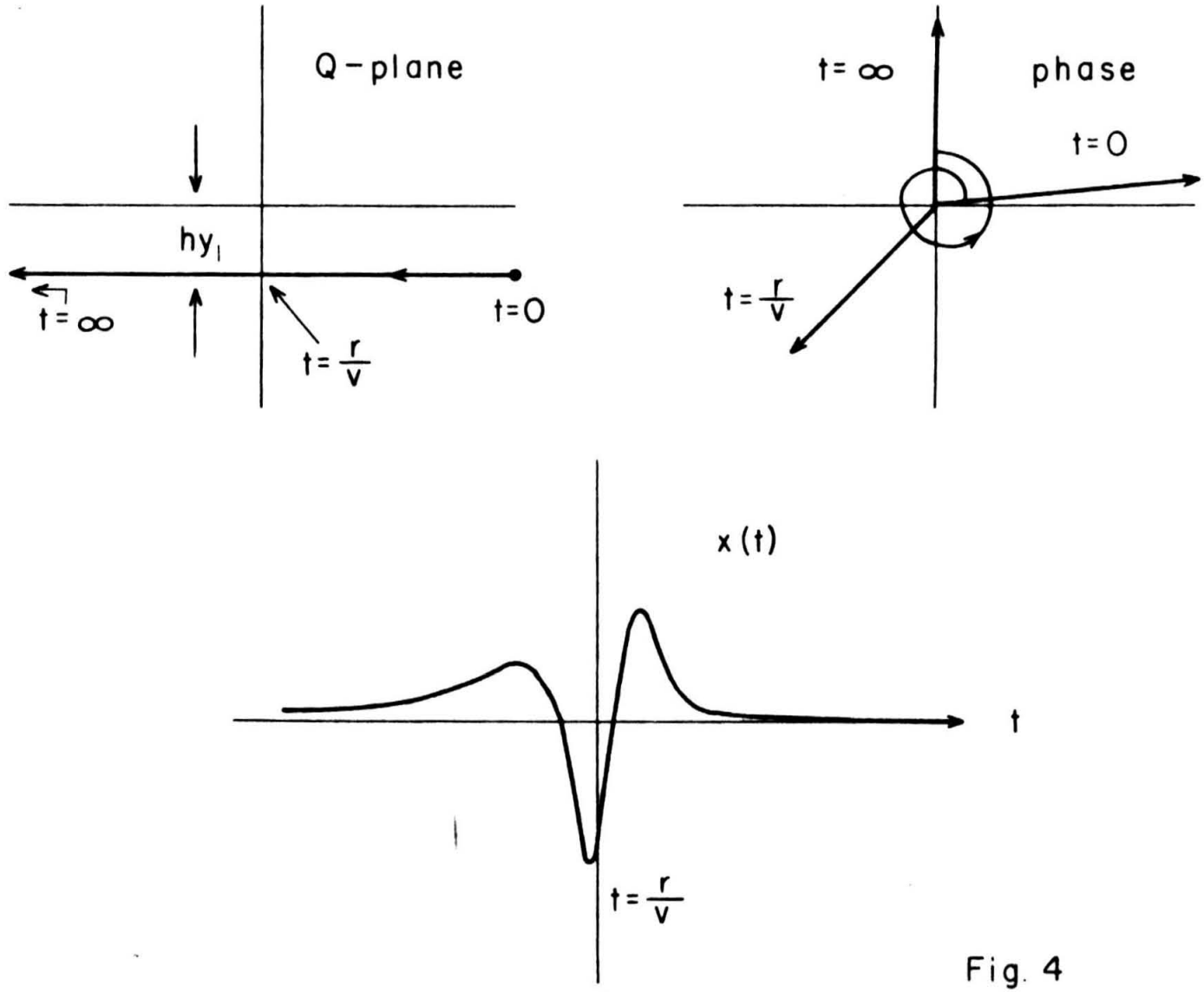
Q-plane
hy_1
$t=\infty$
$t=0$
$t=\frac{r}{v}$
$t=\infty$
phase
$t=0$
$t=\frac{r}{v}$
x(t)
t
$t=\frac{r}{v}$

Fig. 4

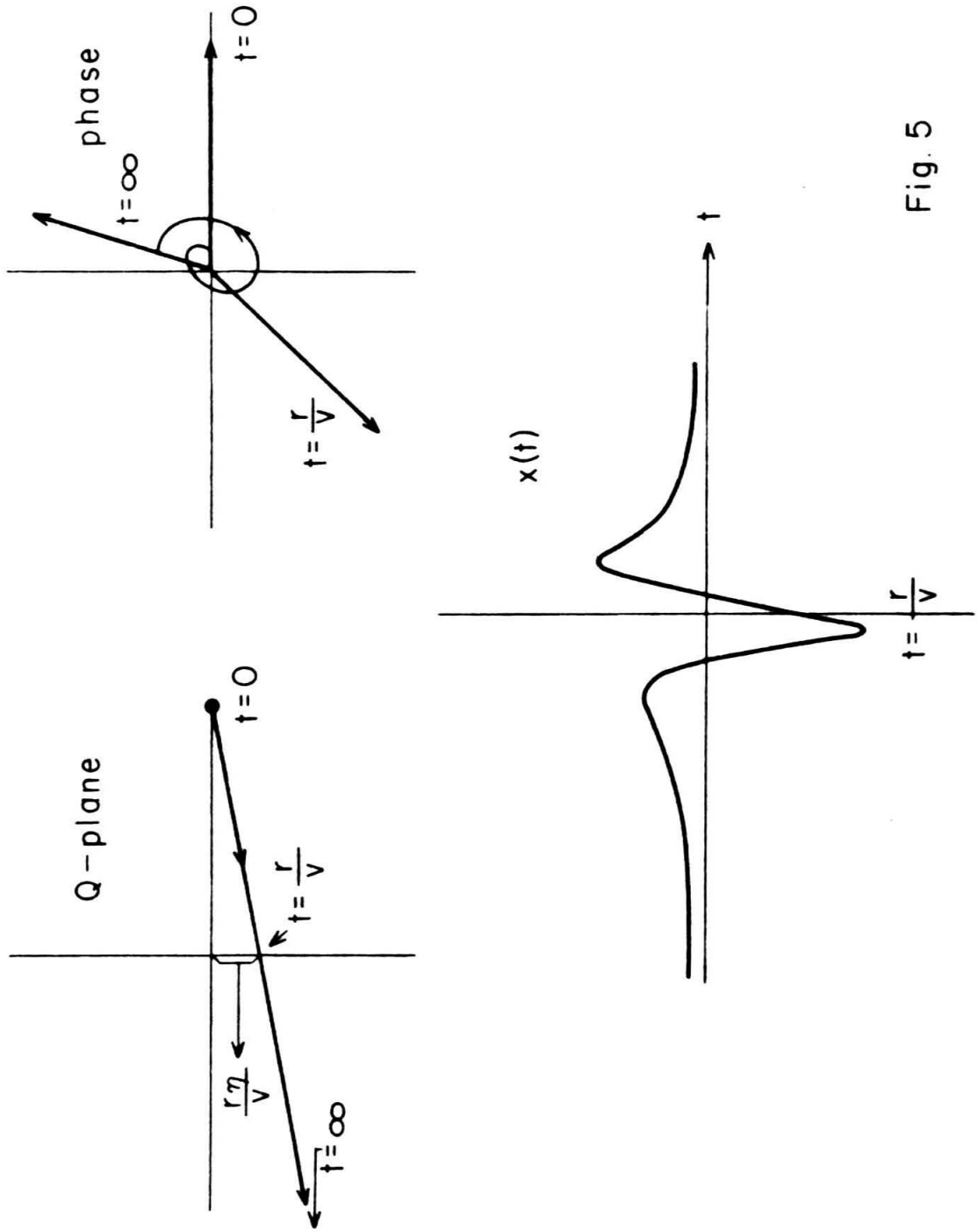

Fig. 5

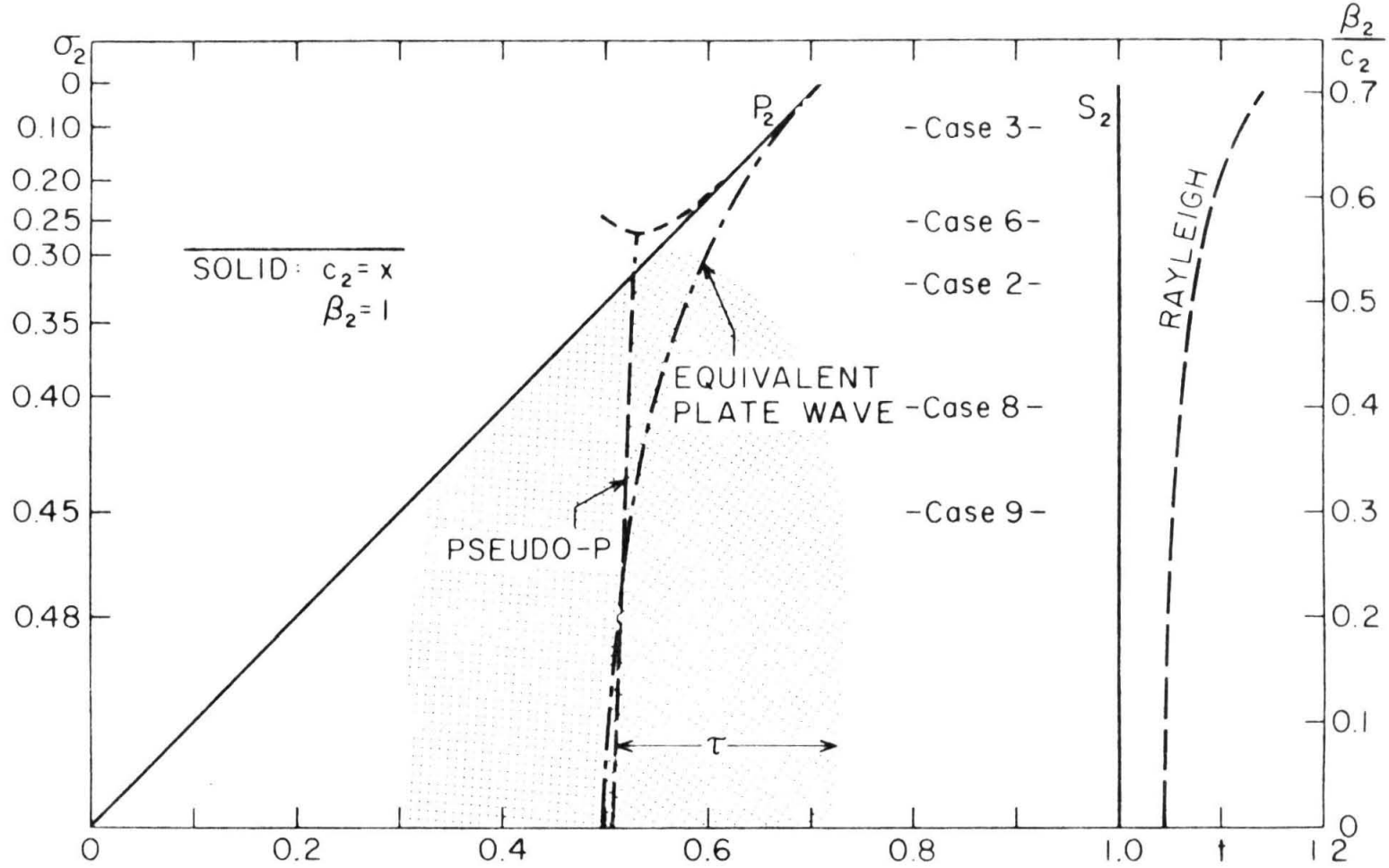
σ_2
0
0.10
0.20
0.25
0.30
0.35
0.40
0.45
0.48
$\frac{\beta_2}{c_2}$
0.7
0.6
0.5
0.4
0.3
0.2
0.1
0
0
0.2
0.4
0.6
0.8
1.0
t
1.2
SOLID: $c_2 = x$
$\beta_2 = 1$
P_2
S_2
RAYLEIGH
-Case 3-
-Case 6-
-Case 2-
-Case 8-
-Case 9-
EQUIVALENT
PLATE WAVE
PSEUDO-P
τ

Fig. 6

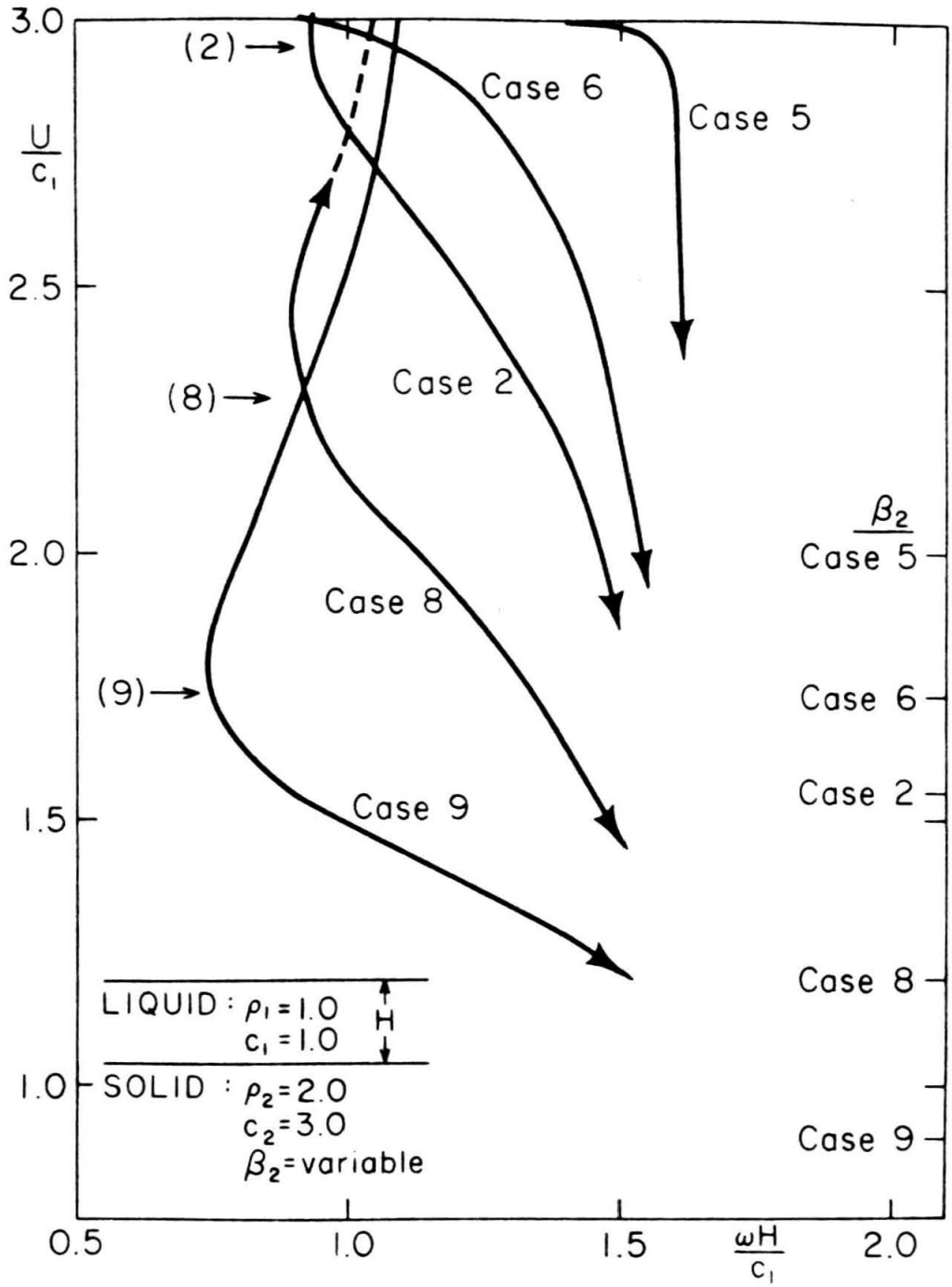
3.0
2.5
2.0
1.5
1.0
U/c1
0.5
1.0
1.5
2.0
ωH/c1
(2)
(8)
(9)
Case 6
Case 5
Case 2
Case 8
Case 9
β2
Case 5
Case 6
Case 2
Case 8
Case 9
LIQUID : ρ1 = 1.0
c1 = 1.0
H
SOLID : ρ2 = 2.0
c2 = 3.0
β2 = variable

Fig. 7

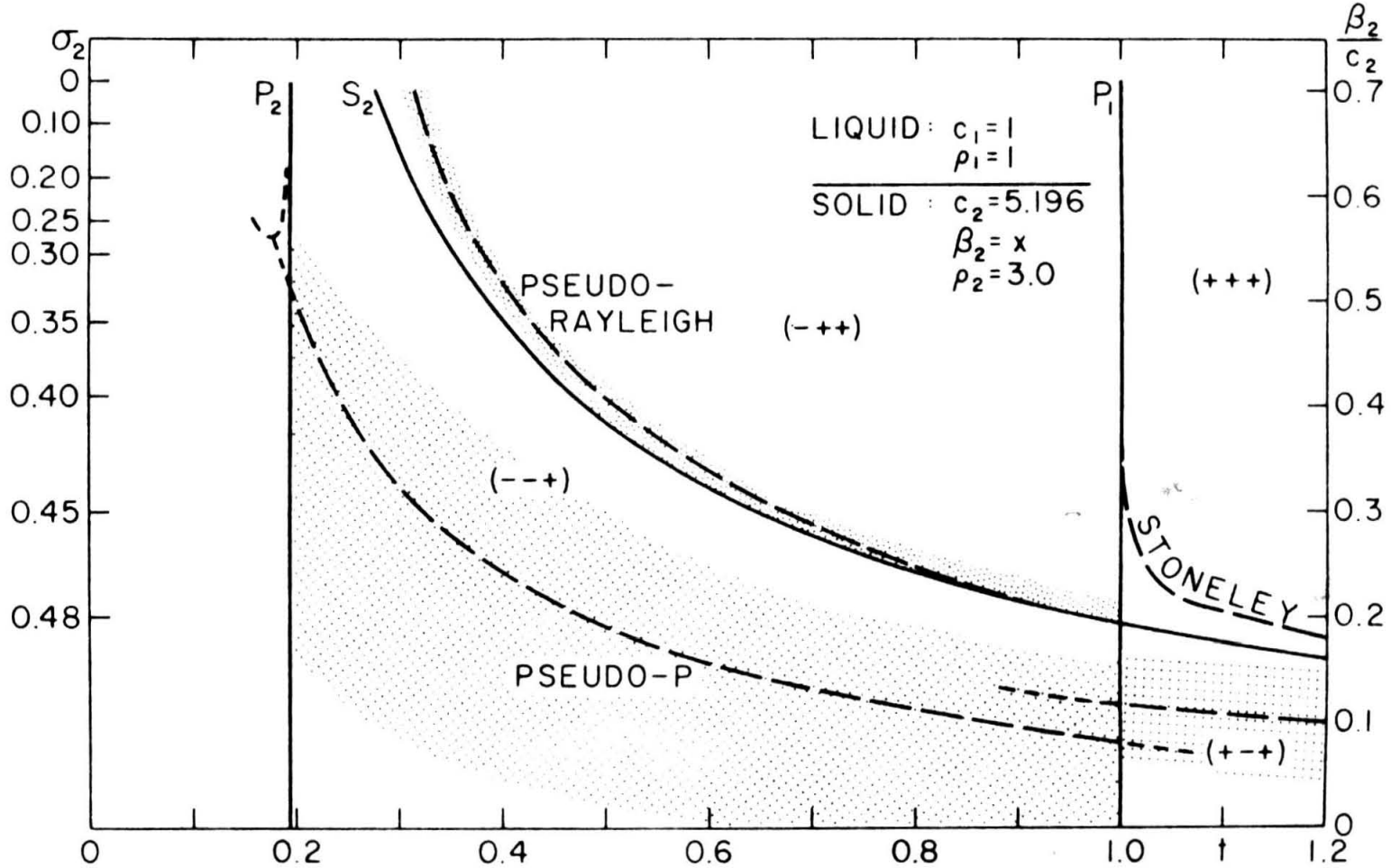
σ_2
$\frac{\beta_2}{c_2}$
0
0.10
0.20
0.25
0.30
0.35
0.40
0.45
0.48
0.7
0.6
0.5
0.4
0.3
0.2
0.1
0
P_2
S_2
P_1
LIQUID: $c_1 = 1$
$\rho_1 = 1$
SOLID: $c_2 = 5.196$
$\beta_2 = x$
$\rho_2 = 3.0$
PSEUDO-
RAYLEIGH
(-++)
(+++)
(--+)
STONELEY
PSEUDO-P
(+-+)
0
0.2
0.4
0.6
0.8
1.0
t
1.2

Fig. 8

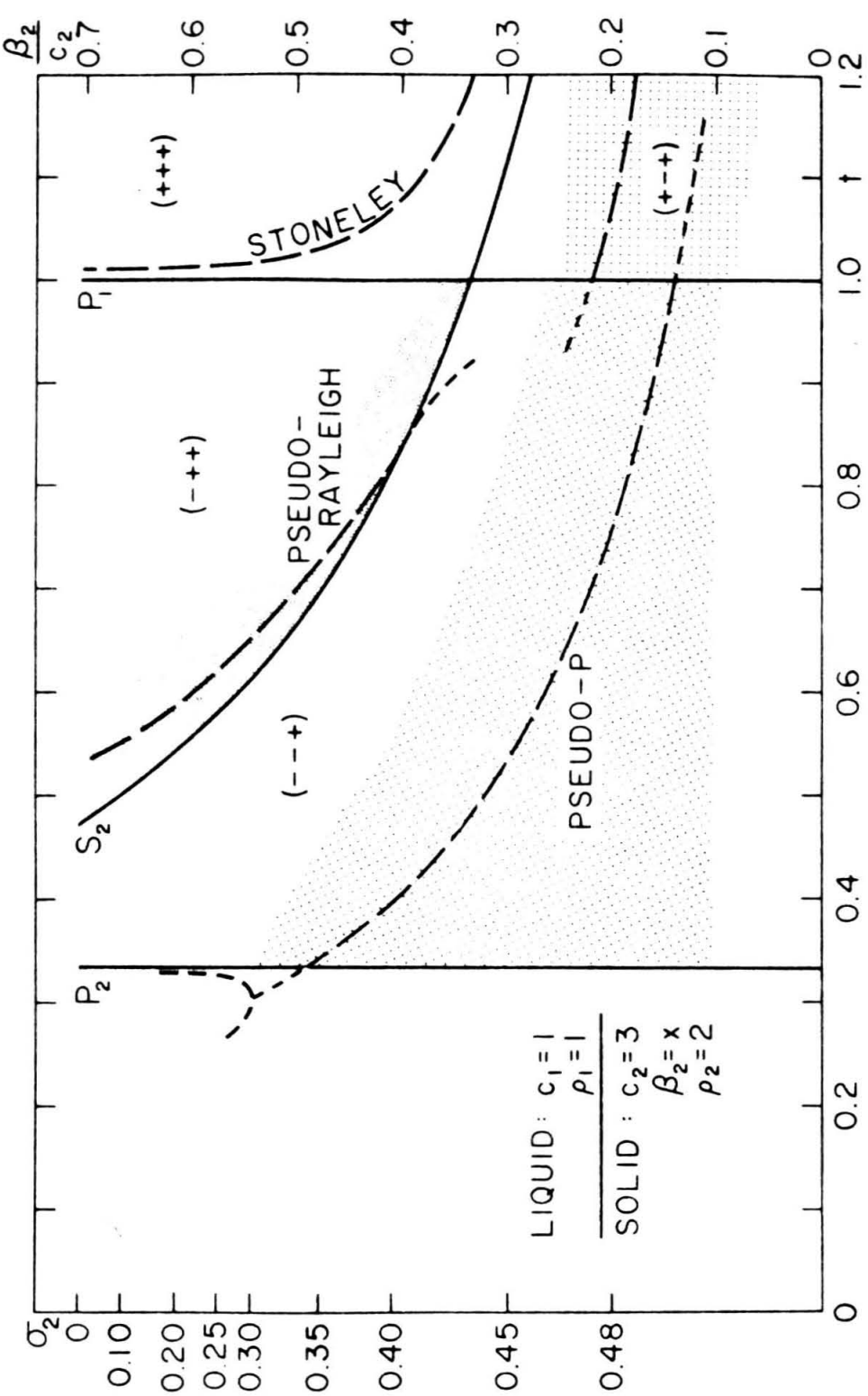
β_2
c_2
0.7
0.6
0.5
0.4
0.3
0.2
0.1
0
1.2
t
1.0
0.8
0.6
0.4
0.2
0
σ_2
0
0.10
0.20
0.25
0.30
0.35
0.40
0.45
0.48
(+++)
STONELEY
P_1
(-++)
PSEUDO-
RAYLEIGH
S_2
(--+)
P_2
PSEUDO-P
(+-+)
LIQUID : $c_1 = 1$
$\rho_1 = 1$
SOLID : $c_2 = 3$
$\beta_2 = x$
$\rho_2 = 2$

Fig. 9

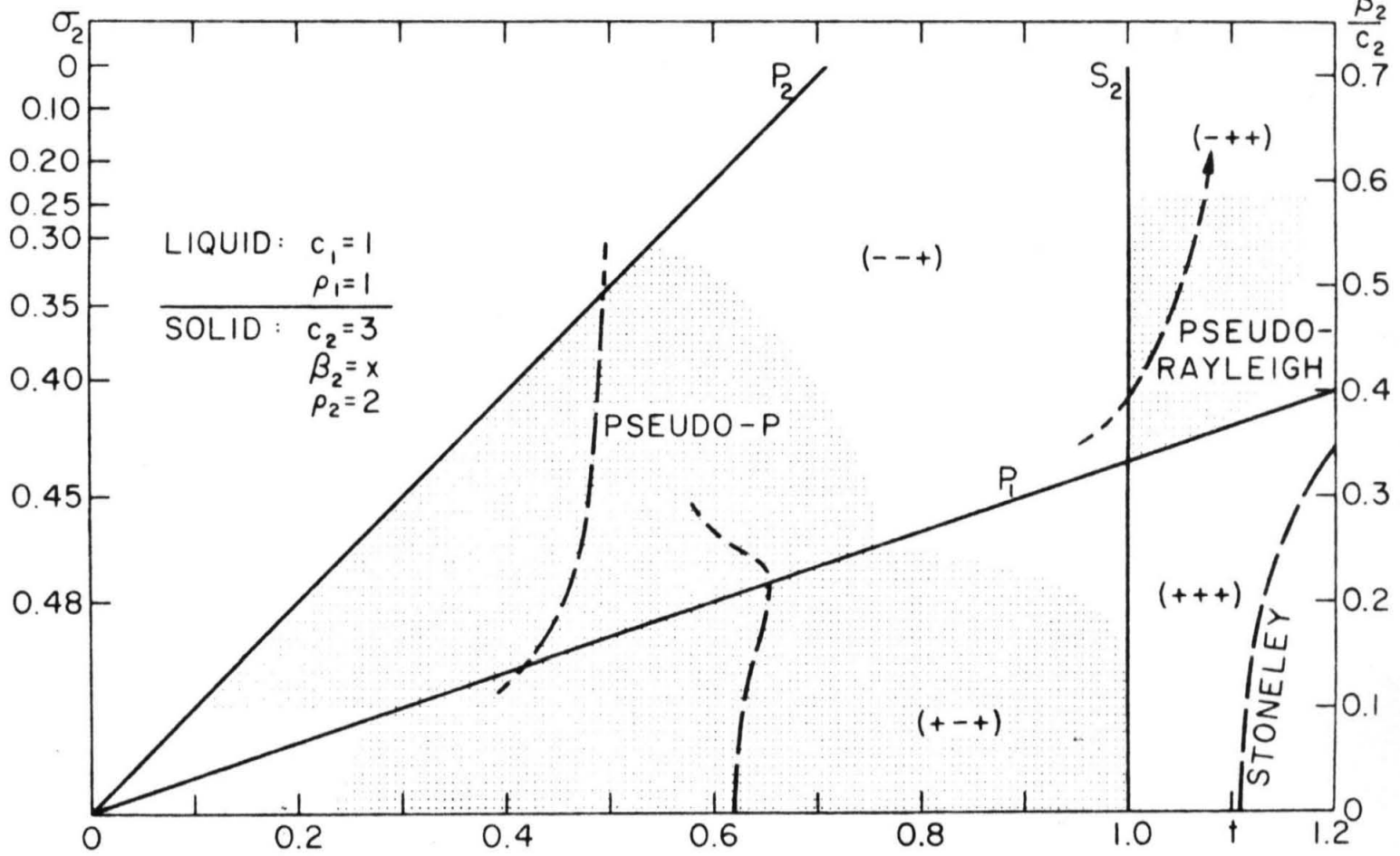
σ_2
0
0.10
0.20
0.25
0.30
0.35
0.40
0.45
0.48
$\frac{\beta_2}{c_2}$
0.7
0.6
0.5
0.4
0.3
0.2
0.1
0
LIQUID: $c_1 = 1$
$\rho_1 = 1$
SOLID: $c_2 = 3$
$\beta_2 = x$
$\rho_2 = 2$
P_2
S_2
(- - +)
(- + +)
PSEUDO-P
PSEUDO-RAYLEIGH
P_1
(+ + +)
(+ - +)
STONELEY
0
0.2
0.4
0.6
0.8
1.0
t
1.2

Fig. 10

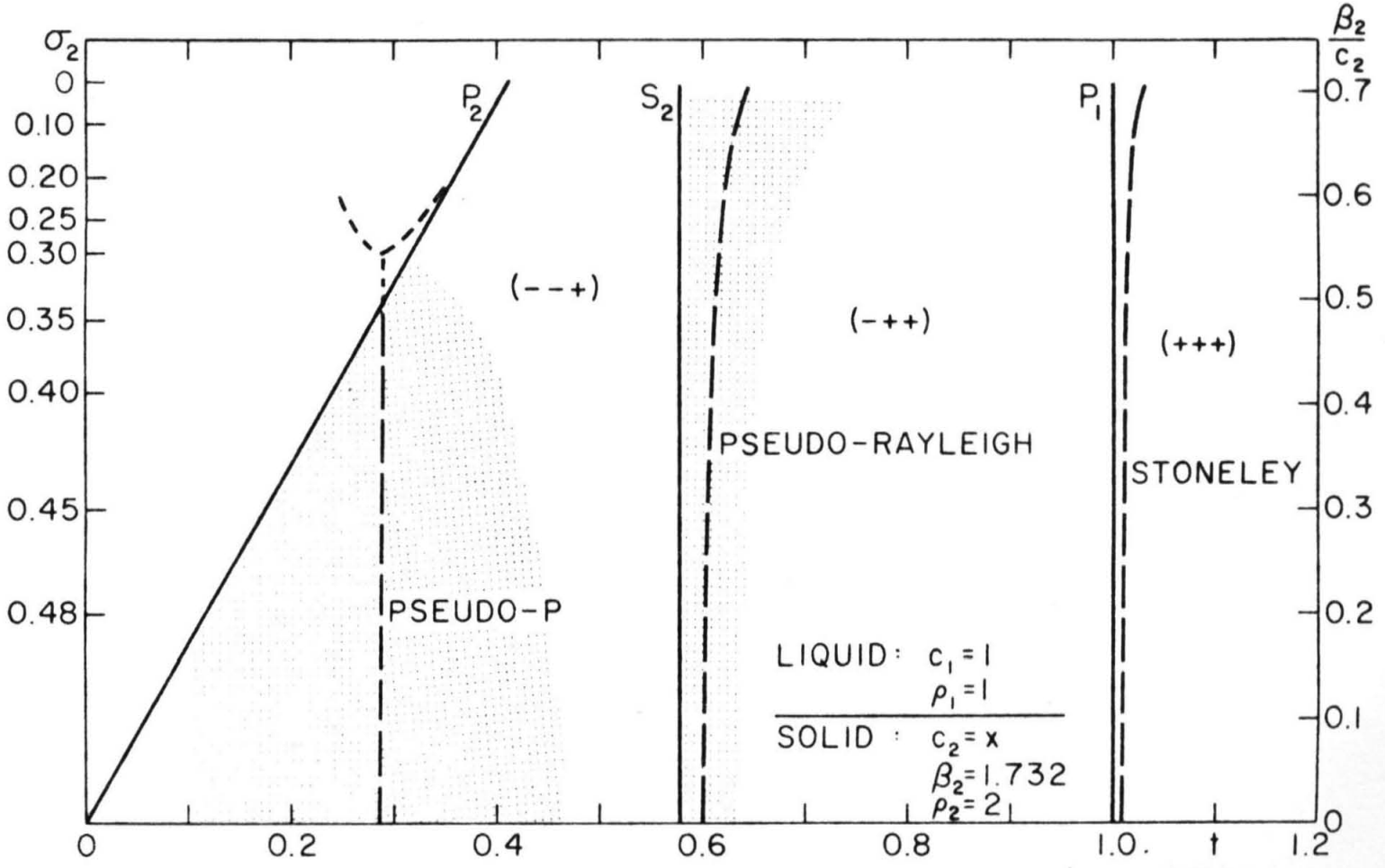
σ_2
0
0.10
0.20
0.25
0.30
0.35
0.40
0.45
0.48
$\frac{\beta_2}{c_2}$
0.7
0.6
0.5
0.4
0.3
0.2
0.1
0
0
0.2
0.4
0.6
0.8
1.0
t
1.2
P_2
S_2
P_1
(--+)
(-++)
(+++)
PSEUDO-P
PSEUDO-RAYLEIGH
STONELEY
LIQUID : $c_1 = 1$
$\rho_1 = 1$
SOLID : $c_2 = x$
$\beta_2 = 1.732$
$\rho_2 = 2$

Fig. 11

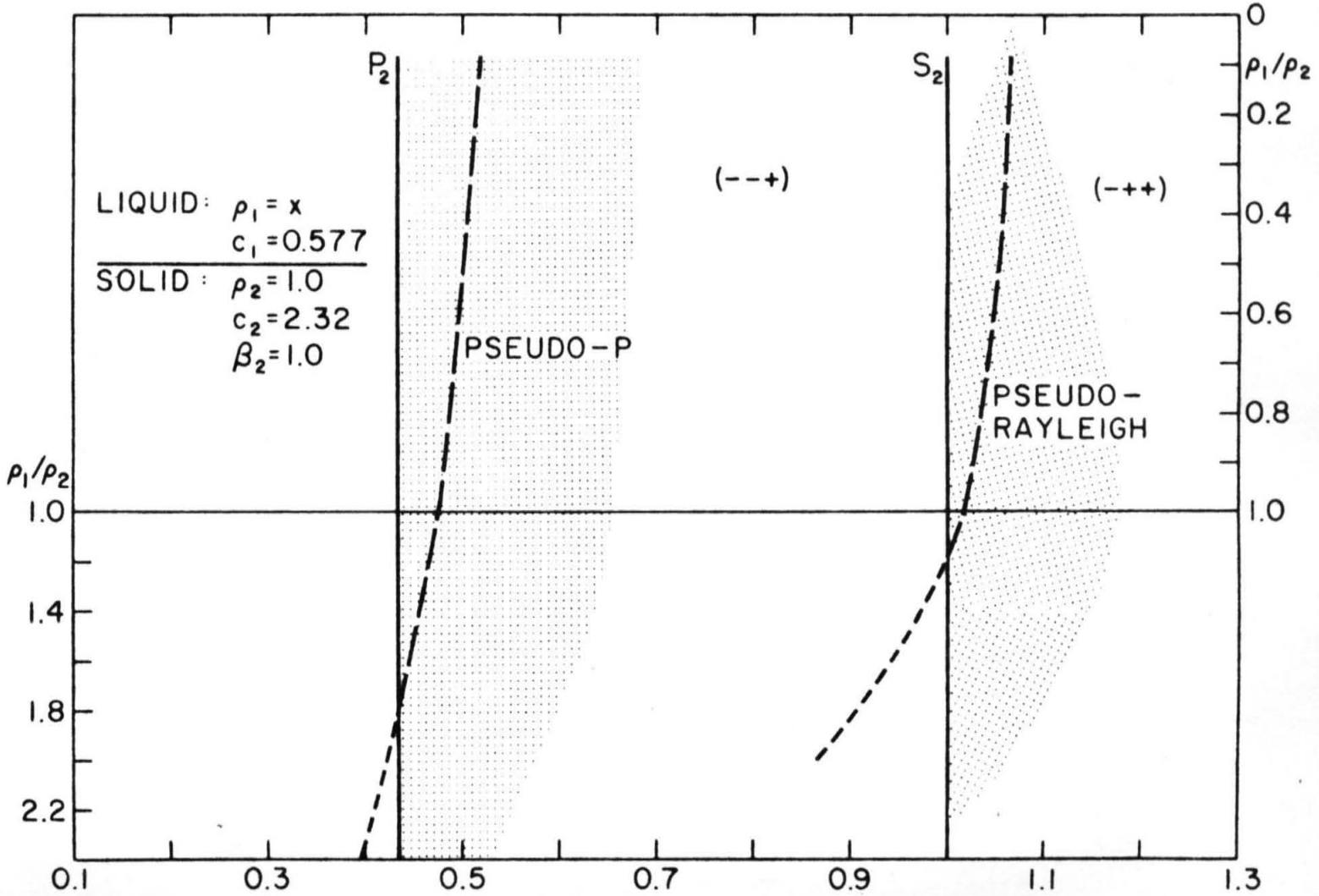
LIQUID: $\rho_1 = x$
$c_1 = 0.577$
SOLID: $\rho_2 = 1.0$
$c_2 = 2.32$
$\beta_2 = 1.0$
P_2
S_2
(--+)
(-++)
PSEUDO-P
PSEUDO-RAYLEIGH
ρ_1/ρ_2
0
0.2
0.4
0.6
0.8
1.0
1.4
1.8
2.2
0.1
0.3
0.5
0.7
0.9
1.1
1.3

Fig. 12

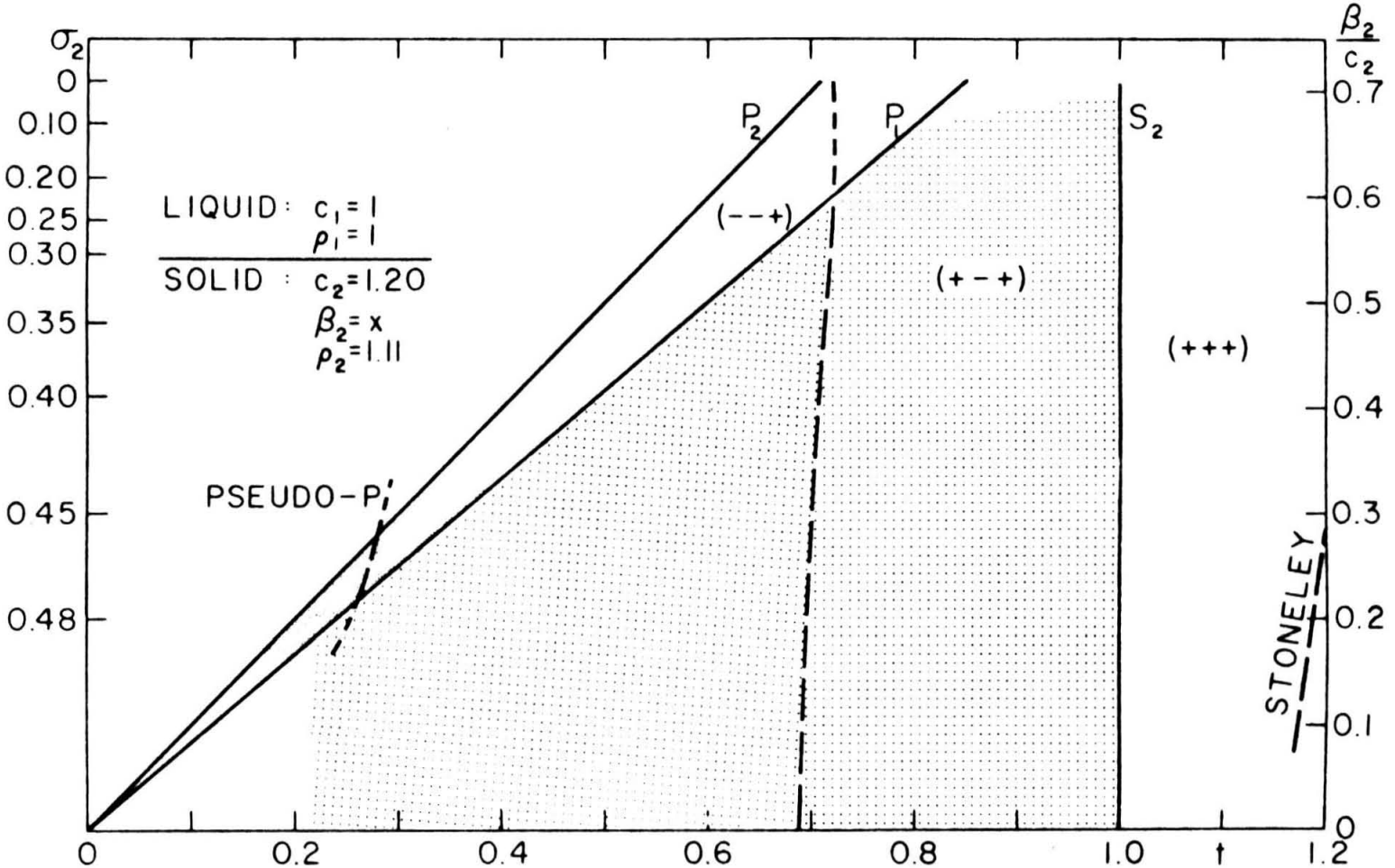
σ_2
0
0.10
0.20
0.25
0.30
0.35
0.40
0.45
0.48
$\frac{\beta_2}{c_2}$
0.7
0.6
0.5
0.4
0.3
0.2
0.1
0
LIQUID : $c_1 = 1$
$\rho_1 = 1$
SOLID : $c_2 = 1.20$
$\beta_2 = x$
$\rho_2 = 1.11$
P_2
P_1
S_2
(--+)
(+-+)
(+++)
PSEUDO-P'
STONELEY
0
0.2
0.4
0.6
0.8
1.0
t
1.2

Fig. 13

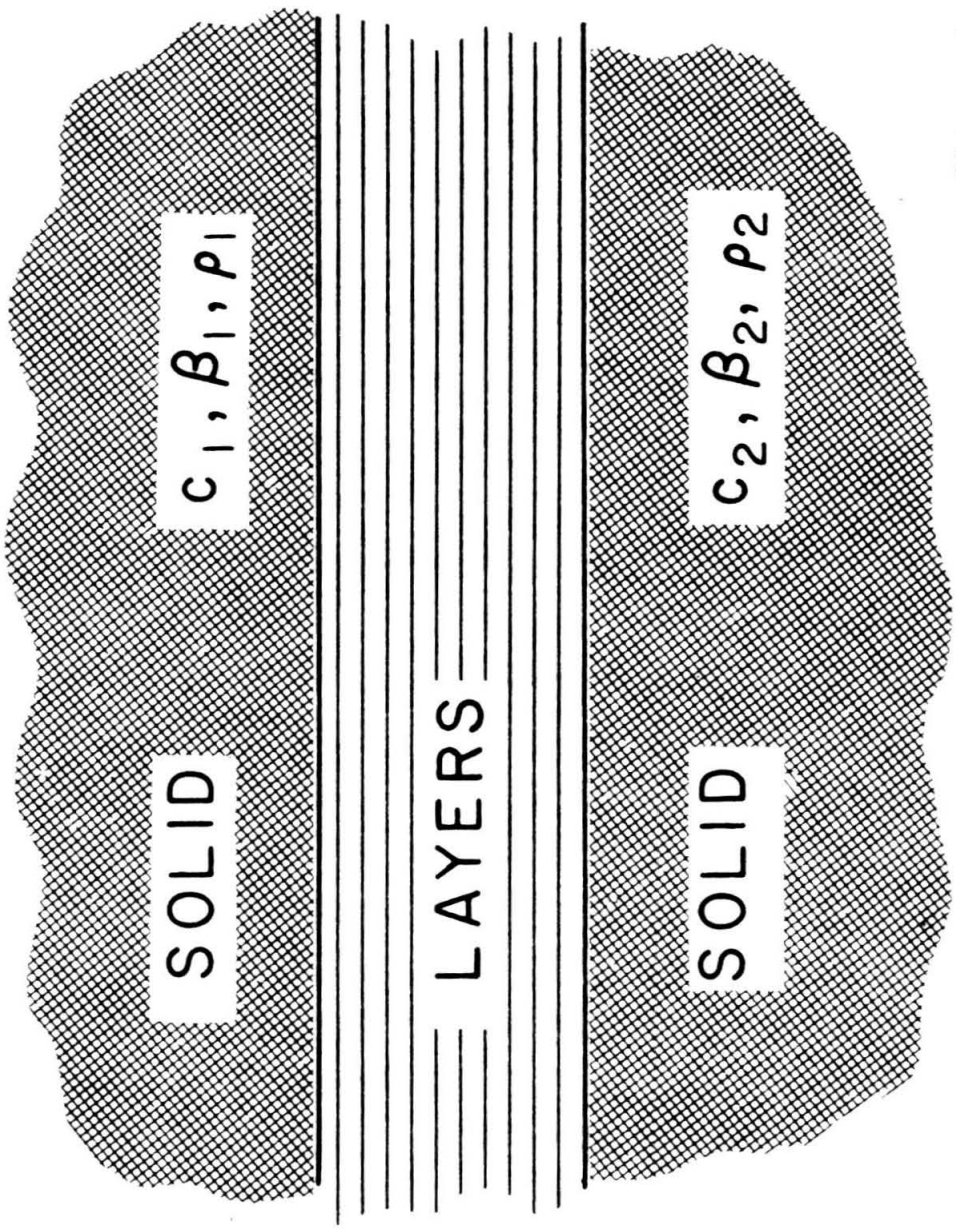

Fig. 14

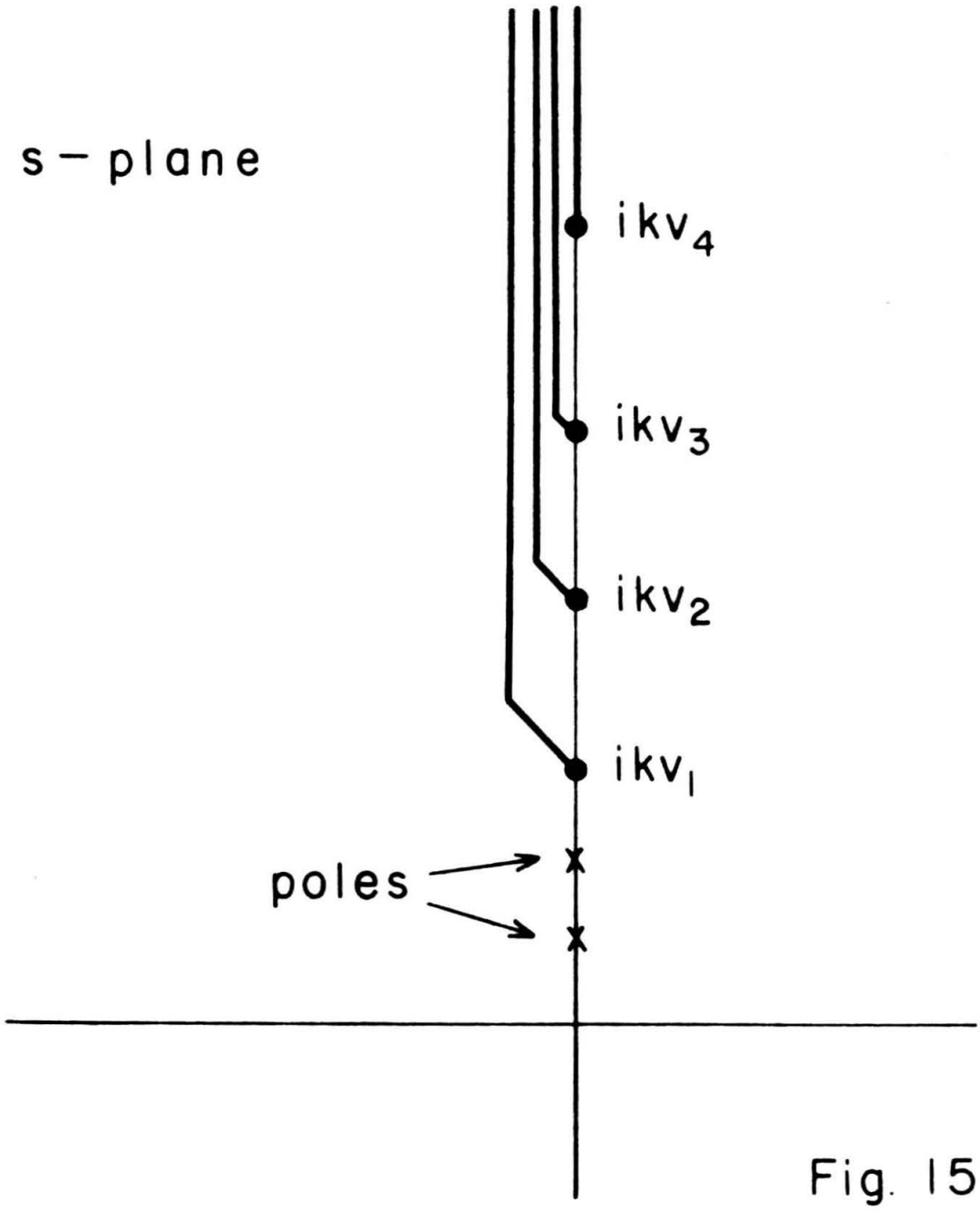

Fig. 15

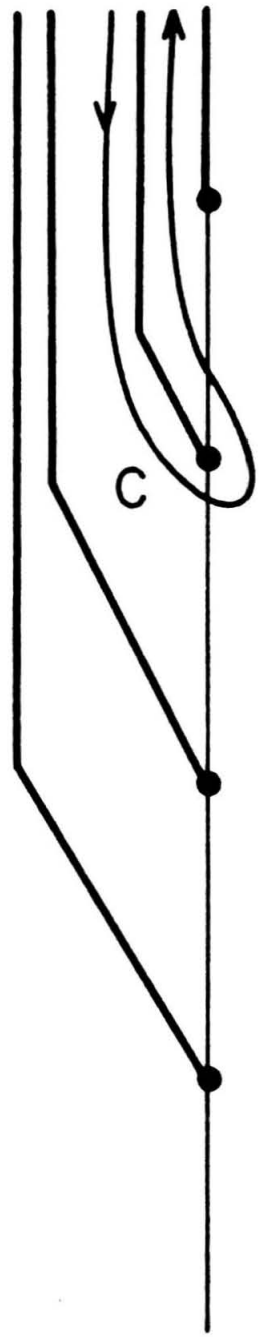

s-plane

Fig. 16

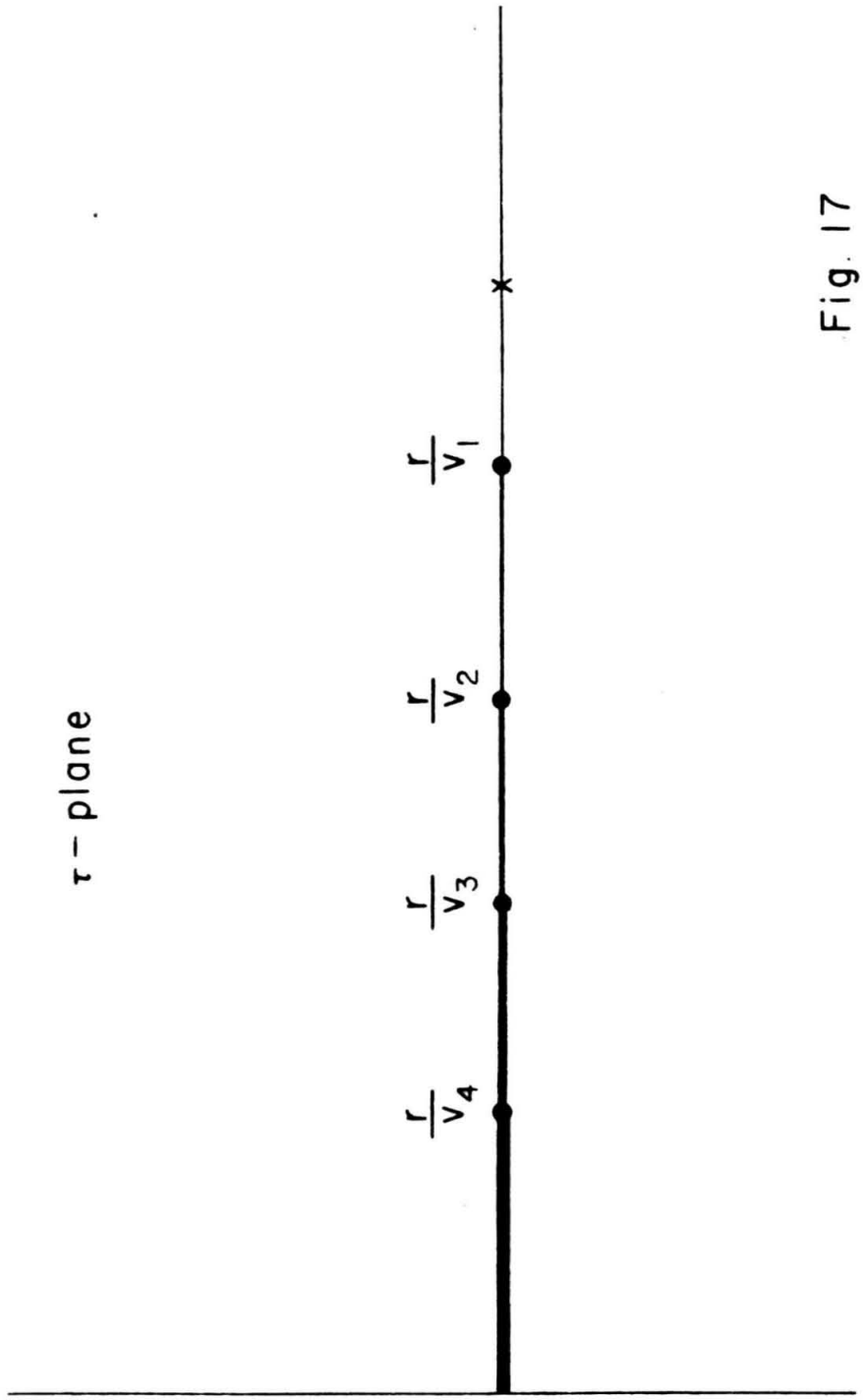

Fig. 17

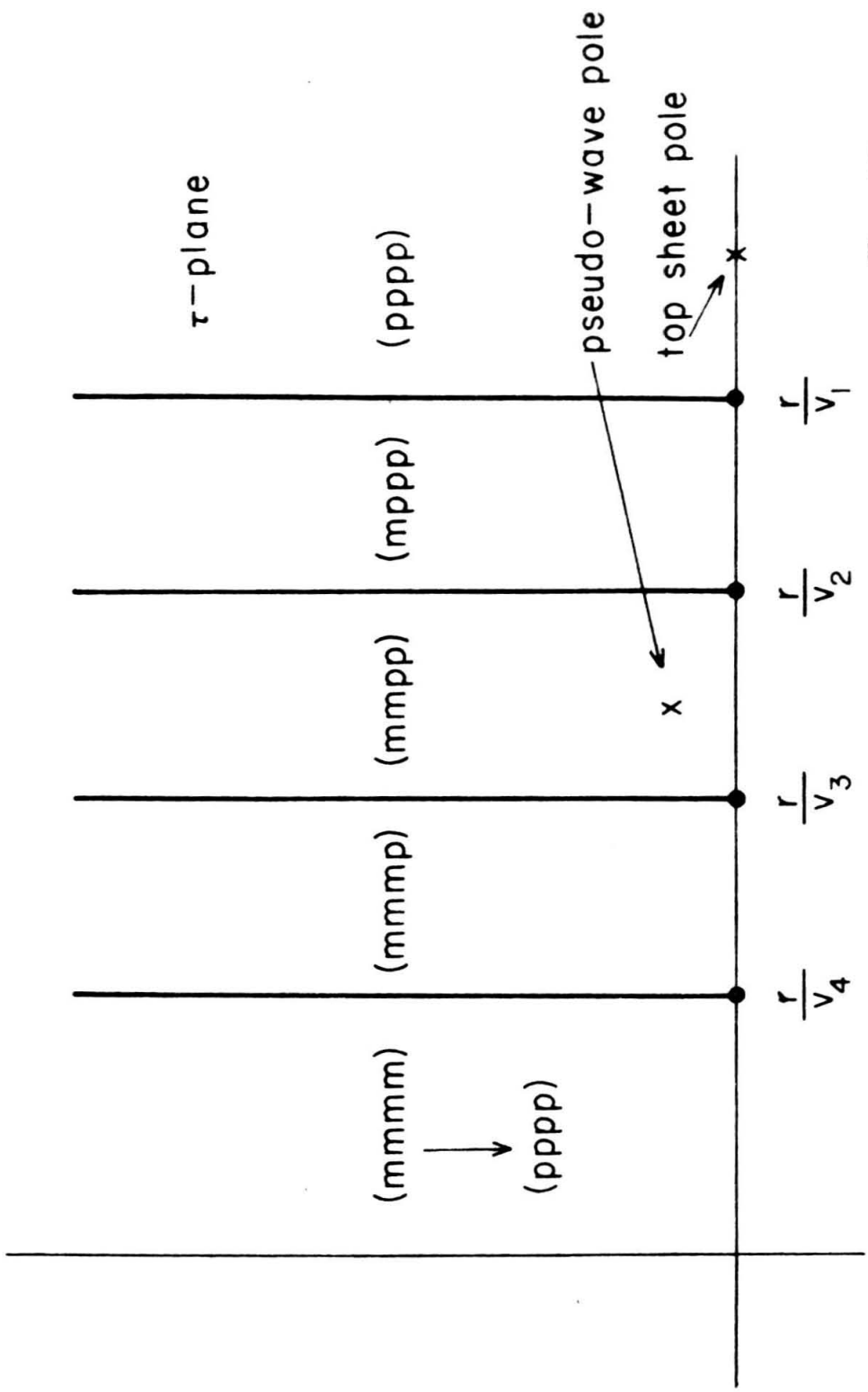
τ-plane
(pppp)
(mppp)
(mmpp)
(mmmp)
(mmmm)
(pppp)
pseudo-wave pole
top sheet pole
x
x
$\frac{r}{v_1}$
$\frac{r}{v_2}$
$\frac{r}{v_3}$
$\frac{r}{v_4}$

Fig. 18

Numerical solution of complex mode problems

Description of problem:

The complex mode problems described in the main body of this thesis were solved by a series of programs coded for the Burroughs 220 computer. The purpose of the program is to find complex zeroes (ω_n) of the period function (f) as a function of the complex parameter k, and to obtain the derivative $d\omega_n/dk$ at each zero. Stated otherwise, it obtains the mapping of the k-plane onto the cut ω_n plane, and computes the complex scale factor of the mapping. The following problems may be handled:

1) Liquid layer over a solid halfspace
2) Solid layer over a solid halfspace
3) Solid halfspace with a free surface
4) Liquid/solid halfspaces in contact
5) Solid/solid halfspaces in contact

The root finding procedure and complex arithmetic are common to all these variations. Explicit coding of the individual functions was employed, since the machine is too slow for general n-layered computations.

Description of computation:

1. Input values of k and ω are generated: manually from the keyboard, or internally, depending on console switch settings. k is taken as a parameter and ω as a trial value.

2. $f(k,\omega)$ is evaluated at k and at $k + \delta k$, the increment being fixed in storage. $f(k + \delta k) - f(k)$ is used to estimate the next trial value of ω by Newton's method (in complex variables). When the correction term $\Delta\omega$ becomes less than $m \cdot \delta k$, the machine assumes that a root has been found. For normalized inputs between 0.1 and 5.0, $m = 20$ and $\delta k = 10^{-6}$ are sufficient to insure repeatability to 5 decimal places. Due to the way in which f is expressed, the magnitude of its individual terms varies as some power (4 or more) of the magnitude of the input variables. Consequently the increment used in the root finding (δk) must be adjusted manually depending on the magnitude of the input quantities. If δk is too small, overflow will occur in the Newton extrapolation, and if δk is too large, inaccuracy is a consequence.

3. (Variations 1 and 2 only) The functions $\partial f/\partial\omega)_\kappa$ and $\frac{\partial f}{\partial \kappa})_\omega$ which have been explicitly coded, are evaluated, and U, defined by $-\frac{\partial f}{\partial \kappa}/\frac{\partial f}{\partial \omega}$, is obtained. In investigations of the saddle point one is interested in following the complex locus where Im U = 0. It is therefore necessary to know U to 4+ decimal places. Fluctuations in the root ω_n (due to cutting off the iterations) in the 5th decimal place result in fluctuations of U in the 4th decimal place. This magnification of error occurs even though the derivatives are obtained by analytic formulae rather than by taking small differences. Thus proper

selection of the increment δk is more crucial in obtaining the desired accuracy in the quantity U than in knowing the behavior of $\omega_n(k)$.

4. Output of the complex numbers k, ω_n, and U occurs on the on-line printer. For the non-dispersive problems (variations 3-5) U is set equal to zero.

5. (Variations 1 and 2) The setting of switches on the console determines the selection of new input values of k by arithmetic increments. The new trial value of ω is estimated by: $\omega(\text{trial}) - \omega(\text{old}) = U(\text{old}) \times \text{increment of } k$.

(Variations 3 - 5) The machine awaits input of one or more new physical parameters on the keyboard. Selection of the parameters of interest is accomplished by elementary modifications of the stored program. These parameters are also printed out in the ensuing output of k and ω.

From two to four radicals in f are responsible for the existence of 4 to 16 Riemann surfaces. The sign of the real part of each radical is chosen + or - depending on the setting of certain switches on the console. Whenever data (k and ω) is introduced at the keyboard, an output occurs, specifying the Riemann sheet. In the root finding process f appears to the computer as a single valued function analytic everywhere except along the branch cut, where it is discontinuous. Newton's method

thus breaks down near the branch cut. It has been possible, by judicious choice of inputs, to get close enough to the cut from either side for the behavior of the roots ω_n and of the group velocity to be apparent.

A framework has been established which permits solution of similar problems with a minimum of recoding. It is necessary only to recode the explicit evaluation of $f(\omega,k)$, $\frac{\partial f}{\partial \omega}$ and $\frac{\partial f}{\partial k}$. This is simplified by the following routines:

1) An interpreter which operates on sequentially stored pseudo-instructions in the complex arithmetic mode. Square root and the hyperbolic functions are included in this mode.

2) Routines which evaluate total derivatives by summation of a signal flow graph. It is necessary only to explicitly evaluate individual partial derivatives in the complex mode.

Signal flow graphs as a coding aid

The concept of a signal flow graph may be used as a programming aid in evaluating total derivatives. We will describe a systematic hand programming procedure. Our description, however, might readily be taken as the framework of a compiler with the ability to generate an equivalent program automatically. For example: $f = f(\omega, k, u_1, u_2, \ldots u_j, \ldots u_n)$. The u_j may be functions of each other and functions other variables. The chain of dependence reaches back eventually to the two independent variables ω and k; to define this chain, one must write down all the explicit formulae relating the variables. The total derivatives $\frac{\partial f}{\partial k}$ and $\frac{\partial f}{\partial \omega}$ are obtained by multilinear sums of all the partial derivatives relating the intermediate variables. Explicit expressions for $\frac{\partial f}{\partial \omega}$ and $\frac{\partial f}{\partial k}$ may be too complicated to consider; the partial derivatives $\frac{\partial u_i}{\partial u_j}$ are easily written down. A signal flow graph provides a formalism by which the partial derivatives may be summed.

Signal flow graphs were devised by Mason (1953, 1956) as an aid in the computation of linear gain in feedback amplifiers. The application described here is actually the basic case in which feedback does not enter. The application of the feedback portion of the theory to more general problems having loops of dependence can be easily

made, when and if this becomes desirable. We offer here a short description of the "forward" type of flow graph.

1. When u is a function of v, we write $u = f(v)$. The corresponding flow graph is:

(By "function" we mean an explicit relation). The linear relation obtained from $u = f(v)$ is $du = \frac{\partial u}{\partial v} dv$. The flow graph may be considered to represent this expression also. We assign a "linear gain" g_{vu} to the directed line from v to u and write: $du = g_{vu} dv$.

2. Let x_1 be an explicit function of x_2, x_3, x_4. Then $x_1 = f(x_2, x_3, x_4)$. The corresponding graph is then:

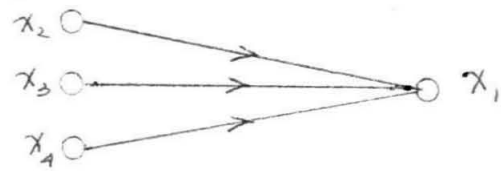

We now write the linear relation between the differentials:

$$dx_1 = \frac{\partial x_1}{\partial x_2} dx_2 + \frac{\partial x_1}{\partial x_3} dx_3 + \frac{\partial x_1}{\partial x_4} dx_4$$

Setting $\frac{\partial u_j}{\partial u_i} = g_{ij}$, the formula becomes:

$$dx_1 = g_{21} dx_2 + g_{31} dx_3 + g_{41} dx_4 = \sum_1^4 g_{i1} dx_i$$

The g_{ij} are called the <u>branch gains</u>. "Transmission" of signal (dependence) along a branch involves multiplication by the branch gain, and confluence of branches going into a node represents summation.

3. Complicated total derivatives may be represented by flow graphs using combinations based on the simple

conventions just described. For example, the following set of equations and flow graph are equivalent:

$$\begin{aligned} f &= f(v,y) \\ v &= v(u,w) \\ y &= y(u,w) \\ u &= u(x) \\ w &= w(u,x) \end{aligned}$$

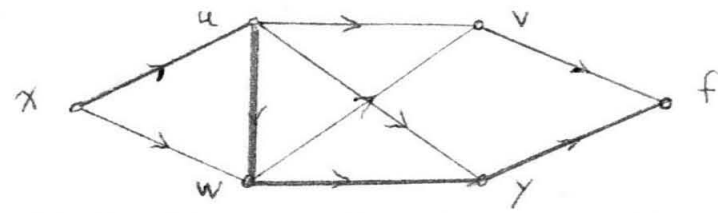

df/dx is the sum of all the linear path gains connecting x to f. There are 6 forward flow paths from x to f. Thus:

$$\frac{df}{dx} = \frac{\partial w}{\partial x}\frac{\partial v}{\partial w}\frac{\partial f}{\partial v} + \frac{\partial w}{\partial x}\frac{\partial y}{\partial w}\frac{\partial f}{\partial y} + \frac{\partial u}{\partial x}\frac{\partial v}{\partial u}\frac{\partial f}{\partial v} + \frac{\partial u}{\partial x}\frac{\partial y}{\partial u}\frac{\partial f}{\partial y}$$

$$+ \underline{\frac{\partial u}{\partial x}\frac{\partial w}{\partial u}\frac{\partial y}{\partial w}\frac{\partial f}{\partial y}} + \frac{\partial u}{\partial x}\frac{\partial w}{\partial u}\frac{\partial v}{\partial w}\frac{\partial f}{\partial v}$$

The fifth term (underlined) is the total path gain along the path x- u- w- y- f (heavy line in the graph). This result could be obtained by careful inspection of the defining equations. When more variables occur, however, the possibility of error in such a procedure increases, and the flow graph is a convenient visual representation of the problem.

4. We now formulate a procedure for evaluating a total derivative, dx_1/dx_n, using the organization afforded by the signal flow graph. First, as many intermediate variables are defined as is convenient, so that the partial (branch) gains g_{ij} are algebraically simple. The variables (nodes) are numbered from 1 to n as follows:

x_1 is the output variable

x_n is the input variable. If there are 2 or more input variables, these are assigned indices n,

n-1, n-2, ...

Every individual branch is directed from a higher numbered node to a lower numbered node. This is possible when feedback is absent. When feedback is present, appropriate transformations will put the graph in a non-feedback configuration (see Mason, 1953, 1956).

When n = 5, the most general graph of the type described is:

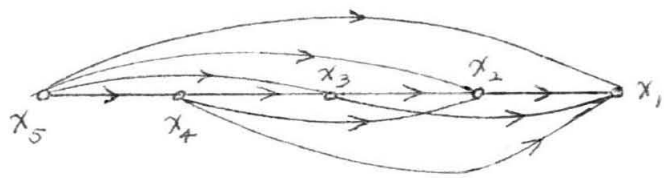

5. The path gains g_{ij} are non-zero only if $i > j$. These quantities may be computed individually and stored in a triangular array. Many of these gains will be zero if no branch exists between the pair of nodes; the graph in paragraph 3 may be thought of as having a branch from v to y with gain $g_{vy} = 0$. We then define dx_1/dx_n to be the gain of the matrix (array).

6. $h_p = dx_1/dx_p$ is defined as the gain of the sub-matrix obtained by deleting all the nodes x_q of index greater than p. Then:

$$h_2 = g_{21}$$

$$h_3 = g_{31} + g_{32}h_2$$

$$h_m = \sum_{p=1}^{m-1} g_{mp}h_p \qquad \text{if } h_1 = 1.$$

This formula is the basis for a computer program which computes successive h_p for p = 2, 3, ..., n, from the stored matrix g_{ij}. h_n is the desired matrix gain. When more than one independent variable is involved, h_n, h_{n-1}, ...etc. are the derivatives of x_1 with respect to the various inputs. When more than one dependent (output) variable is involved, these may be set up individually in the role of x_1.

7. Total derivatives are evaluated explicitly on the Burroughs 220 as follows (in the complex mode):

a. Explicit evaluation of the partial gains must be performed by hand coded complex interpretive commands.

b. A special interpretive command specifying i and j stores the gains in the proper matrix locations.

c. The summation routine operates on the matrix, producing a table of h_p.

References

1. Mason, S. J., Proceedings of the IRE, p.1144, 1953

2. Mason, S. J., Proceedings of the IRE, p. 920, 1956